MAGNETRON SPUTTER GROWN METAL DOPED VANADIUM OXIDE THIN FILMS FOR TERAHERTZ BOLOMETERS

A Thesis Submitted
to the Graduate School of Engineering and Sciences of
Izmir Institute of Technology
in Partial Fulfillment of Requirement for Degree

DOCTOR OF PHILOSOPHY

in Materials Science and Engineering

by

Hakan ALABOZ

January 2018

IZMIR

We approve the thesis of **Hakan ALABOZ**

Examine Committee Members:

Prof. Dr. Gülnur AYGÜN ÖZYÜZER
Department of Physics, Izmir Institute of Technology

Prof. Dr. Hasan EFEOĞLU
Department of Electric and Electronics Engineering, Ataturk University

Asst. Prof. Dr. Enver TARHAN
Department of Physics, Izmir Institute of Technology

Prof. Dr. Ekrem ÖZDEMİR
Department of Chemical Engineering, Izmir Institute of Technology

Prof. Dr. Aysun AKŞİT
Department of Textile Engineering, Dokuz Eylül University

January 12, 2018

Prof. Dr. Mustafa DEMİR
Head of the Department of Materials Science and Engineering

Prof. Dr. Aysun SOFUOĞLU
Dean of the Graduate School of Engineering

ACKNOWLEDGMENTS

I would like to express my sincere gratitude to my supervisor Prof. Dr. Gülnur Aygün OZYUZER for her patience and guidance throughout my Ph.D. thesis. I am grateful for her contributions of time, ideas to make my Ph.D. experience productive. I also would like to thank Prof. Dr. Lütfi OZYUZER for sharing his experience both in the experiment and theoretical part of the terahertz region. He has taught me to be aware of my strengths, work hard on my weaknesses, and he has inspired me each and every day with his own example of extraordinary hard work. It was a great experience to work with their group and perform my research in their labs. Without both Assoc. Prof. Dr. Gülnur AYGUN OZYUZER's and Prof. Dr. Lütfi OZYUZER's valuable guidance and support, it would not be possible to conduct this thesis.

I would like to thank Prof. Hasan EFEOGLU for his valuable comments and guidance in microelectronics.

I would like to thank all members of the OZYUZER's group especially my colleagues Yasemin DEMIRHAN and Batuhan MULLA for good friendship and their general support as well as support for etching and antenna simulation part of the thesis.

Finally, I would like to thank my wife for her patience, support, and love through this stage.

I would like to acknowledge that this research was supported by TUBITAK project no 115F549.

ABSTRACT

MAGNETRON SPUTTER GROWN METAL DOPED VANADIUM OXIDE THIN FILMS FOR TERAHERTZ BOLOMETERS

Terahertz (THz) studies and hence technological improvements have increased and that caused expansion of application of THz waves. Applications of THz region have been expanded in many areas such as security, medical imaging, detection of explosives, nondestructive tests and wireless communication recently. THz radiation passes through many plastic materials, clothing but it reflects from metals and it is used in the detection of a lot of well known explosive materials. In spite of mentioned advantages and a wide range of application area, constructing a detector which is low cost, compact and uncooled is difficult and this causes the industry to improve slowly. Now, detectors which are widely used in THz region are pyroelectric, Schottky barrier diodes, field effect transistors and they have disadvantages such as low sensitivity, hard to construct an array and low speed. Instead of these detectors, superconducting bolometers are presented but they require liquid helium cooling. It is thought that VO_x will be a premium technology for THz region due to its success in the infrared region. In this thesis, VO_x:Au thin films were produced by DC magnetron sputtering and properties of these films were optimized for uncooled bolometer that operates at THz region. Polycrystalline VO_x:Au thin films which have $\cong$-1.7 % K^{-1} temperature coefficient resistance (TCR) and 0.07 Ωcm resistivity values were obtained. Increasing TCR values mostly depend on sputtering parameters such as gas and Au dope rates. These parameters were changed until the best TCR value was achieved and with Au doping, high resistance values of the films decreased to acceptable levels hence it decreased Johnson noise of the bolometer. Originally, these thin films which were sputtered on high resistivity silicon wafers and doped with Au, provided the bolometer to operate in THz region efficiently. The antenna design on the device was made by CST Microwave Studio, the antenna resonance was arranged to $\cong$0.6 THz which is related to our THz source operating frequency.

Keywords: THz, Uncooled bolometer, Vanadium oxide

ÖZET

TERAHERTZ BOLOMETRELERİ İÇİN MANYETİK SAÇTIRMA İLE BÜYÜTÜLMÜŞ METAL KATKILI VANADYUM OKSİT İNCE FİLMLERİ

Terahertz (THz) bölgesindeki çalışmalar ve bunun sonucu olan teknolojik gelişmeler son dönemde artmıştır ve bunun sonucu olarak THz bölgesinin uygulama alanlarının genişlemesine neden olmuştur. Günümüzde terahertz bölgesinin uygulama alanları güvenlikten medikal görüntülemeye, patlayıcı tespitinden, örneklere zarar vermeden yapılabilen testlere ve geniş bant kablosuz iletişime kadar birçok alana yayılmıştır. Terahertz ışıması birçok plastikten, kıyafetlerden geçer, metallerden yansır ve bilinen birçok patlayıcı malzemesinin tespitinde kullanılabilir. Bahsedilen tüm bu avantajları ve uygulama alanlarının çokluğuna rağmen, ucuz, küçük boyutlu ve soğutmasız THz dedektör yapmanın zorluğu sektörün yavaş ilerlemesine neden olmaktadır. Şu anda yaygın olarak THz alanında kullanılan dedektörler, piroelekrik, Schottky bariyer diyotları, alan etkili transistörler, golay hücreleridir ve bunların düşük duyarlılık, bir dizi haline getirme zorluğu, düşük hızda çalışmaları gibi dezavantajları vardır. Bu dedektörler dışında, süperiletken bolometreler yapılmıştır ancak bu hassas bolometrelerin sıvı helyum ile soğutulmaları gerekmektedir. Kızılötesi alanındaki başarısı nedeniyle VO_x in, terahertz bölgesi için de gelecek vaat edeceği düşünülmektedir. Bu tezin kapsamında VO_x:Au filmler DC manyetik saçtırma ile üretilmiş ve filmin özellikleri THz bölgesinde çalışacak soğutmasız bir detektöre uygun hale getirilmiştir. Çoklu kristal yapıda $\cong$-%1.7 K^{-1} sıcaklık direnç katsayılı (TCR) ve 0.07 Ωcm özdirenç değerine sahip filmler üretilmiştir. TCR değerini iyileştirmek, gaz oranları veya Au katkılama oranları gibi kaplama parametrelerine bağlıdır. Bu parametreler en iyi TCR değeri elde edilinceye kadar değiştirilmiş ve aynı zamanda yüksek direnç değerlerini kabul edilebilir düzeylere indirerek bolometrenin Johnson gürültüsü düşürülmüştür. Özgün olarak, yüksek özdirenç silikon yongalar üzerine büyütülmüş ve altın katkılandırılmış bu filmler, bolometrenin THz bölgesinde verimli bir şekilde çalışmasını sağlayacaktır. Anten tasarımı CST Microwave Studio ile yapılmış ve resonansı, grubumuzun elinde bulunan kaynağın çalışma frekansına uyacak şekilde $\cong$0.6THz'e tepki vermesi için tasarlanmıştır.

Anahtar Kelimeler: THz, Soğutmasız bolometre, Vanadyum oksit

TABLE OF CONTENTS

LIST OF FIGURES

LIST OF TABLES

CHAPTER 1

INTRODUCTION

1.1 Terahertz radiation

Terahertz (THz) region of the electromagnetic spectrum is widely known as an unexplored part of the spectrum and it is described from 1 to 10 THz frequency range (Tonouchi 2007). THz region in electromagnetic spectrum and applications that are related to frequencies are shown in Fig. 1.1.

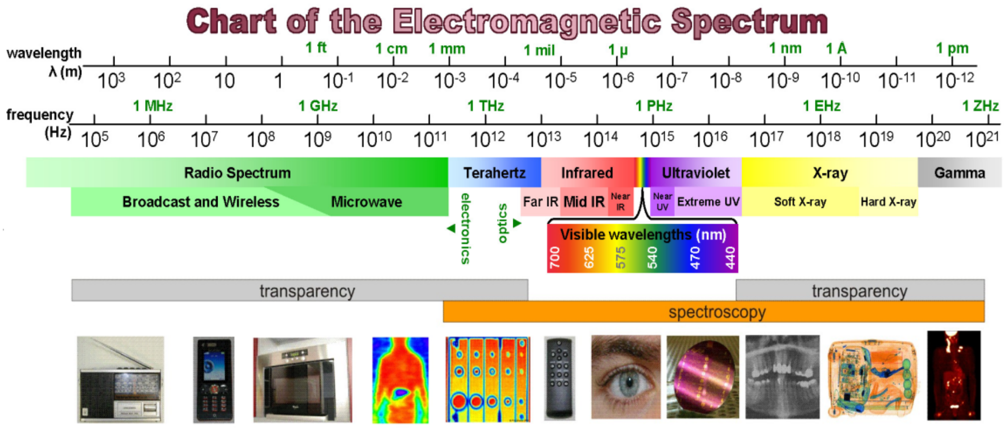

Figure 1.1 Electromagnetic Spectrum
(SURA 2006)

THz region includes a part of submillimeter (0.1-3 THz) range hence both electronics and photonics applications are possible for it. In accordance to understand THz domain, specifications of 1 THz frequency are given in Table 1.1.

Table 1.1 Specifications of 1 THz frequency

For 1 THz Frequency		
Temperature	$T=h\upsilon/k_B$	48 K
Wavelength	$\lambda=C/\upsilon$	300 μm
Wavenumber	$k=1/\lambda$	33 cm^{-1}
Photon energy	$E=h\upsilon$	4.14 meV
Period	$\tau=1/\upsilon$	1 ps

Where T is the temperature, h is the Planck's constant, υ is the frequency, k_B is the Boltzmann's constant, λ is the wavelength, C is the speed of light in vacuum, k is the wavenumber, E is the energy and τ is the period.

Far infrared applications rely on optical and thermal devices. Millimeter wave emitters and detectors were derived from microwave solid-state devices. Although THz region has wide application areas such as wireless communication (Nagatsuma et al. 2013) and security imaging (Liu et al. 2007), lack of sensitive and fast detectors as well as high power sources in this region is an obstacle for advance. Due to lack of available THz source and detectors THz region is identified as a gap called THz gap. It has been narrowed by recent studies in microwave electronics at the part of low frequency and photonics at the part of the high-frequency regime. High power sources (Ozyuzer et al. 2007, 2009; Turkoglu et al. 2013) and better detectors (Lei Liu et al. 2009) which have been provided by researchers to the THz region within last decade. In addition to that THz time-domain spectroscopy (TDS) (Han and Zhang 2001) and THz imaging (Jansen et al. 2010) are accepted as two main improvements in THz region. Besides these improvements, there is an increasing demand for different industries for more sensitive detectors and powerful sources. There are several reasons what make THz region popular for several industries. For instance, THz radiation does not ionize biological organisms because of its low photon energy so it can be used in medical imaging applications (Nagel et al. 2002; Woodward et al. 2002; Ouchi et al. 2014). One of the most important properties of the THz radiation is THz wave can go through nonpolar and nonmetallic materials so it can pass through clothes, paper, plastic, dry wood and even walls that are not thick and reflect from metals hence it can be used for detecting guns and hidden weapons. Another essential property of THz radiation comes from its low photon energy. This low energy can only excite low energy resonances and they are related to vibrational modes of gas molecules, phonons. As a consequence certain explosives (Liu et al. 2007), hazardous materials and drugs have specific fingerprints in THz region so they can also be detected with an advance new THz technologies. THz radiation is reflected on metals so common metals behave as perfect reflector for it. For instance, skin depth of a copper is about 90 nm at 1 THz frequency. Although water molecules are polar and water vapor in the atmosphere absorbs especially upper part of the THz radiation, THz radiation is less scattered by fog or dust than infrared radiation. This property also makes it a possible candidate for wireless communication. THz region is needed for various approaches and techniques which are different from other regions that are employed successfully in neighboring bands. For instance, quantum and thermal noise in THz devices that operate at room temperature must be considered since $h\upsilon \cong k_BT$ where h is the Planck's constant, υ is the frequency, k_B is the Boltzmann constant and T is the temperature.

Thermal emission in THz regime is also important for applications. All objects in the universe emit electromagnetic radiation at all frequencies and the emission depends on the temperature of the object. This thermal emission is well described by a theoretical blackbody spectrum and it is shown in Figure 1.2

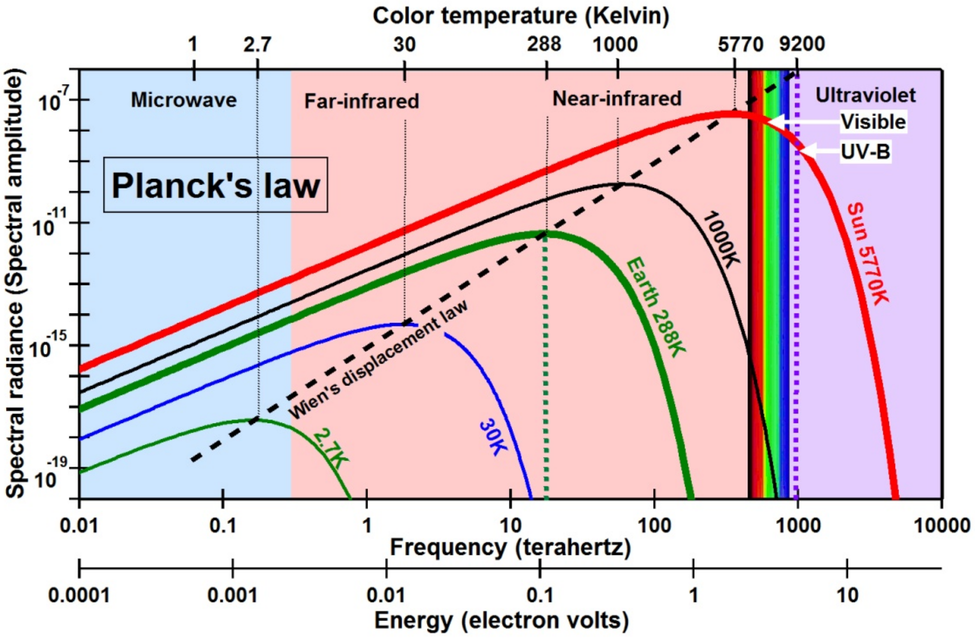

Figure 1.2 Thermal Emission spectrum
(Rogalski 2012)

Cold objects (10 to 100K) such as dust and gas clouds emission which are at THz range in galaxies are weak. Cosmic microwave background radiation emits in the low-frequency THz band.

THz detection is divided into two section; coherent and incoherent. If amplitude and phase of the input field are measured, the detection mechanism is called coherent and if only input fields intensity is measured then it is identified incoherent or direct detection. Although there are several detectors for sensing THz radiation, bolometers are often used. Bolometer principles will be summarized in the following section.

1.2 Principles of Bolometers

Continuous terahertz radiation is detected by thermal devices through the increase in temperature. Detector shows property that changes with temperature. For instance resistivity changes in bolometers, electrical polarization in pyroelectric detectors, gas pressure in Golay cell.

Bolometers are thermal detectors which exhibit the change in resistance of a material with temperature. This material usually named as sensing or absorbing material and it can be metal, semiconductor or superconductor. Representation of a bolometer is given in Fig. 1.3.

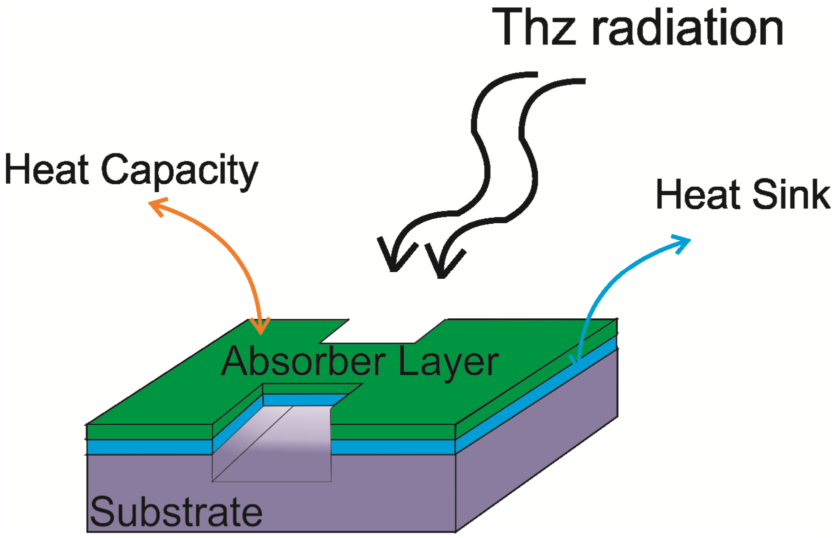

Figure 1.3 Representation of bolometer

Radiation increases temperature of the absorbing layer which is usually a bridge for air bridge bolometer and attached to substrate via thermal heat sink. Temperature change in absorbing layer induces a large change in resistance of the bolometer and this chance can be sensed with an external circuit. Temperature coefficient of resistance is described by Eq. 1.1 and it is a measure of how quickly resistance of the absorbing layer responds to change in temperature.

$$\mathrm{TCR}=\alpha=\frac{1}{R}\frac{dR}{dT} \tag{1.1}$$

where R is the resistance at room temperature and α is the room temperature TCR. It is a crucial parameter which determines responsivity of the bolometer. Sensing material of an ideal bolometer must have high TCR and low resistivity value. This feature can be achieved by fine-tuning between material choice and growth conditions and it will be discussed in following sections of this thesis. For a good sensitivity, absorber layer must have a low heat capacity and good absorptivity. Supporting substrate also must have low heat capacity and high thermal conductivity. Time constant or response time of the bolometer is given by Eq. 1.2 and it is related to thermal conductance and heat capacity values.

$$\tau = \frac{C}{G} \tag{1.2}$$

where C is the heat capacity of the absorbing layer and G is the thermal conductance of the bolometer. Another prominent parameter for bolometer is noise equivalent power (NEP) and it is calculated by Eq. 1.3.

$$NEP = \sqrt{(4k_B \gamma T^2 G)} \tag{1.3}$$

where k_B is the Boltzmann constant and T is the temperature. For instance, the most sensitive superconducting bolometer may reach 10^{-19} W/Hz$^{1/2}$ NEP values but they need to be cooled down to 50 mK to reach that ultra-low noise levels (Morozov et al. 2011). In contrast to cooled ones, uncooled bolometers have 10^{-12} W/Hz$^{1/2}$ NEP values. Lower NEP values also indicate sensitivity of the bolometer. Detectivity is another performance parameter of the bolometers and it is calculated by Eq. 1.4

$$D = \frac{\sqrt{A}}{NEP} \tag{1.4}$$

where A is the area of the absorbing layer. There is a trade-offs between these parameters. Thermal conductance G can be increased and it will enhance response time of a bolometer but it will also increase NEP value. In this case, sensitivity of the bolometer will decrease. Alternatively, heat capacity of the absorbing layer can be reduced by reducing the area of the absorbing layer.

Total noise of the bolometer is determined by Eq. 1.5.

$$\sqrt{V_n^2} = \sqrt{V_J^2} + \sqrt{V_{1/f}^2} + \sqrt{V_T^2} + \sqrt{V_B^2} \tag{1.5}$$

where V_J is the Johnson noise, V_B is the background noise, V_T is the thermal noise and $V_{1/f}$ is the excess electrical noise. $V_{1/f}$ is related to frequency and keeping modulation frequency in high levels can prevent this noise. For uncooled bolometers, Johnson noise is the dominant noise and it will be defined and discussed in chapter 2. Finally, voltage responsivity of the bolometer is described by Eq. 1.6.

$$R_V = \frac{I_b R \alpha \eta}{G\sqrt{(1+\tau^2\omega^2)}} \tag{1.6}$$

where I_b is the applied current, R is the resistance of the bolometer, η is the absorptivity and ω is the radial modulation frequency of the signal. It is clearly seen that improving TCR value will enhance responsivity of the detector.

In the following chapter, the literature review for the vanadium oxide thin films will be summarized and motivation of this study will be presented.

1.3 Literature Review: Vanadium Oxide as a Sensing Material

Oxide phases of vanadium have been used in many research and various applications due to their unique properties (Morin 1959; Ko and Ramanathan 2009; Podraza et al. 2012). Most of the vanadium oxide (VO_x) phases have semiconductor-metal transition (SMT) induced by heat and light. Although there are many other phases that are well known like V_2O_3, V_3O_5, and VO_2, V_6O_{11}, there are also less known phases like V_5O_9 and V_8O_{15} that have a semiconducting metal transition (SMT) at individual temperatures. Their SMTs and related temperatures are shown in Fig. 1.4.

They can be categorized and formalized into two groups which are V_nO_{2n+1} and V_nO_{2n-1} also known as Magneli phases (Magneli 1948). Crystal phases of several vanadium oxides and one of molybdenum doped vanadium oxide phase are given Fig. 1.5

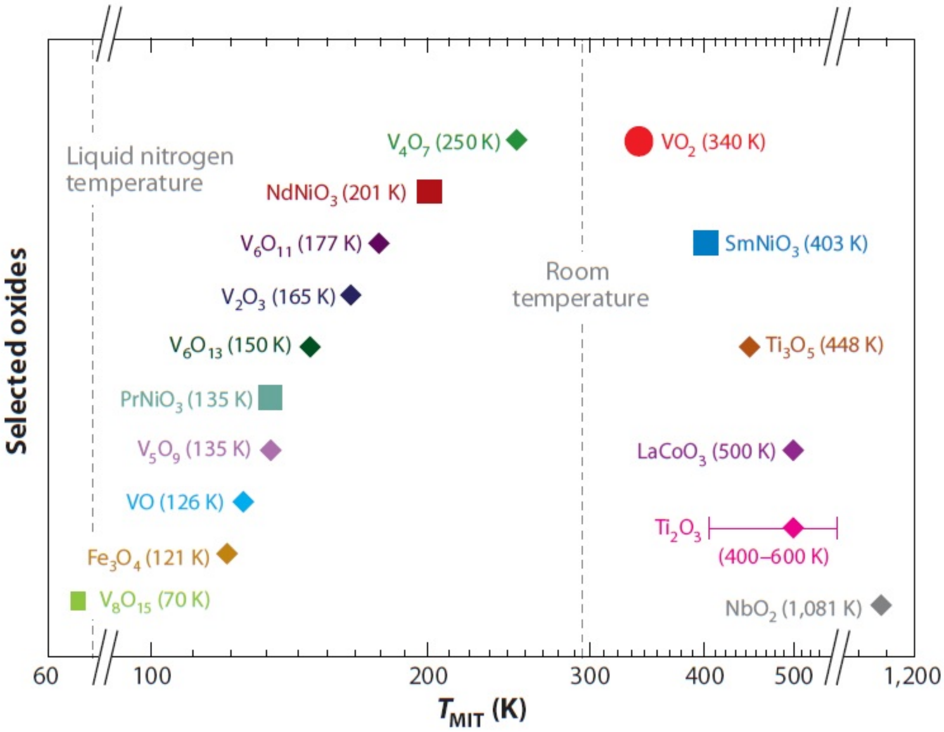

Figure 1.4 SMT of the selected oxide structures of vanadium and other metal oxides (Yang et al. 2011)

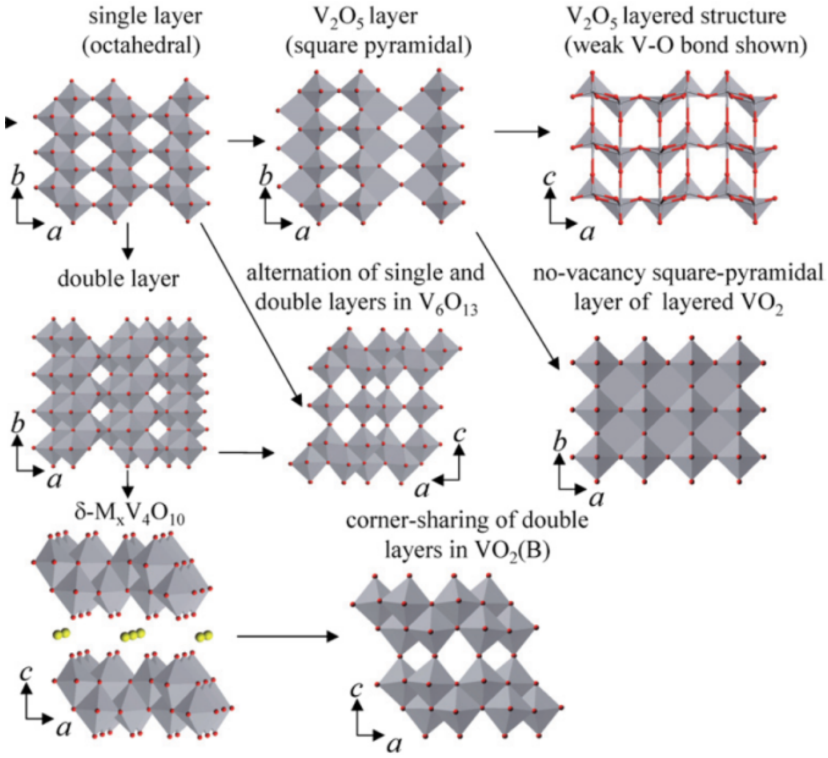

Figure 1.5 Several Crystal Phases of Vanadium Oxide Structures
(Rampelberg et al. 2015)

However, VO_x properties can be implemented in many applications in the field of civil as well as military life such as industrial process control and surveillance. Although researchers used VO_x in memory materials (Radu et al. 2011), photovoltaics (Hancox et al. 2011), optical switching (Choi et al. 2011), hybrid metamaterials (Liu et al. 2016), micro batteries (Root 2011), VO_x thin films have been favorable material for bolometer since barium strontium titanate has limitations. It has developed at Honeywell and patented (Wood 1995) in the mid-90s and it is one of the most used sensing material for infrared bolometers along with amorphous silicon (Syllaios et al. 2000; Ajmera et al. 2010). There are plenty of other materials which are used as thermal sensitive elements such as metal films (Moreno et al. 2007; Shie et al. 1996), YBaCuO (Jagtap et al. 2012), $Bi_2Sr_2CaCu_2O_{1+\delta}$ (Semerci et al. 2016) and Si-Ge alloys (Cheng and Almasri 2009). VO_x thin films have at least five times better TCR values than most metal films, lower impedance than amorphous silicon at same TCR value, low 1/f noise and are compatible with CMOS technology. One of the most prominent vanadium oxides is VO_2 which has a structural change at 68°C along with four orders of magnitude resistivity change. Although VO_2 has four orders of magnitude resistance change around SMT temperature and this property could be useful for thermal detectors, its hysteresis and high resistance properties restrain its detection capability. For instance, resistivity of VO_2 films is 10^4 Ωcm at room temperature and it is way beyond acceptable levels for uncooled bolometers (Gurvitch et al. 2010). Although it is shown that phase transition temperature can be changed with doping (Jiazhen et al. 2008), transition mechanism is not fully understood. Transition behavior has been known for decades and there are two main theories that discuss whether the change in crystal structure prompts the change in electronic structure or vice versa (Adler et al. 1967; Biermann et al. 2005). Basically, these two model point out the role of lattice instabilities. While defenders of Pierls model think that force behind transition caused by electron-phonon interaction and Mott Hubbard model supporters think that the force caused by electron-electron correlations. Later research confirmed that transition takes 80fs and that is half of a period of lattice vibration (Cavalleri et al. 2005). This finding supports that Mott Hubbard model is more suitable for VO_2 transition which is shown in Fig. 1.6. A striking report has been published recently by a group in Oak Ridge Laboratory (Budai et al. 2014).

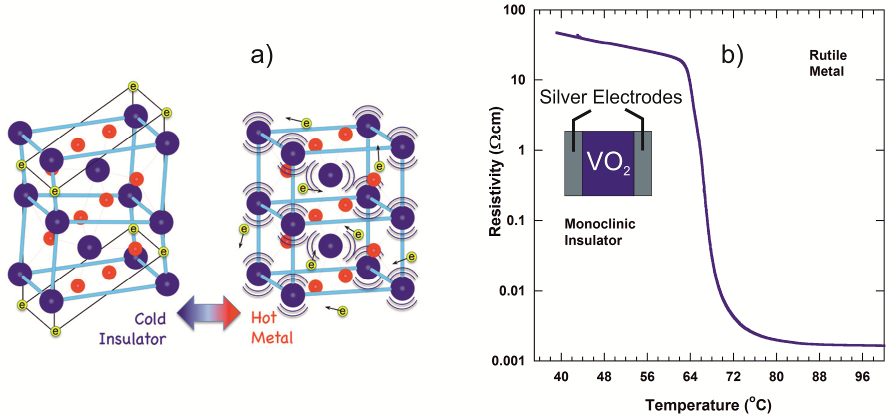

Figure 1.6 a) Change in the crystal structure of vanadium dioxide during the transition. Blue spheres represent vanadium and red spheres represent oxygen atoms (Oak Ridge Laboratory 2015)b) Transition behavior of VO_2 (Yüce 2015).

Studies are performed to expand application areas of VO_2 even though transition mechanism is not fully explained. For instance, Soltani claimed that transition temperature of VO_2 can be shifted to lower temperatures such as 45˚C by tungsten co-doping. This effect can be seen in Fig. 1.7.

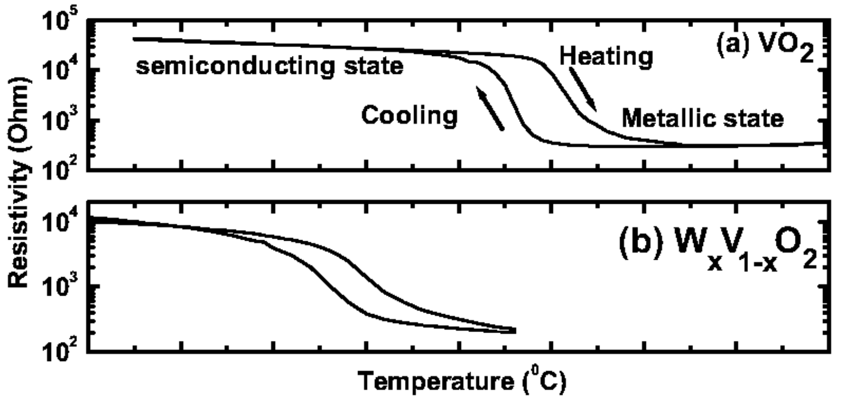

Figure 1.7 Effect of tungsten co-doping on transition temperature of vanadium oxide films

(Soltani et al. 2004)

Even transition temperature decreases to room temperature, hysteresis behavior of the transition between heating and cooling is still an obstacle to achieve a good sensitive material from VO$_2$ for bolometers. To clarify this problem, think about a hypothetical situation which a bolometer placed at a working point T$_0$, R$_0$. T$_0$ represents the working temperature of VO$_2$ bolometer and R$_0$ is a resistance value at this point. When infrared radiation reaches sensitive area of a bolometer, film temperature will be increased and resistance will change enormously. When the radiation removes, bolometer tries to back to its original temperature and resistance values but because of hysteresis behavior, resistance will not be back to its origin. In short, the path of the heating and cooling differ from each other shown in Fig. 1.8.

Detailed explanation was provided by Gurvitch and his colleagues. They stated that hysteresis is not the only problem for producing a bolometer from VO$_2$ material. Keeping bolometer at a constant operating temperature (for VO$_2$ around transition temperature) also causes problems for readout circuits.

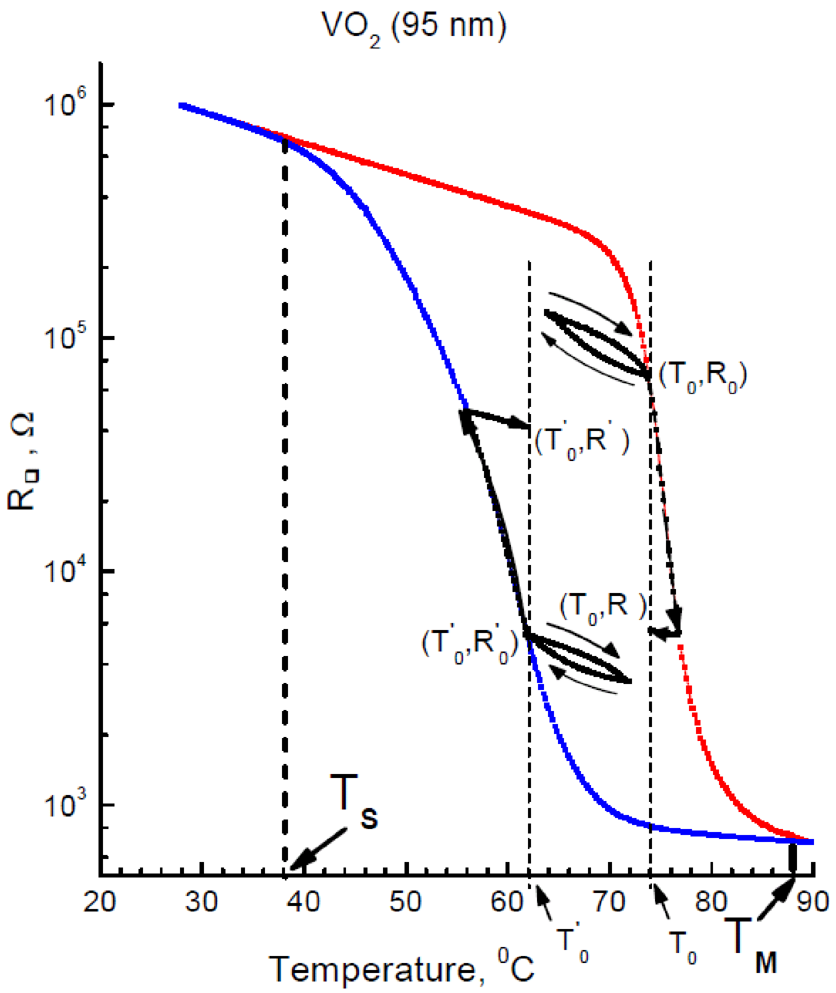

Figure 1.8 How hysteresis behavior causes problems in bolometers (Gurvitch et al. 2010)

Honeywell is well known for their infrared detector researches and they developed a new solution for proper usage of vanadium oxide in bolometers. They also realize that transition causes many problems for bolometer structures. Instead of using VO_2 films they used multi oxide films which contains V_2O_3, V_2O_5 and VO_2 oxide phases of vanadium. The study was a classified US project to develop IR imaging system. There were two important outputs of this study, one of them was creating stable, high TCR bolometer material from vanadium oxide and another one was creating a new design for this type of bolometers (Wood 1993). Relation between electrical resistivity and temperature is shown in Fig. 1.9.

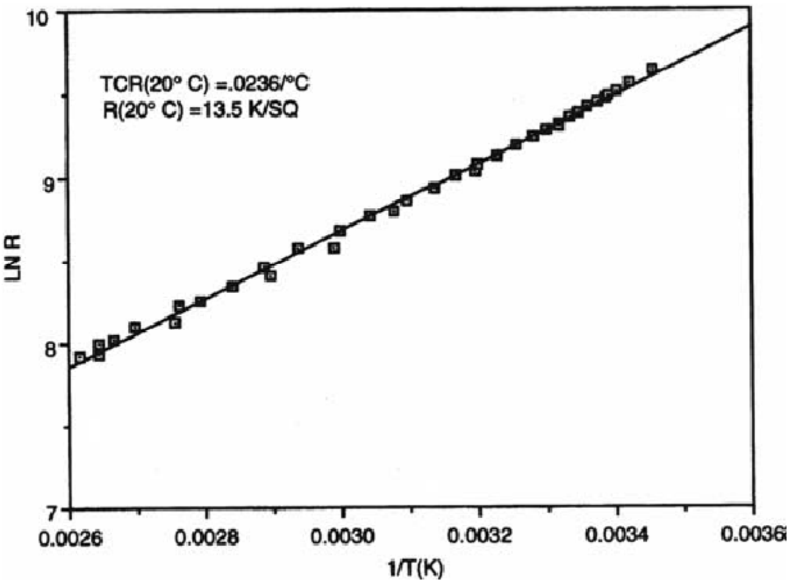

Figure 1.9 Electrical resistivity versus temperature of mixed vanadium oxide film (Wood 1993)

After this success, mixed vanadium oxide dominates commercial bolometer systems and researchers also realize that in contrast to VO_2 thin films, VO_x film has stable TCR over a wide range temperature. Although vanadium oxide films have high resistance, recent studies claimed that resistance values can be reduced with doping metal such as gold (Smith et al. 2014). Moreover, VO_x has low 1/f noise and suitable thermal time constant with low manufacturing cost (Rogalski 2009). Due to these advantages VO_x thin films have been used as bolometer material at IR and they have been obtained by several different techniques that include reactive sputtering (Kusano et al. 1998), evaporation (Case 1984), metal organic decomposition (Son et al. 2012), RF magnetron sputtering (Castro et al. 2013), pulsed laser deposition (Narayandas et al. 2003) and sol-gel methods (Dachuan et al. 1996). Even though many diverse methods can be employed to fabricate VO_x thin films, acquiring desired electrical and optical properties is still a challenge because many oxide phases of vanadium are not stable. Oxide phases of vanadium are highly sensitive to very small changes in sputtering conditions such as oxygen partial pressure and temperature so the composition of the film may change unintentionally. Several groups focus their research to find a suitable fabrication method for improving VO_x thin film properties at infrared region (Soltani et al. 2004; Y. H. Han et al. 2005). They tried to obtain high TCR value along with low resistance. In order to do optimization, it is crucial to understand what the essential parameters for each growing technique that alter resulting film properties. According to literature, doping and substrates also change film properties so they must be considered in the optimization process. Literature summary of VO_x thin films will be given beyond this point with some of the crucial parameters which are transition property, TCR, substrate, deposition technique and temperature will be stress for each work.

Although doping effect of metals in vanadium oxide films such as tungsten (Jin, et al. 1998), molybdenum (Hanlon, et al. 2003), titanium (Kakiuchida et al. 2007), chromium (Metcalf et al. 2007) doping was investigated by different groups, Smith was the first to use gold for TCR improvement and build an IR bolometer array on films. It is also indicated that it is possible to achieve low resistance values without sacrificing TCR values (Smith et al. 2014).

Mixed oxides of vanadium films were produced not only on silicon, it was also grown on quartz substrates and Chen et al. reported that annealed films at 500°C provide -1.86 % K^{-1} TCR and films had no transition near room temperature (Chen et al. 2000). This property can be seen in Fig. 1.10. In this study heat treatment was applied in both during and post depositing process. Substrates were heated at 300°C during deposition and films were post-annealed at 500°C in an oxidizing atmosphere after deposition.

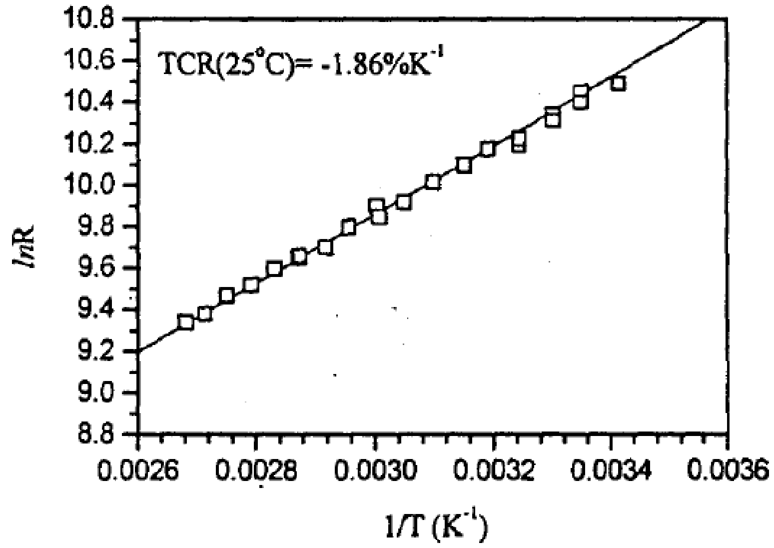

Figure 1.10 Resistance versus temperature behavior for annealed VO_x films
(Chen et al. 2000)

Moreover, it is stated that resistivity of the films increases with annealing. It can be concluded that annealing conditions are also crucial for obtaining oxygen-rich vanadium oxide states. In other word, annealing conditions determine oxidation or deoxidation to obtain higher or lower level oxide of vanadium. Although study claims that -1.86 % K^{-1} TCR value without transition between 273 to 373 K, post-annealing conditions were not provided clearly.

The comparison was also made in the literature in terms of sensitive materials. Gonzales et al. reported that microbolometer array which is made of VO_x thin films had a better response time and signal noise ratio (SNR) than Nb-based ones (González, et al. 2003). RF sputtering was used for obtaining VO_x films and it was not reported any thermal annealing neither during sputtering nor post sputtering process. VO_x thin film TCR values were not provided and research focused on only comparison of performance values of bolometer from VO_x and Nb-based ones as shown in Fig. 1.11.

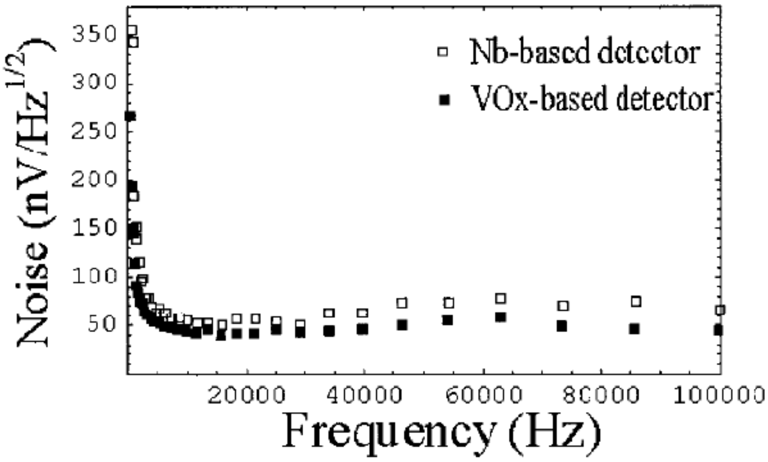

Figure 1.11 Noise frequency spectrum for Nb and VOx based detectors (González and Boreman 2003)

As indicated in the research Nb-based detector had noise voltage spectrum of 54.3 ±2.7 $nVHz^{1/2}$ while VO_x based had 44.3 ± 2 $nVHz^{1/2}$ at 12kHz.

It was also reported that VO_x films properties can be changed with heat treatment at temperature lower than 450°C for ion beam sputtered films (Wang, et al. 2006). These films were also deposited on silicon substrate and Si_3N_4 buffer layer and it was indicated in the article that only annealed films exhibited transition as shown in Figure 1.12. But information about surface morphology of deposited films or composition of oxide phases in these films except VO_2 phases was not provided. However, study presented optimum conditions of VO_x films which were produced by ion beam sputtering and have -2.3 % K^{-1} TCR without transition over 293 to 353 K.

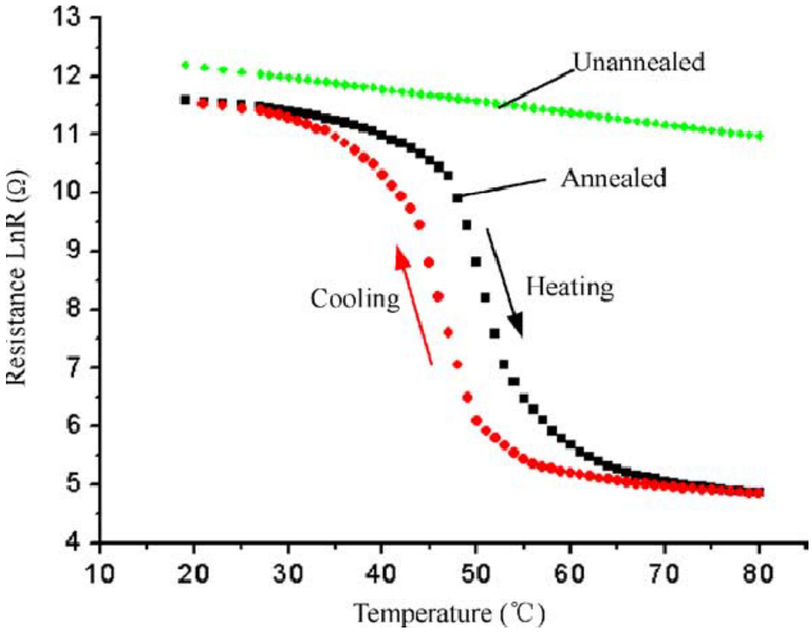

Figure 1.12 Resistance of both Unannealed and Annealed Films
(Wang et al. 2006)

There is also an innovative aspect in film preparation in the literature such as in Lv 's work. System design shown in Figure 1.13 was used to increase deposition rate and film quality.

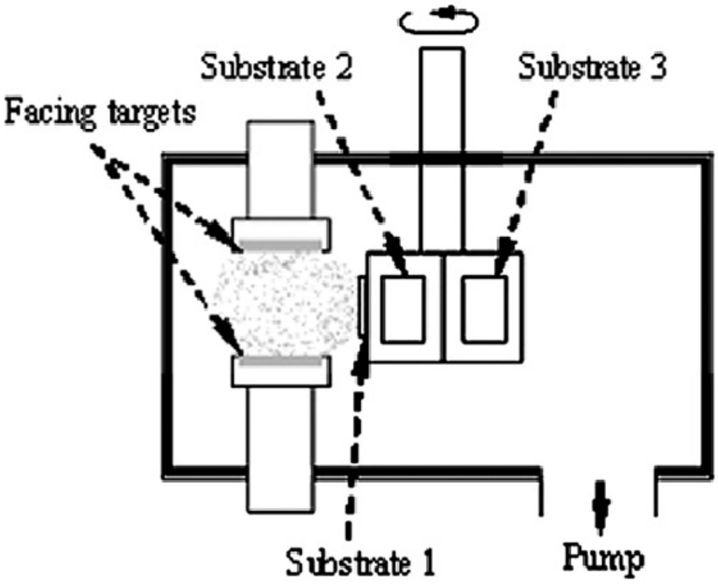

Figure 1.13 Schematic Diagram of the Facing Targets Equipment from Lv's Work
(Lv et al. 2007)

Facing targets were used to depositing VO_x thin films in this system. It is also mentioned that vacuum annealing was performed to decrease resistance. Films exhibited TCR above -4 % K^{-1}. It was claimed that surface properties were improved after annealing. But that effect was only reported when VO_x films were grown on Pyrex glass substrate (Lv et al. 2007).

VO_x thin films which are deposited by ion beam sputtering usually need additional heating during deposition or post-annealing at elevated temperatures. Temperature above 400°C is not suitable for CMOS technology. In order to overcome this problem, Dai et al. suggested production of VO_x thin films which were deposited by DC sputtering at comparatively low temperatures between 200 and 220°C. Si/Si_3N_4 was chosen as a substrate. Dai's group investigated the effect of DC power, deposition time and deposition temperature for optimum conditions which are high TCR and reasonable resistivity were given. It was also concluded that with higher sputtering power, lower resistivity values can be achieved as shown in Fig. 1.14.

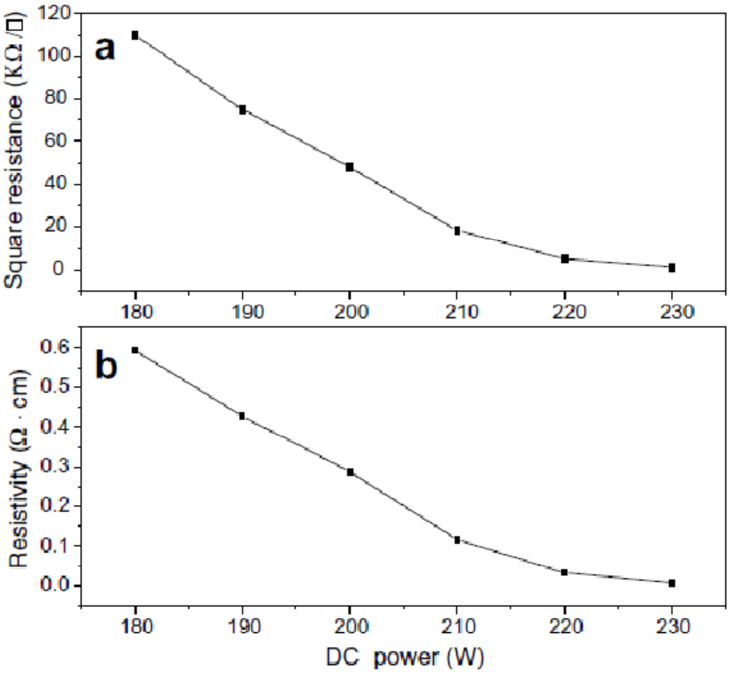

Figure 1.14 Influence of DC power on Electronic Properties of VOx Films (Dai et al. 2008)

One of the important results from their work is, lower deposition temperatures are favorable for obtaining films that have low resistivity values. Other important result extracted as a relation between DC power and VO_x film resistivity. DC Power dependence of deposited film resistivity was presented and they concluded with higher DC power during sputtering caused lower resistivity values. Films did not exhibit a transition from 20 to 80°C and film with the optimum condition had a TCR value of -2.05 % K^{-1} (Dai et al. 2008).

Although sputtering technique is common for thin film production, VO_x thin films were prepared by several other different methods, for instance, metal organic decomposition (MOD) in Son's work (Son's et al. 2012). Films were grown on fused quartz and Si/SiO_2 substrates. Films' composition when heated above 500°C was investigated as well as resistance values. It was concluded that films which were grown on quartz substrates have better TCR than Si/SiO_2. It was stated films on different substrates have different activation energies due to intrinsic and extrinsic stress (Cui and Ramanathan 2011). Films have a TCR above -4 % K^{-1} also exhibited 4 orders of magnitude resistivity change at about 52°C (Son et al. 2012).

Another popular method for obtaining VO_x film is pulsed DC sputtering on porous silicon substrates using Si_3N_4/SiO_2 buffer layers. It can be concluded that porous silicon was used due to its easy fabrication process. As mentioned before these layers provide better growing background for VO_x films and insulating as well as supporting layer for the bolometer structure. Substrates were heated at 250°C during deposition. Wang reported that deposited films did not exhibit a transition between 290 and 350 K and have -3.5 % K^{-1} TCR value. Along with all satisfying properties of the films, they have 128 kΩ/ square sheet resistance at room temperature which is not favorably for bolometer applications. However, Wang's group showed that IR bolometer from these films has a good detectivity and responsivity values (Wang et al. 2012).

Wang presented an infrared bolometer which was made of mixed oxide vanadium films. Films were deposited by ion sputtering methods and annealing was performed just after deposition. VO_x films were deposited on silicon substrates with buffer layers Si_3N_4/SiO_2. Although Wang's group defined films as mixed oxides, films have a wide transition between 310 and 330 K. They also reported their films have an average -6.5 % K^{-1} TCR between 296 and 310 K interval. It is also mentioned that films have nanostructure property which provides lower noise with high TCR value (Wang et al. 2013).

Wei et al. investigated the effect of oxygen concentration as well as sputtering voltage on TCR during reactive dc magnetron sputtering process. Si/Si_3N_4 was chosen as substrate and substrate was heated at 300°C. Research focused on effect of sputtering voltage on film properties. It is claimed that lower sputtering voltage gave higher TCR and it was also stated that oxidation on the target during deposition affected film properties greatly. It was also suggested working constant current mode (Berg and Nyberg 2005) and precleaning of the target is crucial for obtaining desired film properties (Wei et al. 2014).

Chen et al. investigated post-annealing effect on the films which were deposited by DC reactive magnetron sputtering technique. Si/Si_3N_4 was used as a substrate and both substrate heating during deposition and post-annealing were performed. Films were heated to 200°C during deposition and performed different annealing temperatures from 200 to 300°C in the N_2 environment. It is indicated that there is no significant change in the film surface after annealing, but detailed information was not given. There are similar reports from literature claimed that post-annealing decreases resistivity and the reason behind it can be related to oxygen loss (Öksüzoğlu et al. 2013) or grain growth (Li et al. 2005). It was also concluded that post-annealing decreases resistance without making a significant change in TCR can be related to the content of VO_2 nanocrystals. Achieved TCR values were between -2 and -2.39 % K^{-1}. It was also underlined that films which were performed post-annealing at 200°C did not change film composition (Chen et al. 2014).

DC magnetron sputtering has been chosen because it provides large area uniformity and high deposition rate. TCR values of VO_x thin films vary in the literature (Chen et al. 2006; Dai et al. 2008; B. Wang et al. 2013). The reason behind acquiring various TCR values is related to deposition techniques, deposition or post-annealing temperatures, and oxygen partial pressure during deposition. There are several results from the literature that provides a guidance on new works about VO_x thin films.

- There is a common agreement on suitable VO_x thin films for bolometer applications, which they must have resistivity below 10 Ωcm with a TCR near -2 % /K (Fieldhouse et al. 2009).
- Substrate choice has an impact on film properties in terms of surface roughness, adhesion, and TCR.
- Temperature both during and after deposition can be performed to increase or decrease oxygen in vanadium oxide films.
- Studies also showed that higher TCR values (Lv et al. 2007) can be achieved but reproducibility of these films are also important.
- Favorable techniques for obtaining films that have high TCR and low resistivity values are pulsed DC or substrate bias DC magnetron sputtering (Cabarcos et al. 2011; Smith et al. 2014).
- Doping with varying metals changed film properties but it must be optimized carefully. Gold doping solution has been proposed recently (Smith et al. 2014) to solve high resistance problem of VO_x films, but work mostly focused on bolometer application at IR region. We propose

a comparison between this new approach and the old one for instance post-annealing.

In this dissertation, we focused on changes in the electrical properties as well as structural properties of dc sputtered VO_x thin films just after annealing or gold doping. In addition to that VO_x films with different oxygen partial pressures were fabricated at room temperature then post-annealing was performed. Hence, oxygen partial pressure and post-annealing effect on TCR were also investigated. All the processes including post-annealing were performed under 400°C in quartz furnace nitrogen environment, therefore, it is also compatible with complementary metal oxide semiconductor (CMOS) technology. Moreover, we reported that a certain amount of co-sputtering gold during VO_x deposition decreases film resistance accompanied with the slight change of film composition and TCR, but did not change film surface.

1.4 Motivation

Vanadium oxide thin films have been used as a sensing material and they proved their compatibility at the infrared region. There are several detectors which operate at THz region but their disadvantage is an obstacle in advance. Their advantages and disadvantages are given in Table 1.2.

In addition to advantages in Table 1.2, vanadium oxide thin films have low 1/f noise, high TCR and they can be produced compatible with CMOS process. Optimized VO_x thin films will be a great candidate for uncooled bolometer that operates THz frequency. We proposed VO_x as a sensing material at THz region and investigated the best solution for obtaining high TCR along with low resistivity. In order to operate vanadium oxide uncooled bolometer at THz frequency, antenna structure must be designed.

Table 1.2 Terahertz Detectors

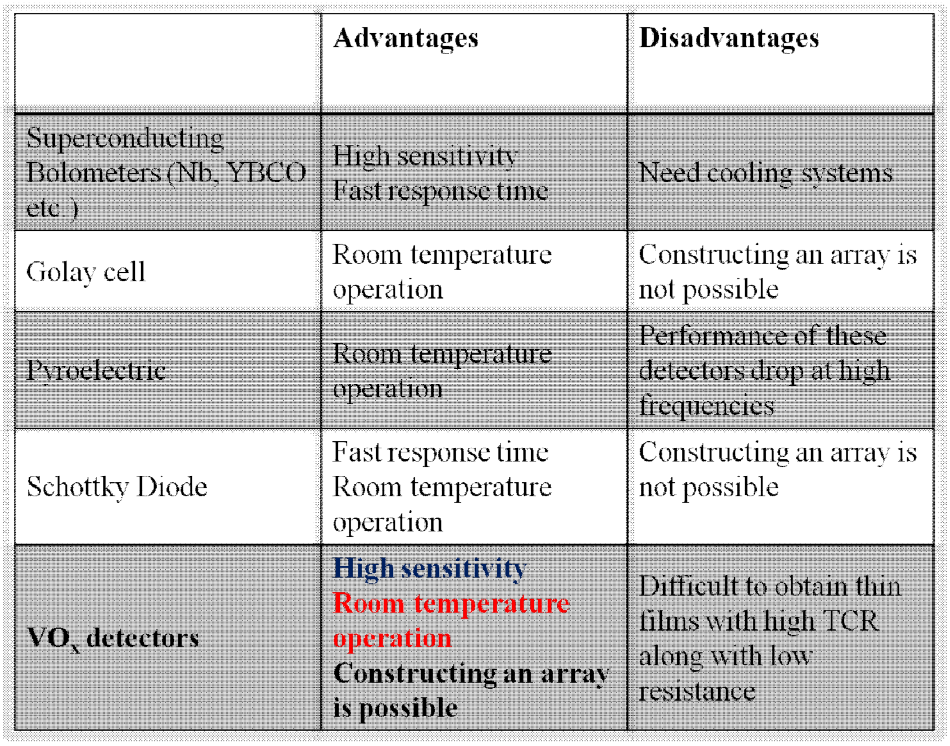

	Advantages	**Disadvantages**
Superconducting Bolometers (Nb, YBCO etc.)	High sensitivity Fast response time	Need cooling systems
Golay cell	Room temperature operation	Constructing an array is not possible
Pyroelectric	Room temperature operation	Performance of these detectors drop at high frequencies
Schottky Diode	Fast response time Room temperature operation	Constructing an array is not possible
VO_x detectors	**High sensitivity** **Room temperature operation** **Constructing an array is possible**	Difficult to obtain thin films with high TCR along with low resistance

In this dissertation, a brief summary of the applied methods was given in Chapter 2. Structural characterization, compositional analysis and electrical characterization of these films were discussed in Chapter 3. Antenna design and effect of geometrical parameters on antenna resonance frequency as well as reflection coefficient were given in Chapter 3. Conclusion and discussion of results were given in Chapter 4.

CHAPTER 2

MATERIALS AND METHODS

2.1 Substrate Selection and Silicon Oxide Layer Growth

In this dissertation, high resistivity floating zone silicon (HRFZSi) wafer was used as a substrate. There are three main reasons to choose HRFZSi as a substrate. It is one of the low loss materials in terahertz region, thermal conductance of HRFZSi (1.5 W/cmK) is higher than GaAs (0.37 W/cmK) and it is suitable for various microfabrication steps. In order to stabilize bridge structure and ensure film quality, oxide layer was grown on HRFZSi wafer. In this section silicon oxide growth mechanism and experimental details were given.

Silicon dioxide (SiO_2) layers have been used in semiconductor industry for various purposes. These can be summarized as passivation of high field areas on the semiconductors, masking, insulating film ($\rho > 10^{20} \Omega cm$) in the gate part of transistors and final circuit protection. Reproducible and stable interface between silicon and silicon dioxide makes SiO_2 prominent material for the semiconductor industry. Required quality and thickness change by related application. For instance, high-quality silicon oxide layer is needed for metal oxide semiconductor (MOS) transistors. In order to obtain silicon oxide, silicon is equally important as oxygen and it can be supplied from external source. In this case, silicon in gaseous form (usually SiH_4) supplied system hence silicon consumption from the substrate is not needed. Silicon oxide growth can be performed various ways but in general thermal oxide growth can be divided into 3 groups which are dry, wet and pyrogenic. Although a thin layer of silicon dioxide (approx. 20 Angstroms) is formed onto silicon layer at room temperature without any treatment, controlled growing of thicker silicon dioxide layers need special methods. Thermal growth of SiO_2 involves the heating of a silicon wafer in a furnace and stream of gas mixtures or steam at elevated temperature that is usually between 600 and 1250°C. High temperature helps the diffusion of oxidant through the surface to silicon interface expeditiously. This method provides two main advantages;

1)External source of silicon is not needed hence simple system is enough

2)Thickness of the substrate is diminished and it is beneficial for some applications.

Two widely used methods schematics of thermally growth of silicon dioxide are given in Fig. 2.1 and their reactions are given in equation 2.1 and 2.2.

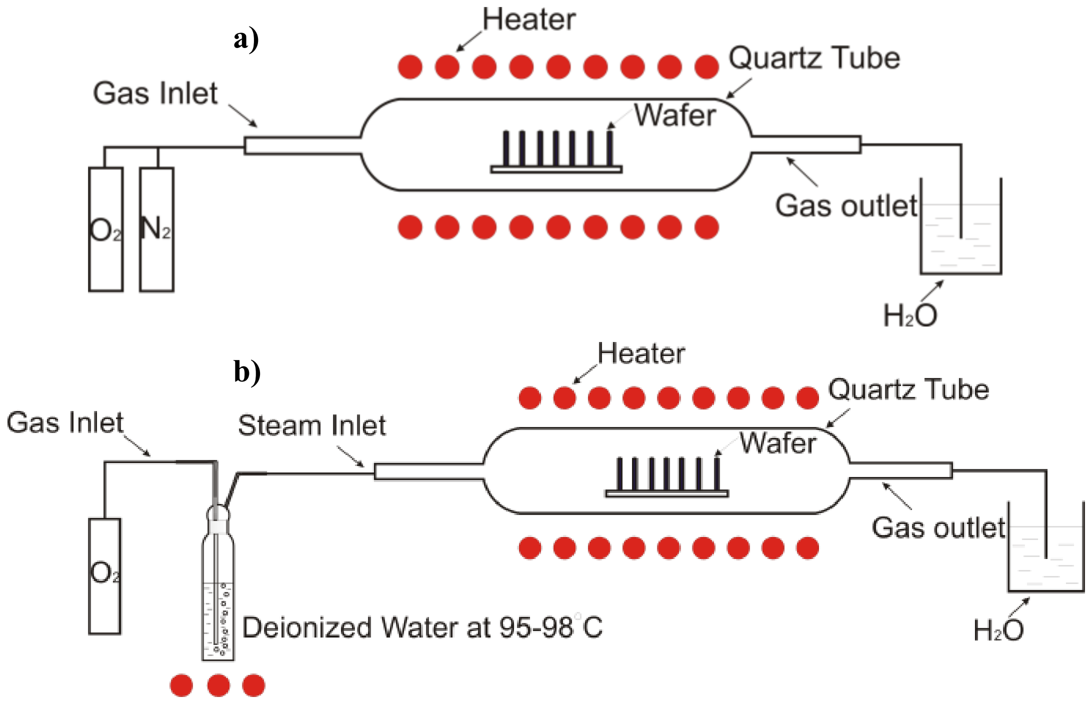

Figure 2.1 Schematic representation of a) dry oxidation b) wet oxidation

$$Si + 2H_2O \xrightarrow{\qquad} SiO_2 + H_2 \text{(wet oxidation)} \qquad (2.1)$$

$$Si + O_2 \xrightarrow{\qquad} SiO_2 \text{(dry oxidation)} \qquad (2.2)$$

Differences between these two methods emerge from supplying oxygen in different forms. In dry oxidation, oxygen is supplied as pure O_2 in gas form while silicon wafers is exposed to oxygen in steam form during wet oxidation process. While wet oxidation method yields faster oxidation rate, dry oxidation method provides better oxide layer quality in terms of better adhesion to the silicon surface. As shown in Fig. 2.2 a certain amount of silicon is consumed by both silicon oxide growth methods.

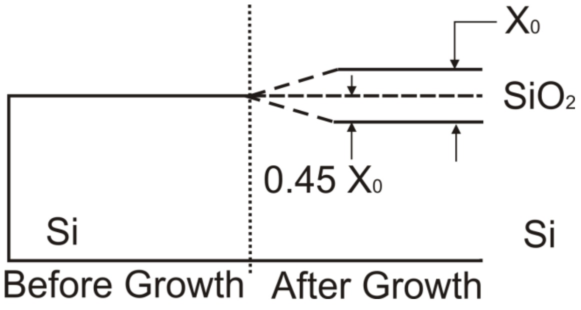

Figure 2.2 Consumed and formed silicon during oxidation process

Relationship between consumed silicon and formed oxide layer is given in Eq. 2.3

$$\frac{\text{Si thickness}}{\text{SiO}_2\text{thickness}}=\frac{\dfrac{\text{Molecular weight (Si)}}{\text{Density (Si)}}}{\dfrac{\text{Molecular weight (SiO}_2\text{)}}{\text{Density (SiO}_2\text{)}}}=\frac{\dfrac{28.9\text{g/mol}}{2.33\text{g/cm}^3}}{\dfrac{60.08\text{g/mol}}{2.21\text{g/cm}^3}}=0.46 \qquad (2.3)$$

Silicon dioxide layer can be formed by three different ways in thermal oxidation process. Oxygen molecules move through the film and react with silicon at the interface between silicon and the native oxide layer. Silicon moves through film and reacts with the oxygen at the film surface or oxygen and silicon both move into film and reaction occurs anywhere between the film and surface. In wet oxidation hydrogen gas out of the film may diffuse into silicon dioxide layer and open a path that electrons can follow. This reduces film quality especially in applications which silicon dioxide layer needed for insulating purposes.

2.1.1 Experimental details

In the scope of this dissertation thermally grown silicon dioxide was intentionally used to satisfy two objectives. SiO_2 layer acted as a supporting layer for bridge structure of bolometer and provided a suitable layer for growing mix oxide phase of vanadium. HRFZSi wafers were used as a substrate. They have high resistivity ($\rho>10^4\Omega$cm) and low losses in THz range. HRFZSi wafers transmittance properties were measured by Bruker Vertex 80v FTIR spectrometer. The beam path of the measurement system and measurement conditions were given in Fig. 2.3 and Table 2.1 respectively. In contrast to frequently used silicon substrates, HRFZSi maintains better transmittance between 0.3 and 1.5 THz region. It is also one of the low loss materials in THz region and optical transmittance of measured HRFZSi wafer was given in results section.

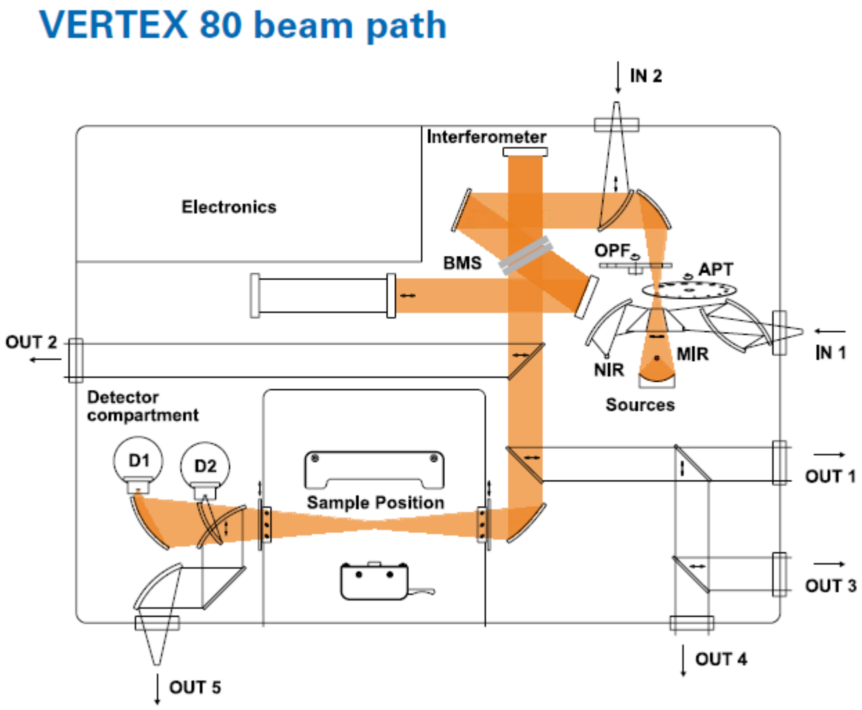

Figure 2.3 Bruker Vertex 80v FTIR Beam path
(Bruker, 2016)

Atmospheric absorption is an undeniable problem especially for THz region and in order to overcome this problem, Bruker company added vacuum compartment for sample measurement in the 80v model. Hence weak spectral features are not masked by moisture absorption, as well as resolution is not affected by CO_2 and H_2O lines.

Table 2.1 FTIR Measurement details

Measurement Type	Background	Sample
Beamsplitter	Mylar	Mylar
Detectors	DTGS	DTGS
Resolution (cm^{-1})	2	2
Scans	1200	1200
Wavenumber Range (cm^{-1})	680-30	60-10
Measurement Pressure (hPa)	<3	<3

In order to grow thermal oxide layer on top of HRFZSi, thermal oxidation setup was used. The interface between silicon and its oxide must be stable when silicon dioxide is used as a supporting layer. Thickness of 150-200 nm thermally grown SiO_2 is enough to support bridge part of the bolometer. In order to achieve high-quality silicon oxide layer, both wet and dry oxide methods were performed. Wet oxidation setup was shown in Fig. 2.4 and 8 standard cubic centimeters per minute (sccm) pure O_2 was sent by MKS gas controller and DI water was heated by a hot plate at 98°C. Wet thermal oxidation performed for one hour at 1000°C.

Figure 2.4 Experimental setup which is used in our laboratory for wet oxidation process

Dry oxidation was also performed for one hour at 1000 °C within air ambient. Acquired thickness from dry oxidation and comparison of obtained SiO_2 layer thickness with both dry and wet oxidation methods were given in results section.

There are lots of ways to measure and confirm oxide layer thickness such as SEM cross-sectional image of the film, ellipsometer, step creation for profilometer measurement and comparing color of produced silicon oxide layer with predefined color chart of silicon dioxide, spectroscopic ellipsometer. Spectroscopic ellipsometer and SEM cross-sectional image methods were used to determine SiO_2 thickness.

2.2 Magnetron Sputtering

In this subsection, production method of vanadium oxide films was explained briefly. Magnetron sputtering technique was chosen for thin film production because of two main advantages of sputtering. Sputtering provides certain advantages comparing to other techniques (i.e thermal evaporation) such as uniformity. General features of the sputtering technique are illustrated Fig. 2.5. Chamber of the sputtering system is evacuated usually to very high vacuum levels (such as 10^{-6} to 10^{-9} Torr) before sputtering to ensure get rid of contaminants. After desired vacuum level is achieved a chemically inert gas such as argon is bled through the control valve and fed the chamber until sputtering pressures were obtained. Sputtering pressure is often between 10^{-3} to 10^{-2} Torr.

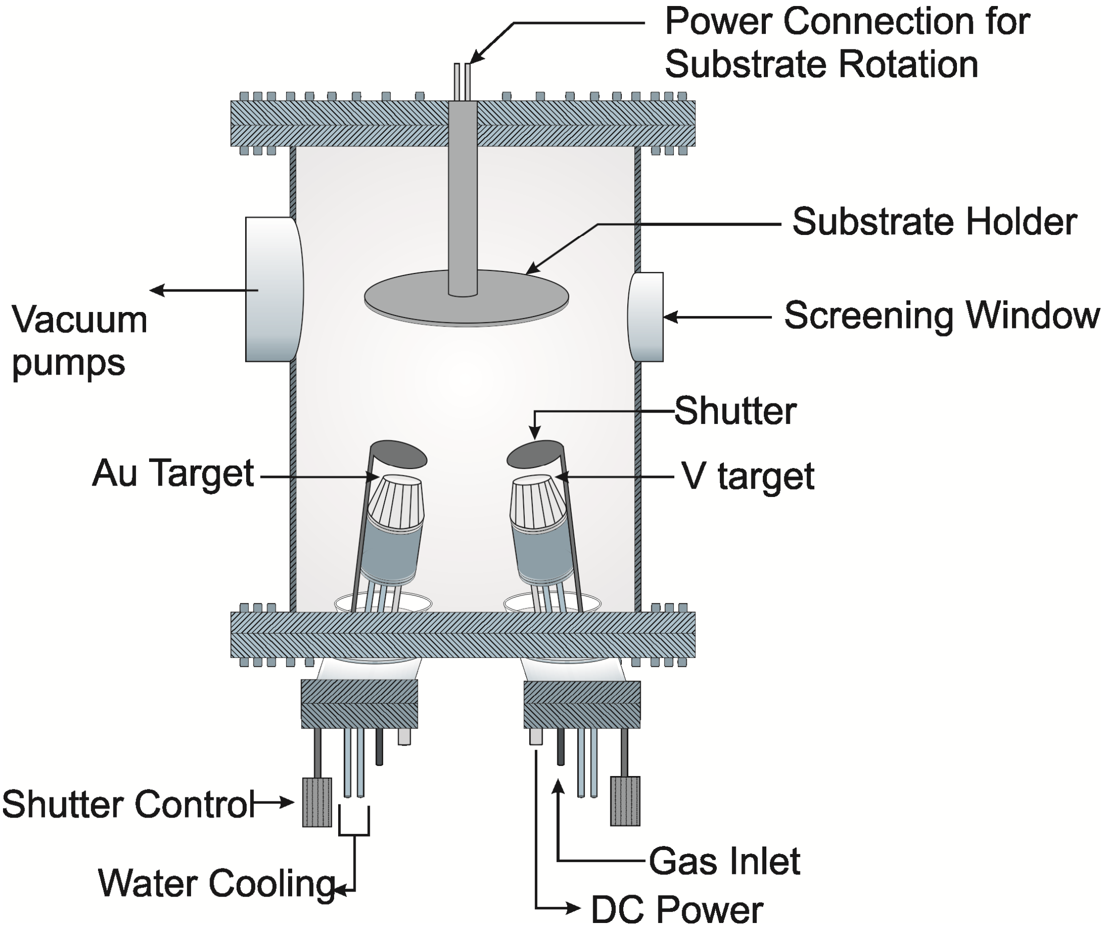

Figure 2.5 Schematically represented sputtering system used in this work

There are cathode and anode in the sputtering system, the cathode is made of a material that is desired to deposit and substrates attached to the anode. High voltage (400V) is applied between electrodes which are usually separated by 15 cm each other and inert gas is ionized then positive ion accelerates to the cathode. Electrical breakdown of the inert gas occurs when electrons accelerate and transfer an energy that is greater than inert gas ionization potential. Inelastic collisions generate a second free electron and a positive ion shown in the Eq. 2.4 and 2.5 or glow called plasma. The term plasma first presented by Langmuir in 1929 and may be determined as weakly ionized gas that exhibits a collective behavior in the presence of applied electromagnetic fields (Tonks and Langmuir 1929).

$$e^{-}+Ar \rightarrow 2e^{-}+Ar^{+} \tag{2.4}$$

$$e^{-}+Ar^{+} \rightarrow Ar+\gamma \tag{2.5}$$

A stray electron near the cathode accelerates to the anode because of electric field and it will collide inert gas along the way through anode and collision produces two different scenarios. Eq. 2.4 represents generation of secondary electron and ionization of inert, Eq. 2.5 represents excitation of inert gas. In the first case, secondary electrons create an avalanche of ions and electrons until gas breakdown. In order to acquire avalanche one secondary electron must ionize at least 10 to 20 gas molecules. After gas breakdown, a current that is usually hundred milliamps starts to flow and the voltage between electrodes drops from 1.5-2 kV to a few hundred Volts. When electrons produce sufficient ions to generate the same number of initial electrons, equilibrium is reached. Beyond this point glow region of plasma becomes a good electrical conductor and potential becomes stable. In order to understand the sputtering mechanism, the structure of the glow discharges in a DC diode system is presented in Fig. 2.6.

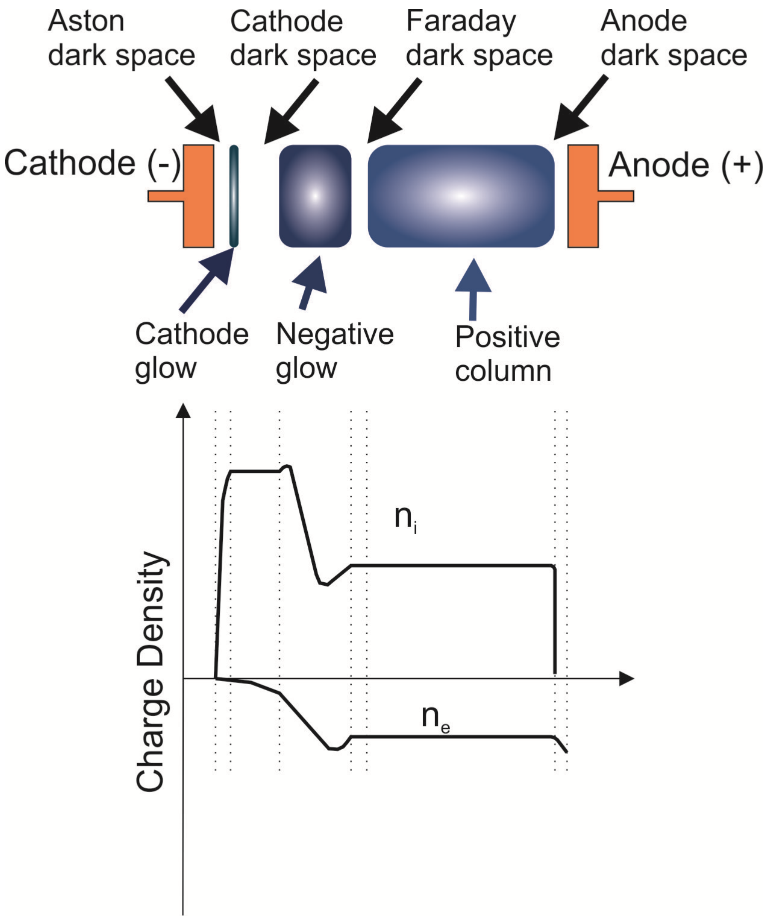

Figure 2.6 Structure of the glow discharge in a DC system

Glow discharge may be divided into several regions between anode and cathode. The most important region all among them is cathode dark space known as Crookes or Hittorf region because of the applied voltage drop across it. The target is maintained at a negative potential related to the substrate and ionized Ar entering Crookes region accelerates toward the target and bombards it. In order to sustain a plasma generation of secondary electrons are needed when cathode is struck by ions. Hence ejection of the atoms from the surface of the target by this bombardment is called sputtering. Bombardment of the target by highly energetic ions may have different results such as listed below and represented in Fig 2.7.

1. producing secondary electrons
2. ion reflection
3. ion implantation
4. structural rearrangement
5. emission of photons

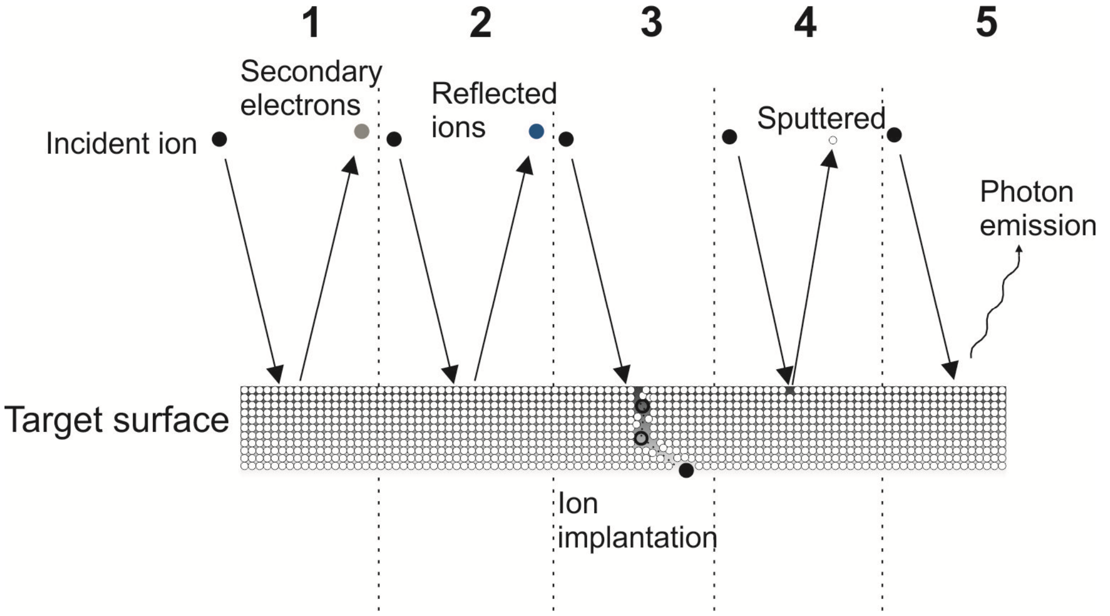

Figure 2.7 Possible results of the collision between highly energetic particles and target atoms

Momentum transfer is taken place when target atoms ejected from target surface and transport to substrate surface. Magnetron source is introduced to overcome low ionization problem in the sputtering system. Hence electrons are trapped in this magnetic field and forced to move in cycloidal curves and this magnetic field provides a longer path for ionization process as shown in Fig. 2.8.

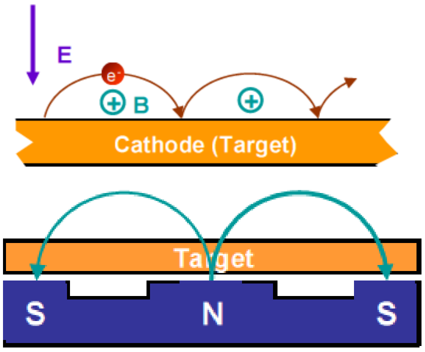

Figure 2.8 Advantage of the Magnetron Sputtering System

2.2.1 Experimental details

VO_x thin films were deposited on high resistivity floating zone silicon (HRFZSi) (100) by DC reactive sputtering at room temperature. Chamber is evacuated to a base pressure of 5 x 10^{-6} Torr just before deposition. In order to obtain contaminant free target surface, 10 minutes presputtering was performed prior to deposition. VO_x thin films were grown at Ar/O_2 mixed gas pressure environment and constant sputtering power at room temperature. Commercially available Plasmaterials high purity (99.95%) vanadium target was used. Substrate holder was connected to a DC motor and it was rotated at 15 RPM in order to improve the uniformity of the film growth. DC magnetron system which is used for this deposition is shown in Fig. 2.9.

In this thesis, film thickness was also optimized to 150 nm. Thickness values for optimized conditions were indicated in Table 2.2. Step creation method was used to measure exact thickness of the sputtered thin film. Thickness optimization was performed by Dektak surface profilometer. Before sputtering process, a small portion of AZ5214 resist dropped onto thickness calibration glass. After deposition, resist was stripped by using acetone and step feature was measured by a surface profilometer. Created step and its surface profilometer measurement result were given in results section. Relation between sputtering time and film thickness was also given in results section.

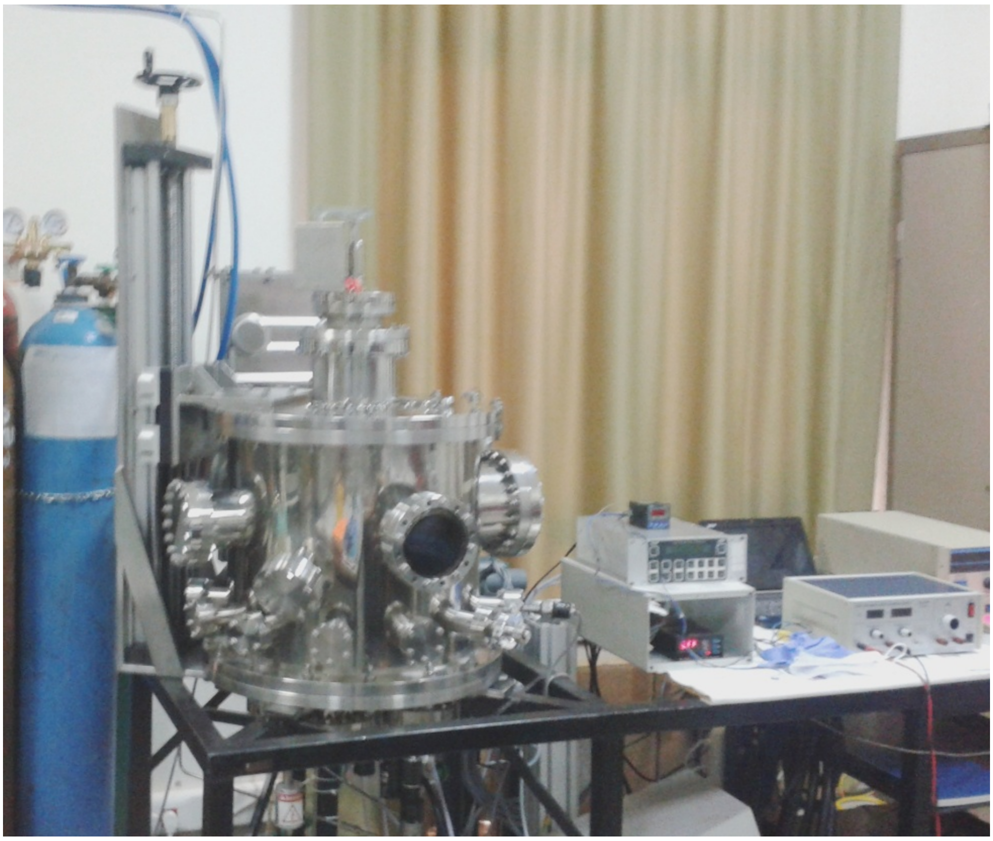

Figure 2.9 The figure shows the DC sputtering system in our laboratory which is used for thin film production

Table 2.2 Constant Sputtering Conditions for all Vanadium Oxide Films (Alaboz et al. 2017)

Deposition Conditions	Value
Substrate temperature	Room Temperature
DC Sputtering Power	50 W
Sputtering Time	30 min
Base Pressure	$5*10^{-6}$ Torr
Working Pressure	$3*10^{-3}$ Torr

In the first part of the experiment, oxygen gas ratio of the sputtered thin films was changed and electrical properties of the films were investigated. In the second part deposition conditions which provided the best TCR value were kept the same and small amount of Au was doped during deposition then electrical properties were investigated after doping.

Oxygen partial pressures during deposition were calculated with Eq. 2.6. Room temperature TCR values for each optimized films were given in result section.

$$\rho_{Oxygen}=[\text{Oxygen (sccm)}]/\ [(\text{Argon (sccm)})+\ (\text{Oxygen (sccm)})] \qquad (2.6)$$

2.3 Experimental Details of Electrical Characterization

Electrical measurements were performed and electrical properties of VO_x samples were characterized between 295 and 350 K on a microprobe station (Janis Microprobe Station) shown in Fig. 2.10. Data was acquired with Keithley multimeter and automatically recorded using Lab View program. The main reason behind the electrical measurement was to ensure that thin film resistance is suitable for bolometer applications. In order to provide a better understanding, short information about the relation between resistance and Johnson noise was given in this section.

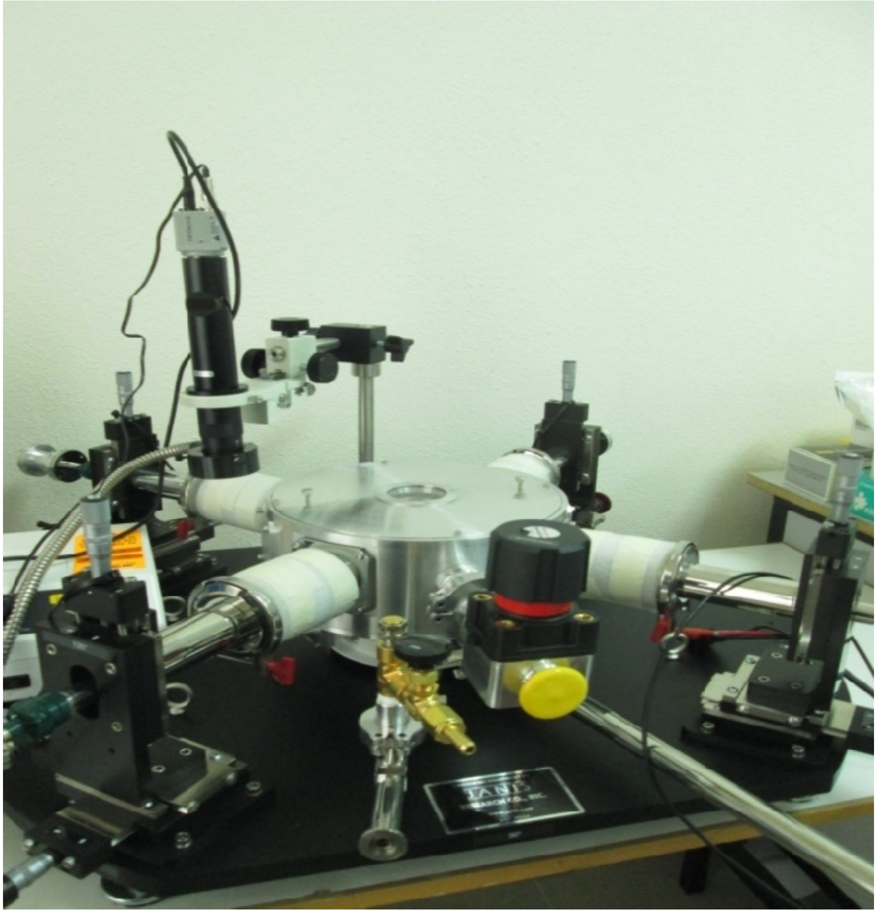

Figure 2.10 Figure shows the Janis Microprobe Station in our laboratory which is used for electrical measurements

Although obtained thin film resistivity was high for bolometer applications, it was decreased by gold doping. Because higher resistivity value causes higher Johnson noise value which is an essential noise for uncooled bolometer and is described by Eq. 2.7.

$$V_{rms} = \sqrt{4k_B TR\Delta f} \tag{2.7}$$

Where T, R, k_B, and Δf are resistor's temperature, resistance, Boltzmann constant, and bandwidth respectively. Johnson noise is generated by the random thermal motion of charge carriers. There are several methods which can be used for decreasing Johnson noise. Decreasing resistivity of the absorbing layer is one of them. To overcome high resistivity problem, doping with different metals was studied by different groups (Smith et al. 2014; Han et al. 2005). But detailed comparison for post-annealing, gold doping, and oxygen partial pressure has not been presented.

2.4 Antenna Fundamentals and Its Design in Microwave Studio

An antenna is a transmitting or receiving system that is designed to radiate or receive electromagnetic waves and it is defined by IEEE (Committee, Antennas, and Society 2014). Most of the antennas behave as reciprocal devices, in other words, they act the same on transmit as on receive. Antennas collect incoming radiation and direct them to a common feed point. In some cases, radio wave focusing on the property of an antenna is explained by analogy with optical wave focusing on the property of a lens. For clarification, related antenna performance parameters and types of the antennas were introduced before simulation of the designed system in this thesis.

There are several parameters which can be used to determine antenna performance such as radiation pattern, directivity, gain, polarization, impedance, bandwidth, scanning and system considerations. In addition to those parameters optimization of resonance frequency and calculation of S parameters are needed to be considered to determine antenna design as well as performance. Bandwidth is explained as a range of frequencies over which important performance parameters are acceptable (Stutzman and Thiele 1998). Two different bandwidth definition were made for narrowband and wideband type antennas. Bandwidth of narrowband antennas usually expresses as a percent of the center frequency and it is determined by Eq. 2.8.

$$B_P = \frac{f_U - f_L}{f_C} \times 100 \tag{2.8}$$

where f_C is the center (design) frequency, f_L is the lower and f_U is the upper frequencies of operation for which satisfactory performance is obtained. For wideband antennas, it is expressed as the ratio of the lower and upper frequencies and it is determined by Eq. 2.9. These terms are shown in the Fig. 2.11

$$B_r = \frac{f_U}{f_L} \tag{2.9}$$

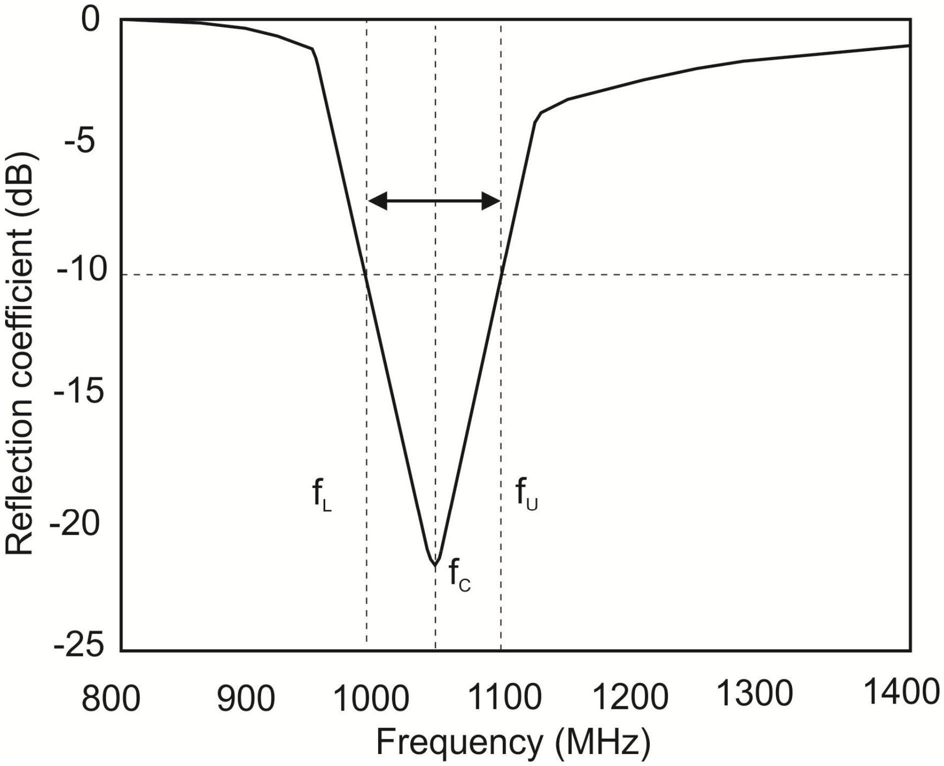

Figure 2.11 Representation of bandwidth calculation parameters at -10 dB

It is mentioned that antennas that have standing waves (as in resonance antennas) have smaller bandwidths than that have traveling waves. f_U and f_L are often represented upper and lower frequencies which satisfy the 90% power and this point is related to -10 dB in the reflection coefficient versus frequency graph. The reflection coefficient is usually plotted by using Eq. 2.10.

$$|\Gamma|_{dB} = 20\log|\Gamma| = 10\log_{10}|\Gamma|^2 \tag{2.10}$$

Before defining types of antennas as well as their advantages and disadvantages, it is useful to define frequency ranges which antennas operate. It was summarized in Table 2.3.

Antennas can be divided into four main groups by their performance as a function of frequency and those groups are electrically small, resonant, broadband and aperture antennas.

Table 2.3 Frequency Ranges and Related Applications

Frequency Band Name	**Frequency Range**	**Application**
Extremely Low Frequency (ELF)	3-30 Hz	Underwater Communication
Super Low Frequency (SLF)	30-300 Hz	AC Power (though not a transmitted wave)
Ultra Low Frequency (ULF)	300-3000 Hz	
Very Low Frequency (VLF)	3-30 kHz	Navigational Beacons
Low Frequency (LF)	30-300 kHz	AM Radio
Medium Frequency (MF)	300-3000 kHz	Aviation and AM Radio
High Frequency (HF)	3-30 MHz	Shortwave Radio
Very High Frequency (VHF)	30-300 MHz	FM Radio
Ultra High Frequency (UHF)	300-3000 MHz	Television, Mobile Phones, GPS
Super High Frequency (SHF)	3-30 GHz	Satellite Links, Wireless Communication
Extremely High Frequency (EHF)	30-300 GHz	Astronomy, Remote Sensing

Electrically small antennas are used at VHF and below, resonant antennas usually from HF to GHz frequencies, broadband antennas from VHF to GHz frequencies and aperture antennas at UHF and above. Electrically small antennas are not sensitive to construction details. Their maximum length must be 0.003λ long where λ is the operating wavelength. Short dipole and small loop are electrically small antennas. Broadband antennas preserve their properties over the wide frequency range. Spiral and log periodic antennas are in this classification. Aperture antennas have a physical aperture through which waves flow. They are often used at UHF and above because their gain increases with frequency. Horn and reflector antennas are two common antennas that are used for UHF operations. Resonant antennas are a good choice when best performance is needed for over a narrow band of frequencies. Half wave dipole, microstrip patch and Yagi antennas are the examples of these types of antennas.

Antenna performance heavily depends on design but there is a trade-off between these parameters hence it is not possible to enhance all these parameters at the same time. Classification of antennas was given as an example and properties of these antennas can be changed with the design. For instance, microstrip antennas usually have narrow bandwidth but there are techniques and approaches that can be used for achieving broadband behavior in microstrip antennas (Kumar and Ray, 2003).

Feeding techniques of antennas are also important for achieving desired performance. Antenna can be fed directly by coaxial probe or microstrip feed line. Indirect methods can be chosen including electromagnetic coupling (also named as proximity coupling), aperture coupling or coplanar waveguide feed. In the direct feeding technique, antenna and feed element have a metallic contact between them. In the scope of this thesis, indirect feed technique was used and antenna was fed by continuous THz wave radiation at far-field region.

In addition to types of antenna and feeding techniques, description of radiation regions was given for better understanding antenna properties. Three field regions of an antenna are defined which are reactive near field, radiating near field and far field. Radiating near-field region is also called Fresnel Zone and Far field is called Fraunhofer Zone. These fields are depicted in Fig. 2.12 based on Balanis' description (C. A. Balanis 1997).

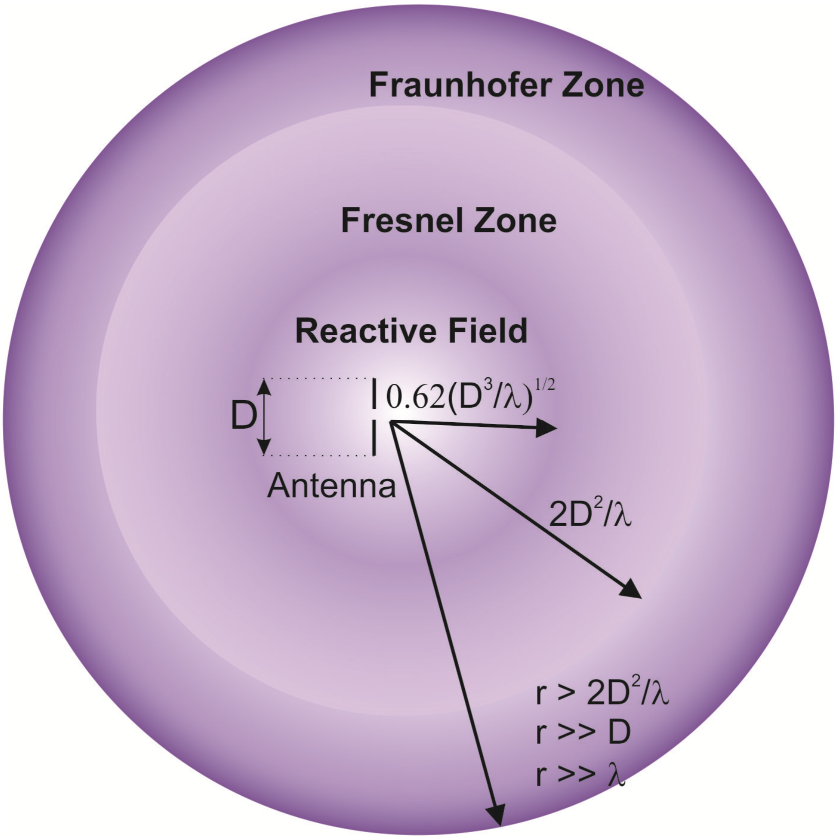

Figure 2.12 Field Regions of an Antenna

where D is the largest dimension of the antenna, λ is the wavelength and r is the radial distance.

Reactive near-field region is defined from antenna surface to radial distance r that is smaller than 0.62 $(D^3/\lambda)^{1/2}$. Radiating near-field region lies between reactive near-field region and far field region. This region can only exist when conditions in Eq. 2.11, 2.12 and 2.13 satisfied.

$$D \rangle r \tag{2.11}$$

$$r \geq 0.62\sqrt{\left(D^3 / \lambda\right)} \tag{2.12}$$

$$r \langle 2D^2 / \lambda \tag{2.13}$$

The last region is named far-field or Fraunhofer region and angular field distribution is independent from the distance from antenna. Conditions which must be satisfied for this region are given in equations 2.14, 2.15 and 2.16.

$$\mathrm{r} \rangle 2\mathrm{D}^2/\lambda \tag{2.14}$$

$$\mathrm{r} \gg \mathrm{D} \tag{2.15}$$

$$\mathrm{r} \gg \lambda \tag{2.16}$$

Amplitude pattern of antenna, both phase and magnitude changes from reactive near field to far field region.

Maxwell equations postulated by Scottish physicist James Clark Maxwell and they are shown in equations 2.17, 2.18, 2.19 and 2.20. These equations described how electric and the magnetic field generated and altered by each other and by the influence of charges or currents.

$$\oint \vec{H} = \vec{J} + \frac{\partial \vec{D}}{\partial t} \text{ (Ampere's Law)} \tag{2.17}$$

$$\oint \vec{E} = -\frac{\partial \vec{B}}{\partial t} \text{ (Faraday's Law of Induction)} \tag{2.18}$$

$$\nabla \vec{B} = 0 \tag{2.19}$$

$$\nabla \vec{D} = \rho \text{ (Gauss's Law)} \tag{2.20}$$

where $\vec{J}$ is the current density vector, $\partial \vec{D} / \partial t$ is the time derivative of the electrical displacement vector $\vec{D}$, $\partial \vec{B} / \partial t$ is the time derivative of magnetic induction vector $\vec{B}$, $\nabla \vec{D}$ is the source density and ρ is the charge density. In principle, antenna properties are extracted from analytical solutions of Maxwell equations and the properties are investigated using with CST Microwave Studio. Designer must choose antenna structure for a specific application and define radiation property of source, field condition then inputs property of all materials (such as dielectric constant) that will be used for antenna structure. Antennas are usually made of metals, for instance, gold and copper, but there are several different materials which can be used as a substrate. All these material properties must be taken into account in the simulation. In addition to that, solver technique must be chosen wisely. A guidance is provided by CST MS for choosing right solver for simulation and it is shown in Fig. 2.13.

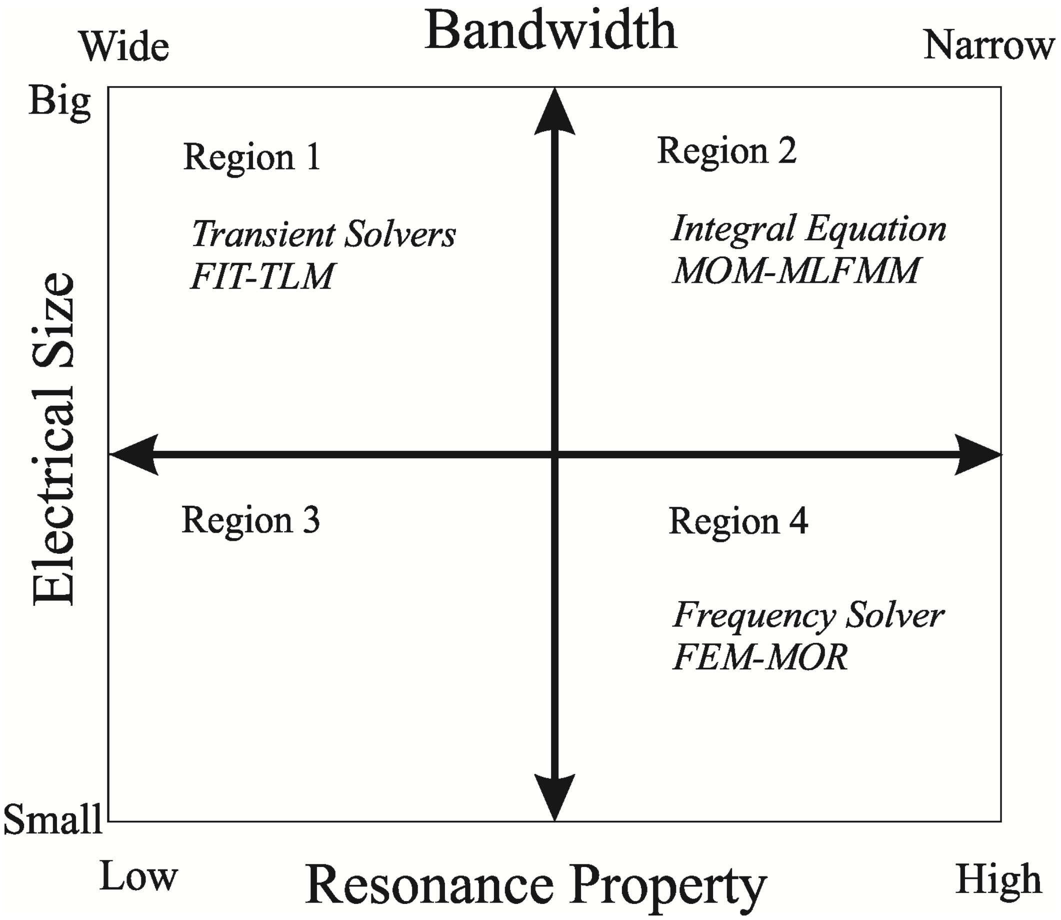

Figure 2.13 Guidance for choosing right solver for desired antenna properties adapted and reanimated from CST manual

In this dissertation log periodic antenna was also simulated and optimized for 0.6 THz frequency. Bowtie antenna is also a log periodic antenna but one of the main differences between them is periodically arranged structures in log periodic antenna. Log periodic antennas' radiation characteristics and their impedance are a logarithm of a frequency and repeat periodically. Both bow tie and log periodic antenna have been used in high-frequency region (Luukanen et al. 2006; Saijo et al. 1999; Lu et al. 2008). General structure of a log periodic antenna and its geometrical parameters are shown in Fig. 2.14. Dimension factor is an important parameter for log periodic antenna and it is defined by Eq. 2.21.

$$\tau = \frac{R_{n+1}}{R_n} < 1 \qquad (2.21)$$

The gap between periodically arranged tooth is given in Eq. 2.22.

$$\sigma = \frac{a_n}{R_n} < 1 \qquad (2.22)$$

Equation 2.22 is valid for every n values. The relation between τ and σ is given Eq. 2.23.

$$\sigma = \sqrt{\tau} \qquad (2.23)$$

This relation is used for achieving broadband self-complementary log-periodic antenna design. Antenna which was designed according to equations 2.21, 2.22 and 2.23 shows stable performance between frequencies $f_n<f<f_{n+1}$. Where f is the frequency. Parameters such as R and a are shown in Fig 2.14.

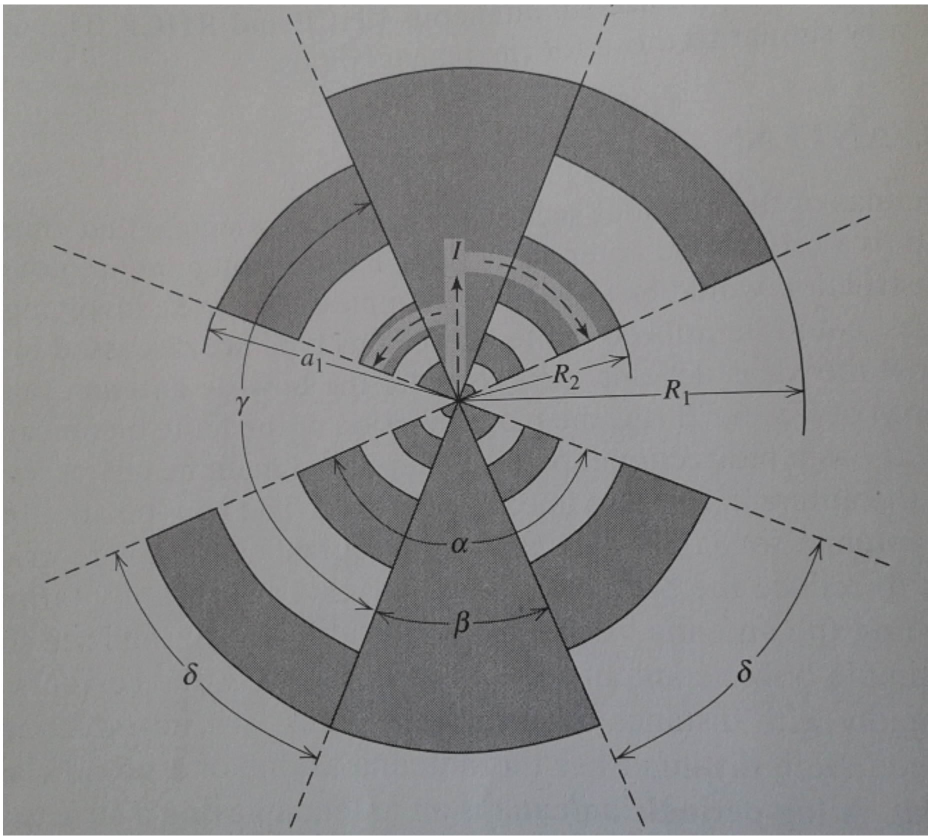

Figure 2.14 Self-complementary structure of a log periodic antenna (Stutzman and Thiele 1998)

2.4.1 Simulation Details

Two different antenna structures which are bow tie and log periodic were investigated and simulated and CST Microwave Studio is used for high-frequency simulation. Antenna structures as well as thin film layers, substrates, and the environment around bolometer were taken into consideration. Frequency solver was chosen and unit cell boundary condition was used for simulation due to designed antenna array will be highly resonant and have relatively small feature. Because continuous terahertz source is far from detector in our THz imaging system, two ports are defined and far field condition was applied as mentioned in equations 2.14, 2.15 and 2.16. Antenna fed indirectly on top of the metal radiating elements. For all designed antennas maximum dimension was 126µm. The designed resonance frequency is 0.6 THz and its related wavelength is about 500µm.

All layers (HRFZSi/SiO_2/VO_x:Au/Au) and a cavity below absorbing area are designed and added to the simulations. Top and cross-section image of the designed structure is shown in the Fig. 2.15.

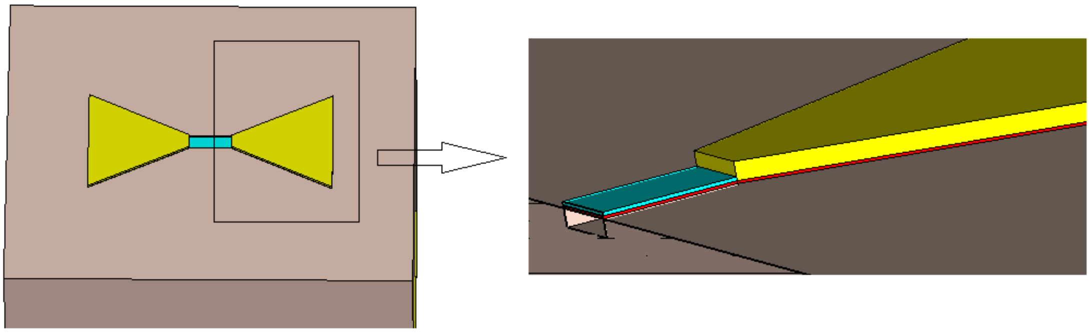

Figure 2.15 Top and cross-section view of the designed bow tie antenna structure

This method is not often used in the literature because it will increase simulation time. Usually, only metal antenna part is simulated alone or only one element of the array is simulated (Guo et al. 2008). Thin film and oxide thickness values are used as mentioned in chapter 2 and simulations focused on two goals;

1) Investigating the effect of geometrical lengths of the antenna and optimizing resonance frequency between 0.15-0.75 THz

2) Decreasing S11 value. It must be lower than -15 dB at optimized resonance frequency since lower S11 is related to lower reflectivity.

In order to achieve these goals, antenna geometries were investigated. These parameters were shown in the Fig. 2.16 and summarized in the result section.

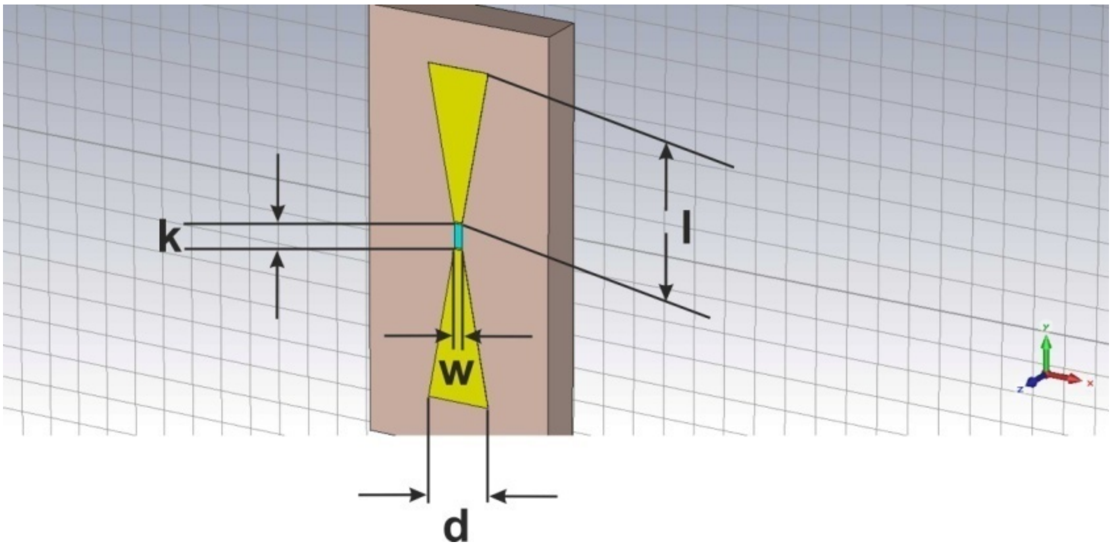

Figure 2.16 Bowtie antenna design in CST Microwave Studio

k is the absorbing area length, w is the absorbing area width, d is related to the bow tie antenna width and l is related to the bow tie antenna length. These parameters are widely investigated for IR frequencies and low THz frequencies (Rauly et al. 2008).

2.5 Lithography for Uncooled Terahertz Bolometer Array Structure

Ultraviolet lithography (UV) was proposed for designed uncooled terahertz bolometer array. A preliminary investigation was done with handmade shadow mask then professional UV Mask was designed in Autocad. Designed and produced shadow masks were given in Fig. 2.17 and 2.18.

Lithography steps were applied as follows;

1. Formation of bridge
2. Formation of contact pads and array
3. Formation of the air bridge

Lithography steps were summarized in Fig. 2.19.

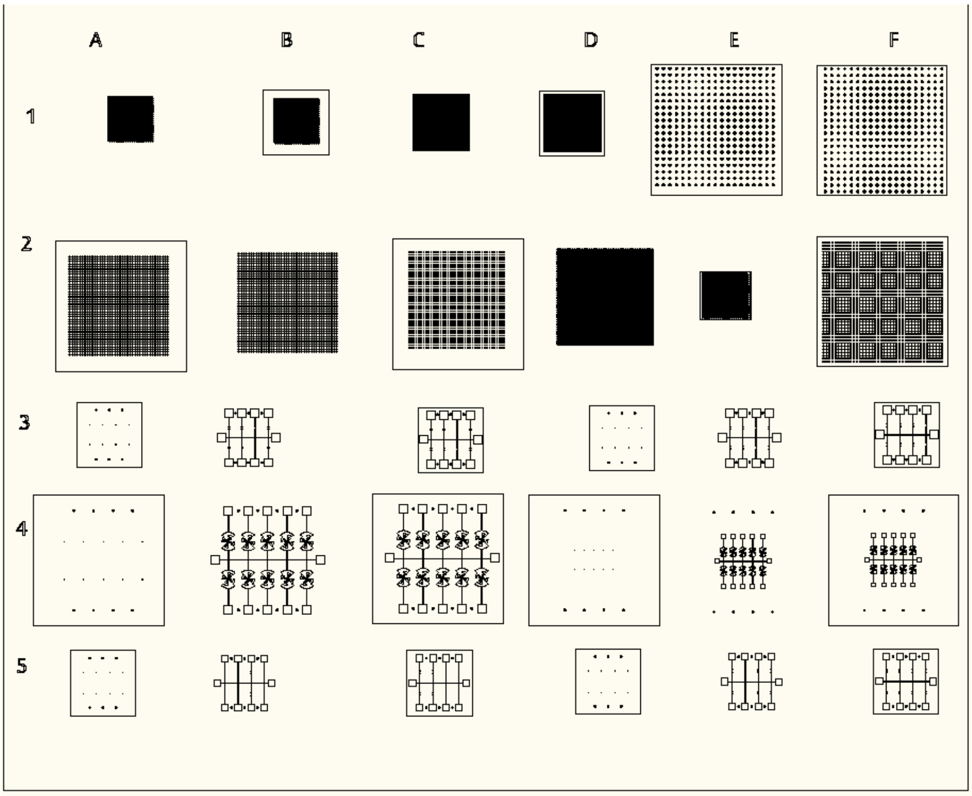

Figure 2.17 UV lithography mask design in Autocad

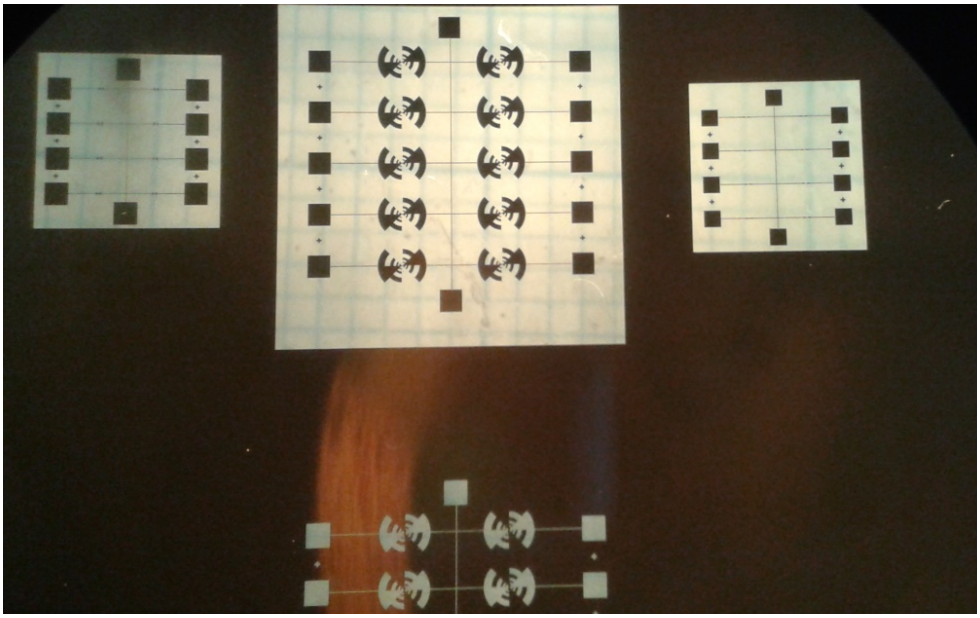

Figure 2.18 Cell of 3C, 4C, 5C and a part of 4B are shown in produced UV Lithography mask

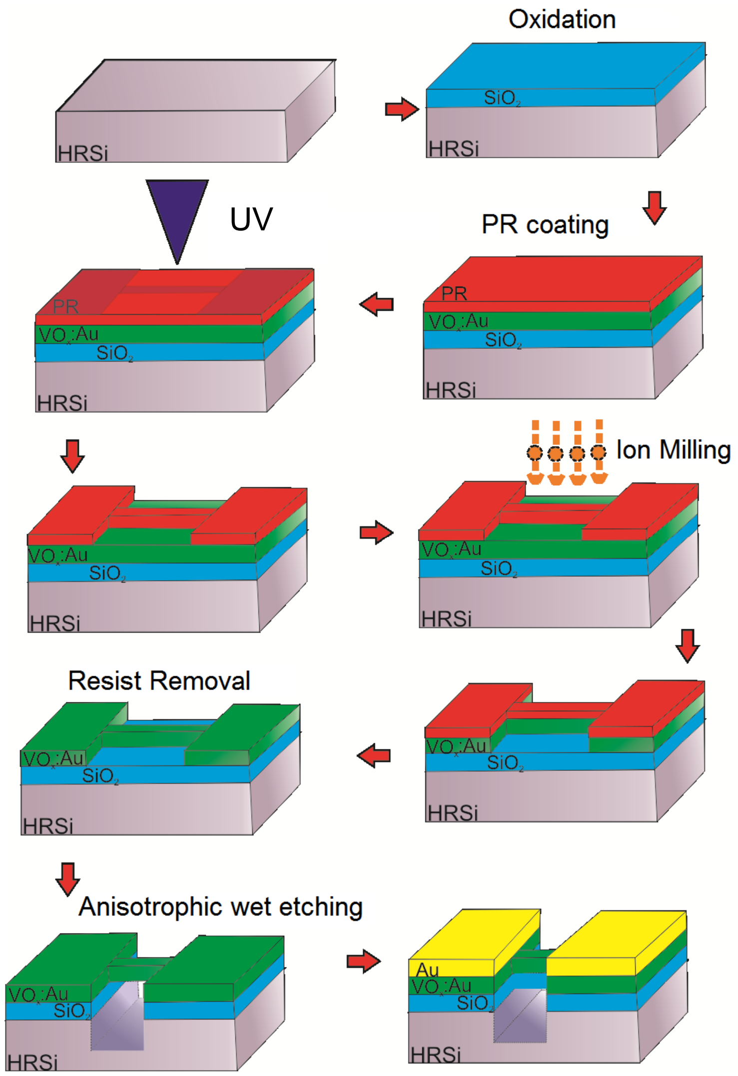

Figure 2.19 Lithography Steps

HRFZSi wafer was cut into 1X1 cm^2 and 5X5 mm^2 pieces with wafer cutter and thermally oxidized. Then AZ5214E photoresist was coated with a spin coater at 3000 RPM and 90˚C soft bake was performed in an oven. 7 seconds UV exposure was employed and bridge structure was formed. Only bridge part was protected by resist and ion milling was performed to etch unprotected areas until reaching silicon substrate. At the second stage, alignment marks and antenna array employed by using thermal evaporation. KOH solution was used to perform wet etching of silicon that was just below the bridge part of the structure. Both results from preliminary work and UV lithography were presented at results section.

CHAPTER 3

RESULTS

3.1 Optical Characterization of Substrate

High resistive floating zone silicon (HRFZSi) wafer transmittance profile between 0.3 to 1.5 THz was given in Fig. 3.1.

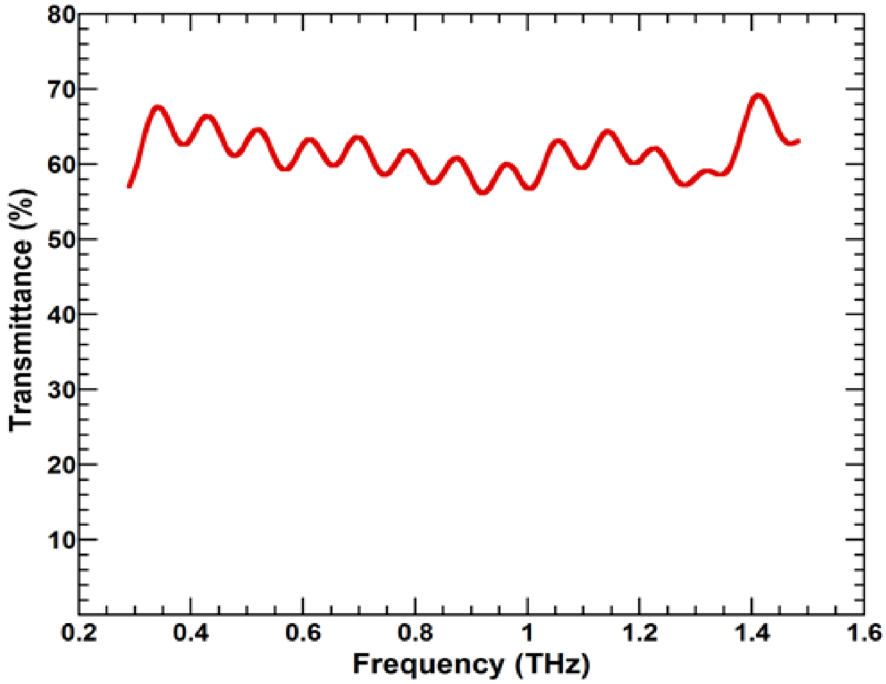

Figure 3.1 Transmittance of 0.5 mm thick HRFZSi wafer between 0.3 and 1.5 THz

HRFZSi had 60-70% transmittance from 0.3 to 1.5 THz region. There was no significant absorption around 0.6 THz. Hence it was confirmed that HRFZSi is a suitable substrate for bolometer applications at THz region.

3.2 Silicon Oxide Layer Thickness Optimization

Oxide layer thicknesses were measured by spectroscopic ellipsometer and confirmed with SEM cross-sectional images. Obtained silicon oxide layer thicknesses which were obtained dry and wet oxidation methods, were given in Table 3.1.

Table 3.1 Comparison of wet and dry oxidation growth rates at 1000˚C for one-hour duration

Wet and dry oxidation growth rates of silicon	
Temperature (˚C)	1000
Dry Oxidation (nm/h)	60
Wet Oxidation (nm/h)	410

Although there is a significant growth rate difference between wet and dry oxidation, dry oxidation is chosen to ensure oxide quality. Relation between oxidation time and obtained oxide thickness is shown in Fig. 3.2.

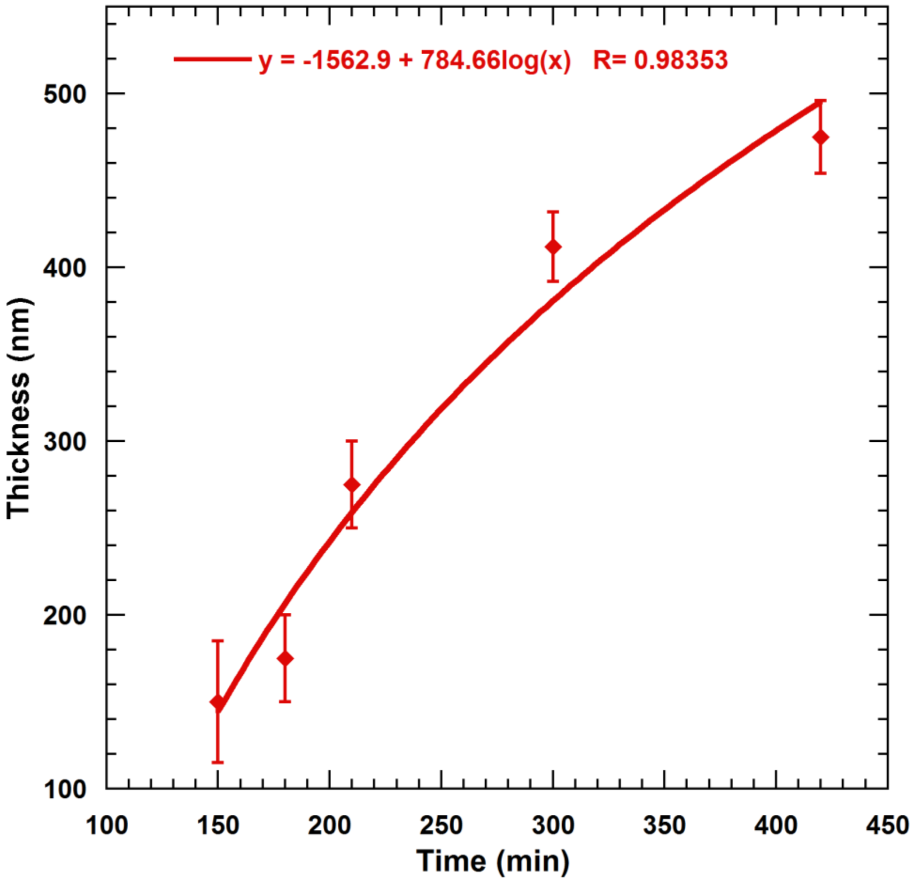

Figure 3.2 Thickness versus time behavior for dry oxidation process at 1000˚C, air ambient

3.3 VO$_x$:Au Film Thickness Optimization

Step creation method was used as described in materials and methods section. One of the steps and its profile along scanning axis were given Fig. 3.3 and 3.4

respectively. Relation between sputtering time and obtained film thickness were given in Fig.3.5.

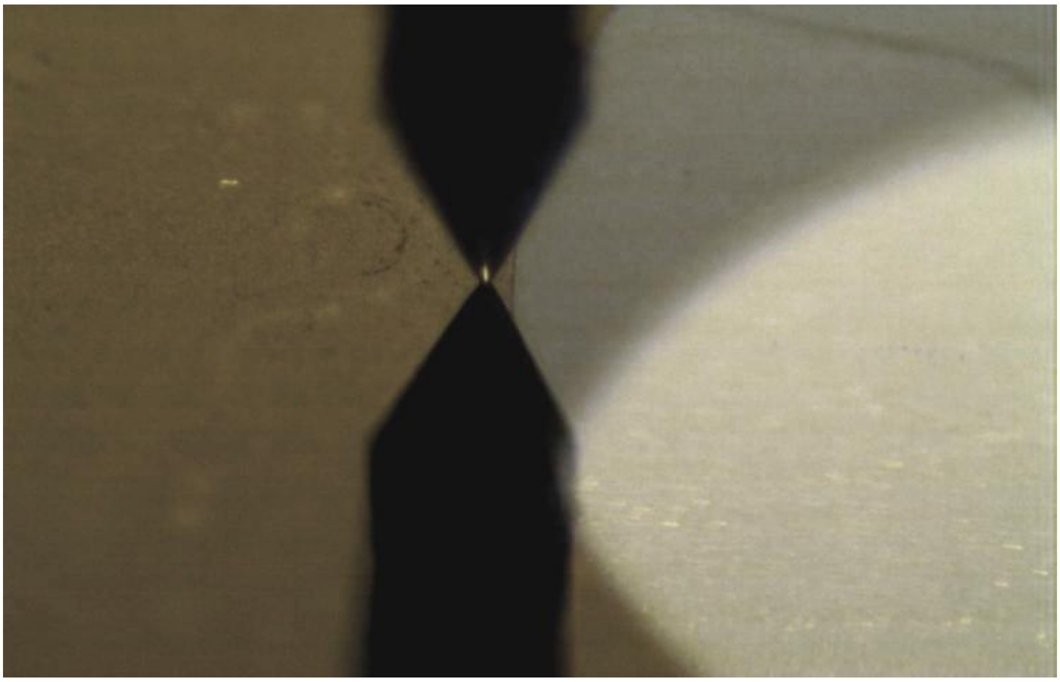

Figure 3.3 Step profile created with AZ5214 drop for thickness measurement

Distinction between film and glass surface were shown in Fig. 3.3. Depth of the created step was shown in Fig. 3.4.

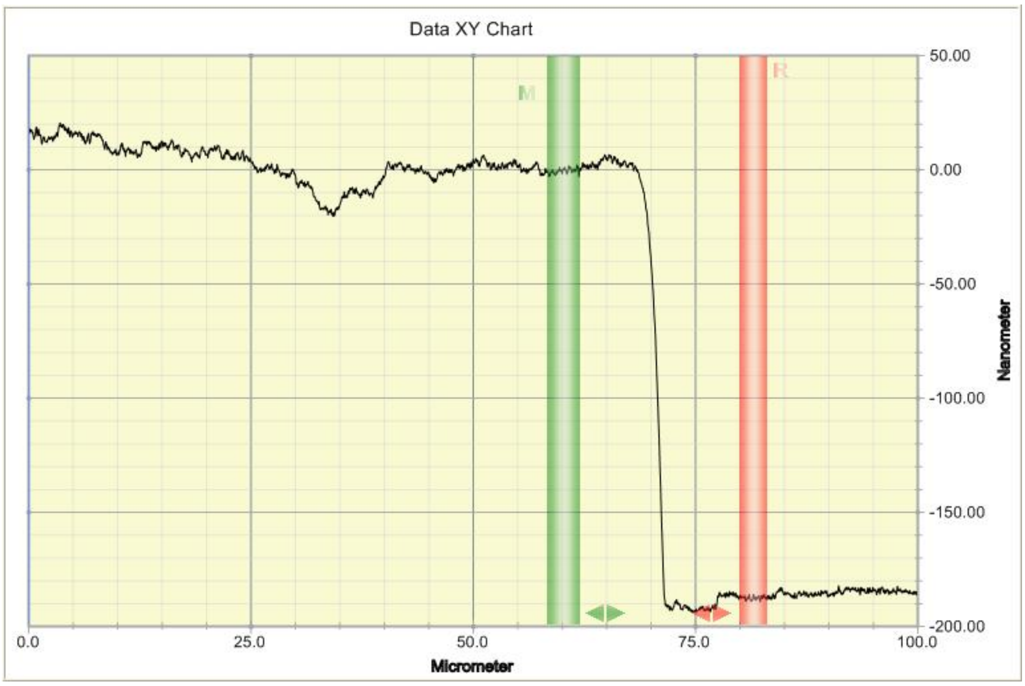

Figure 3.4 Step profile of 187 nm thick VO_x:Au film

Relation between sputtered VO_x:Au thin film and sputtering time were investigated and result was given in Fig. 3.5.

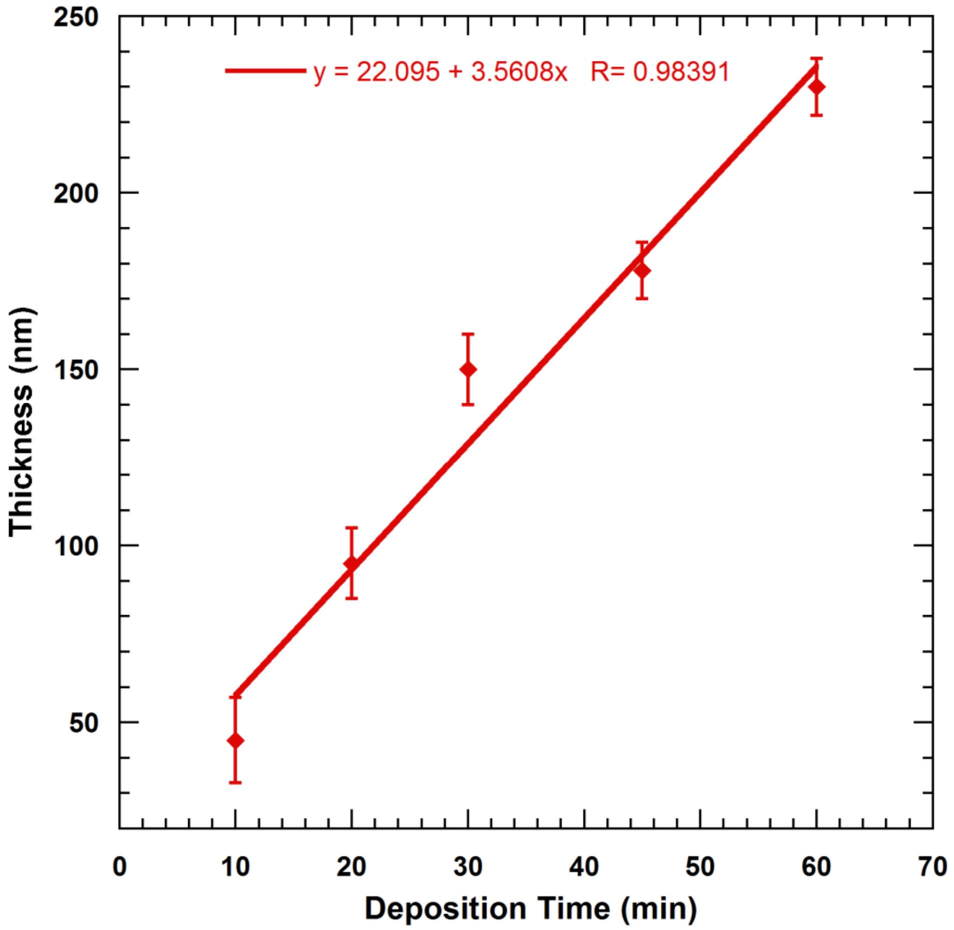

Figure 3.5 Relation between VO_x:Au thickness and deposition time

According to experimental result in Fig. 3.5, optimization was made in terms of thickness of the VO_x:Au film. Thickness of the sputtered VO_x:Au film was fixed to 150 ±10 nm.

3.4 X Ray Diffraction Analysis

X-ray diffraction spectrum was collected from 10 to 65^o and influence of annealing as well as doping effect on the film composition were investigated. The corresponding XRD patterns of as-grown VO_x, annealed VO_x, as grown VO_x:Au and annealed VO_x:Au thin films were shown in Fig. 3.6, 3.7, 3.8 and 3.9.

It was observed that both VO_x and VO_x:Au thin films exhibited multi oxide phase structures. VO_x thin films mainly consisted of V_2O_5 phase along with a small portion of VO_2 and V_6O_{13} phases before annealing process. As shown in Fig. 3.6 and 3.7 diffraction peaks with solid circles could be indexed to orthorhombic pentoxide (JCPDS card no 41-1426) and with solid stars could be indexed to vanadium dioxide (JCPDS card no 43-1051).

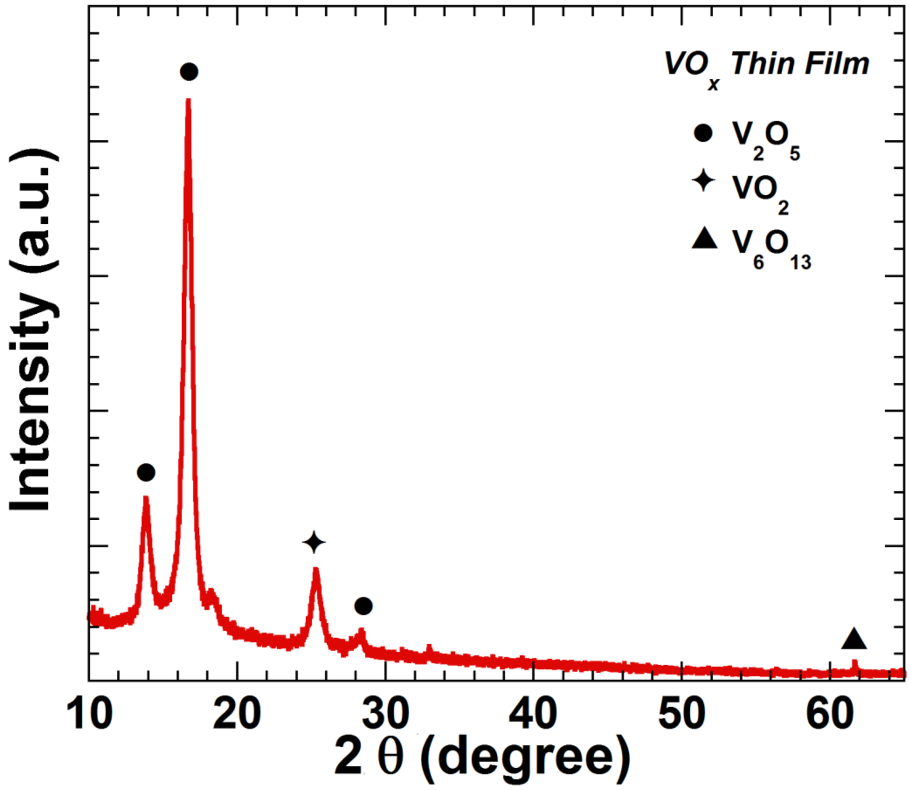

Figure 3.6 X-ray diffraction pattern of as-grown VO$_x$ thin film (Alaboz et al. 2017)

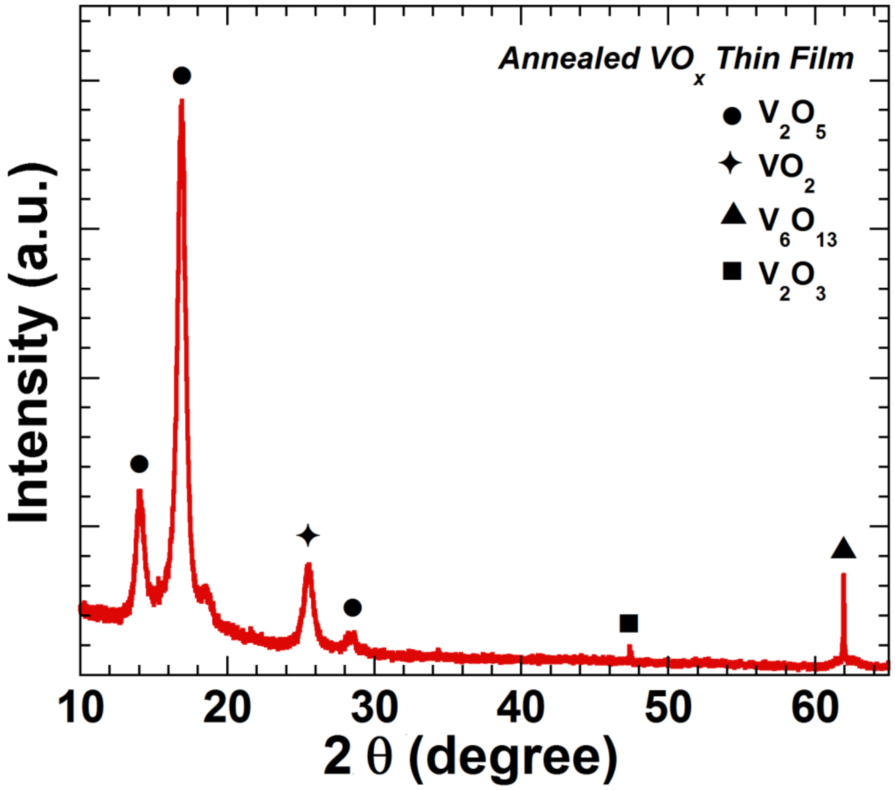

Figure 3.7 X-ray diffraction pattern of annealed VO$_x$ thin film (Alaboz et al. 2017)

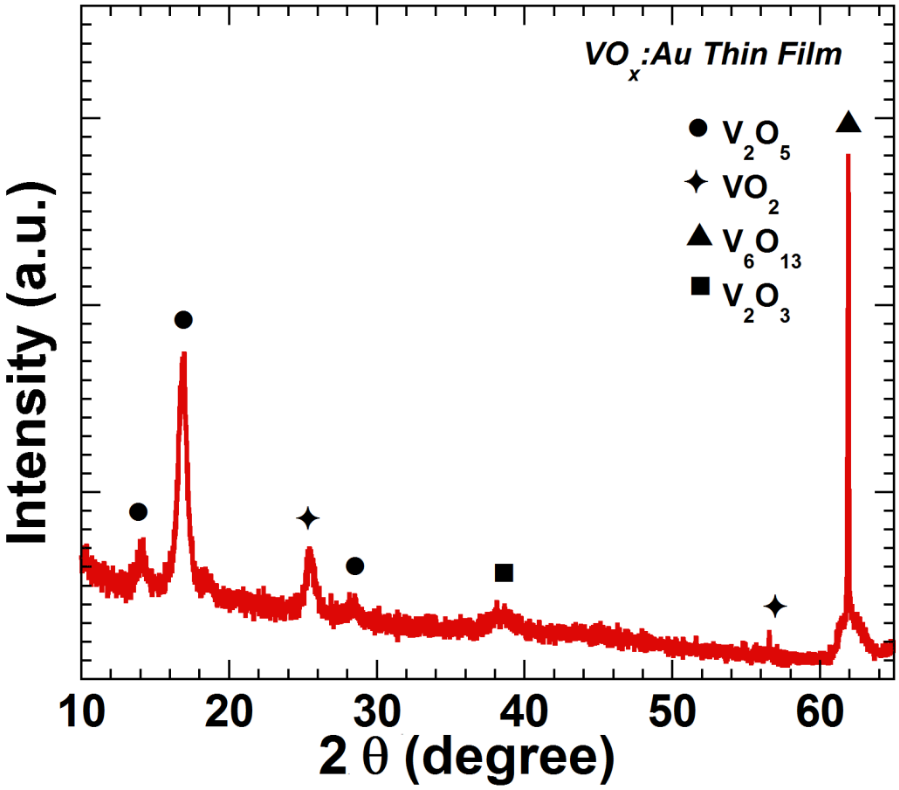

Figure 3.8 X-ray diffraction pattern of as-grown VO_x:Au thin film (Alaboz et al. 2017)

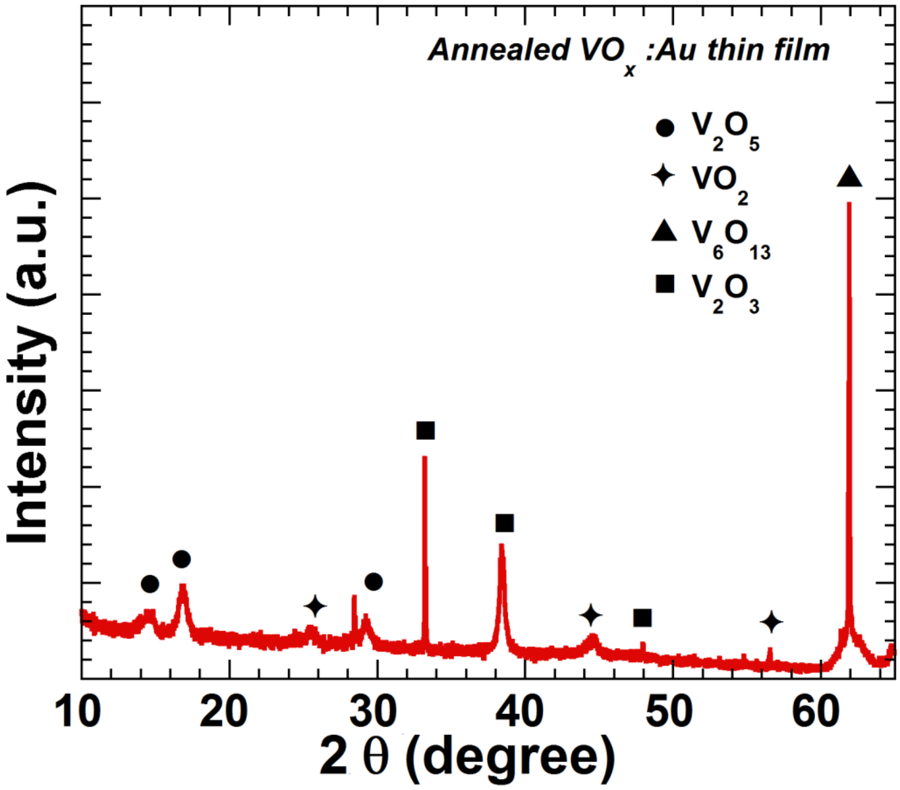

Figure 3.9 X-ray diffraction pattern of annealed VO_x:Au thin film (Alaboz et al. 2017)

It can be seen that VO_x film which was prepared on silicon oxide buffer layer has been consisted of polycrystalline structure with nano-sized grains. It was observed that diffraction peak intensity at 16.7° which was related to (200) V_2O_5 decreased and 61.6° which was related to (042) $V_{16}O_3$ increased just after annealing both for VO_x and VO_x:Au thin films.

In order to investigate annealing effect on film properties VO_x:Au films were also annealed. XRD results indicated that annealing was the main cause of formation of lower oxide phases hence decrease in the x value. It can be seen that V_2O_5 which is a higher oxide phase and has x=2.5 reduced to V_6O_{13} which is a lower oxide phase and has x=2.2. It could be explained that lower oxide phases are more stable for temperature increment than higher oxide phases. Moreover doping gold into VO_x thin films caused a slight change in the structural composition of the films. Gold doped VO_x films consisted of more V_6O_{13} phase and less V_2O_5 than undoped VO_x films. In other words, gold doping decreased x value and restricted to form higher oxide phases in the VO_x film. Annealing had the same effect on VO_x:Au films and annealed VO_x:Au films contain lower oxide phases such as V_2O_3 and V_6O_{13}.

3.5 Scanning Electron Microscopy Analysis

Surface morphologies of the VO_x thin films were investigated and SEM images of the films were shown in Fig. 3.10. In contrast to VO_2 dominated thin films, as deposited VO_x thin film surface is smooth. After annealing, oxide phases and surface morphology of the films were changed.

It can be seen in Fig. 3.10 (a) that film surface was very smooth before anneal which was crucial for lithographic steps and it is an imperative property for bolometer construction. The film may consist of nanograins just before annealing and these grains coalescence into bigger ones which was about 200 nm average size of diameter. Although grain shapes and diameters vary by many conditions which are related to substrate, the buffer layer, and growth temperature, there has been a similar report in the literature (Dou et al. 2015) that indicates annealing is the main driving force to form bigger grains. SEM cross-section image is shown in the Fig. 3.10 c) and it was taken for confirming film thickness and silicon oxide layer thickness.

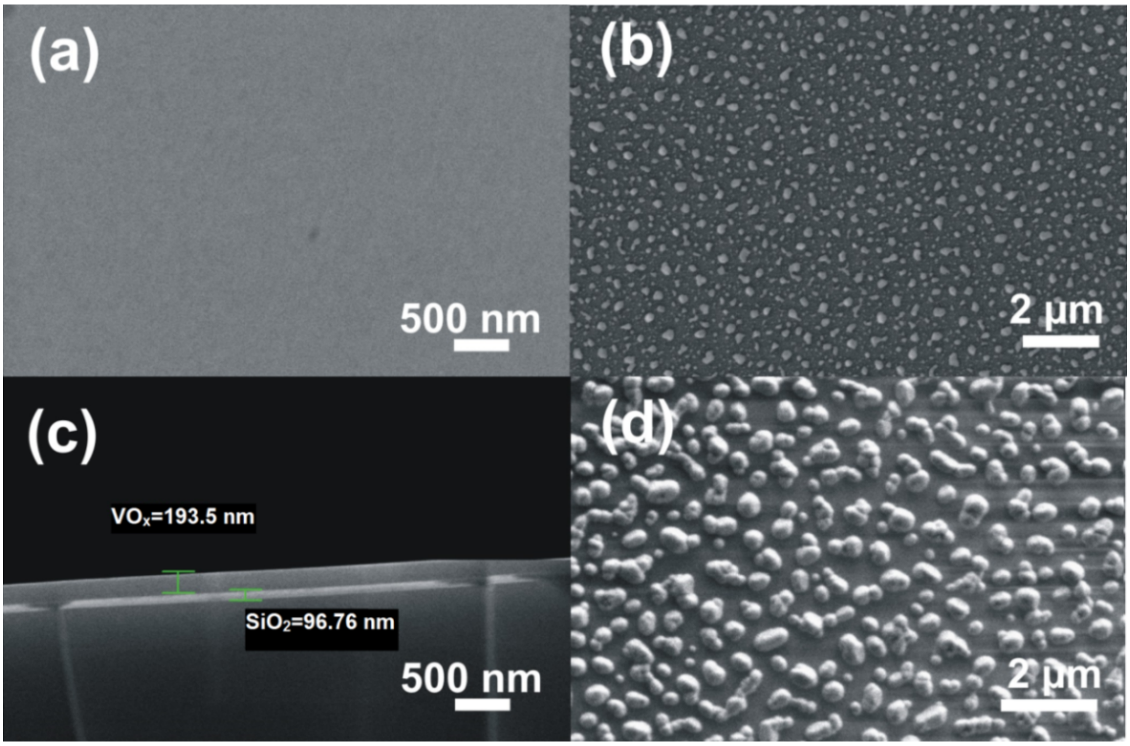

Figure 3.10 a) As grown VO_x multi oxide phase thin film fabricated at room temperature b)Annealed VO_x thin film c) Cross-sectional image of VO_x film d) VO_2 dominated films fabricated at 550°C on sapphire substrate (Alaboz et al. 2017)

We successfully optimized the thickness of the VO_x film for bolometric applications on the top of the SiO_2 support layer. SiO_2 layers thickness were also confirmed by spectroscopic ellipsometer. It is clear that after post-annealing VO_x film surface on a silicon substrate (Fig. 3.10 (b)) is becoming similar to VO_2 on sapphire substrates which deposited at elevated temperatures like 550 °C (Fig. 3.10 (d)) after annealing in terms of grain shapes and size. Their respective average grain sizes are 200 nm for annealed VO_x films and 350 nm for VO_2 films. In contrast to annealed VO_x films, VO_x:Au films which were fabricated by DC magnetron sputtering at room temperature also had same flat surfaces similar to as grown VO_x films.

3.6 Electrical characterization

Electrical behavior of sputtered films was investigated and room temperature resistivity values along with TCR values of these films were summarized in Table 3.2.

Table 3.2 Oxygen partial pressure and doping effect on room temperature TCR of the films
(Alaboz et al. 2017)

ρ_{Oxygen} Oxygen Partial Pressure (%)	Gold Doping	Annealing	TCR (-%)	Room Temperature Resistivity (Ωcm)
8	-	-	1.54 ± 0.05	0.250
9	-	-	1.60 ± 0.04	0.150
10	-	-	1.77 ± 0.04	0.080
10	performed	-	1.67 ± 0.06	0.031
10	-	performed	1.55 ± 0.06	0.075

It can be seen that increasing oxygen partial pressures of the film during the deposition process caused TCR increment of the films. Similar behavior was observed in the literature (Subrahmanyam et al. 2008) at room temperature DC sputtered VO_x thin films.

In the experimental part, optimum TCR value -1.77 K^{-1} was achieved at 10% oxygen partial pressure at room temperature deposition. Linear fitted electrical behavior of thin films was shown in Fig. 3.11, 3.12, 3.13 and measurement data of the selected thin film was shown in Fig. 3.14. Surface property of annealed film was discussed and it can be seen that in Fig. 3.13 and Fig. 3.10 annealing decreases film resistivity but increases film surface roughness. Flat surface is crucial for preventing additional reflections from the surface of the absorbing layer. Flat surface is also crucial for lithography process. Gold doping was performed for the film which has the best TCR value and it decreased resistivity of the film significantly without altering film surface.

It was also observed that film resistivity with optimum TCR value can be decreased with gold doping without sacrificing TCR value. Fabricated films are highly reproducible and stable between 8% to 10% oxygen partial pressure levels but VO_x films which were fabricated at the higher oxygen partial pressures exhibited unstable electrical properties hence measurements did not reveal any consistent behavior. Film resistivity and TCR values versus oxygen partial pressure values were shown in Fig. 3.16 and 3.17.

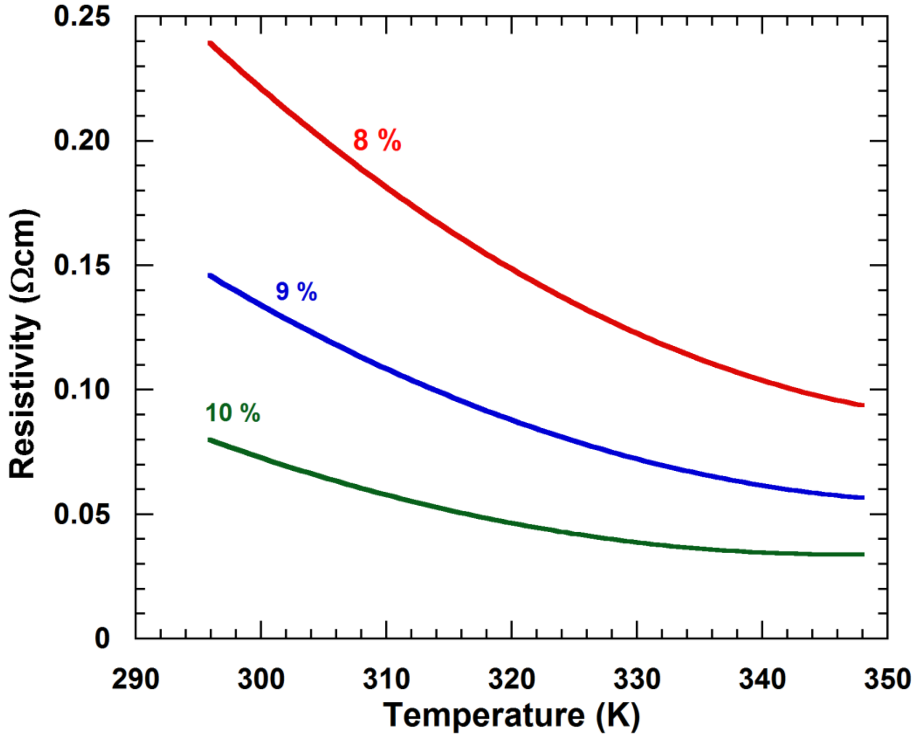

Figure 3.11 Resistivity of VO_x thin films that are produced at different oxygen partial pressure environments between 290 and 350 K (Alaboz et al. 2017)

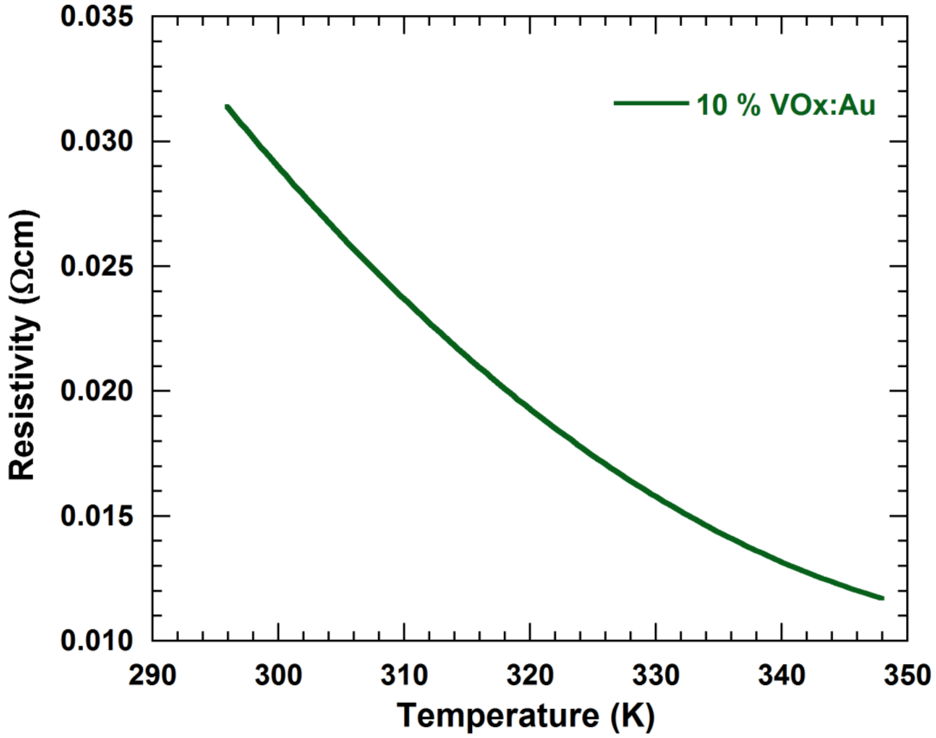

Figure 3.12 Effect of gold doping on resistivity of the VO_x:Au thin film that is produced 10% oxygen partial pressure environment (Alaboz et al. 2017)

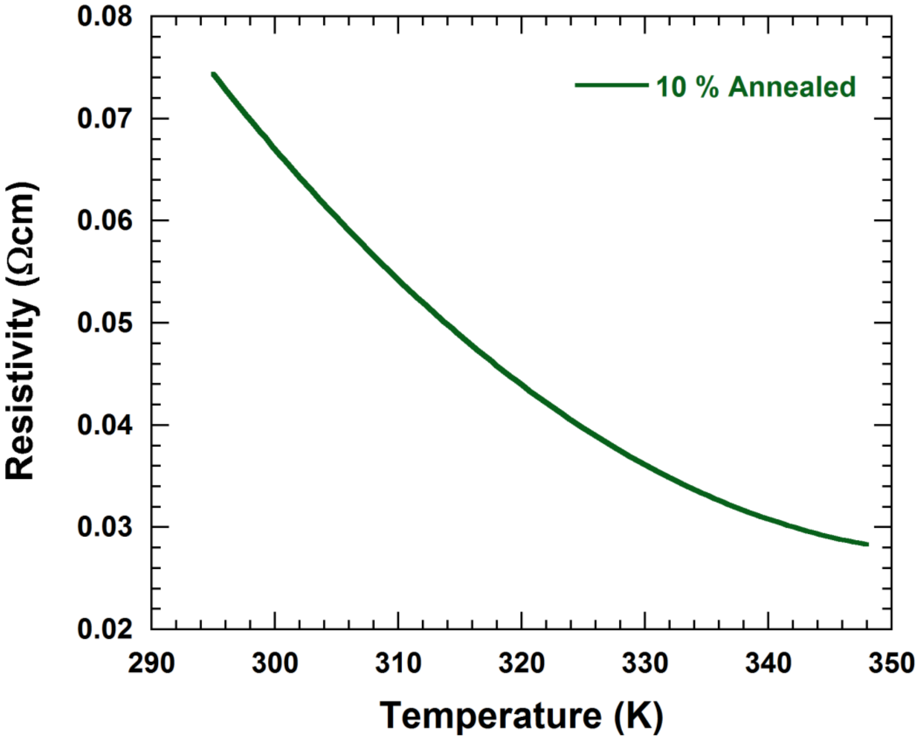

Figure 3.13 Effect of annealing on resistivity of VO_x thin film that is produced 10% oxygen partial pressure environment
(Alaboz et al. 2017)

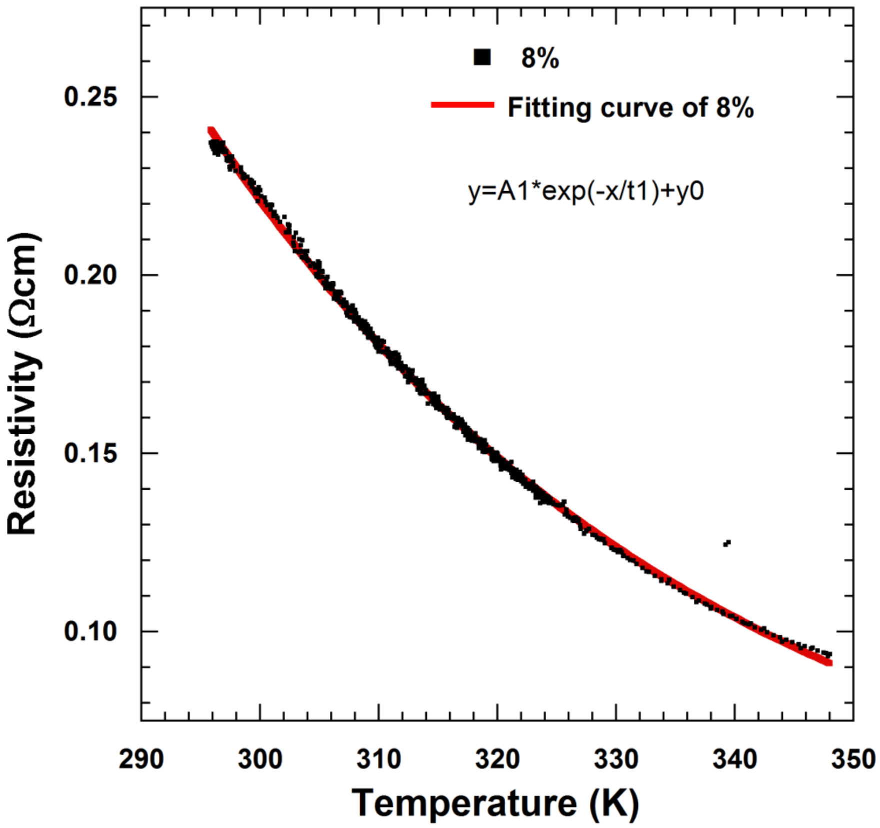

Figure 3.14 Measurement data of the VO_x thin film that is produced 8% oxygen partial pressure environment and its fitting curve

Aging behavior of the VO_x:Au films have also been investigated. Same film electrical behavior was measured just after the sputtering process and six months later. Comparison of electrical behavior between freshly produced and six months air exposed film is given in Fig. 3.15. Vacuum desiccators were not used and films exposed air environment for six months directly. It can be seen that there is a slight increase in resistance after six months.

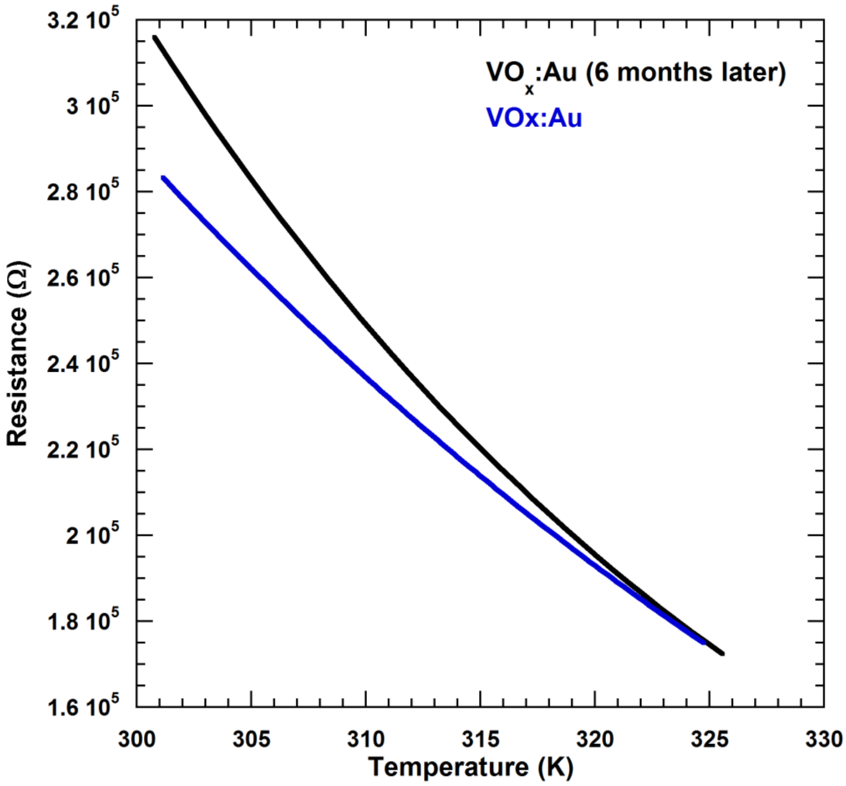

Figure 3.15 Comparison of electrical behaviors of sputtered and 6 months air exposed VO_x:Au thin film

Fig. 3.15 indicates that after six months vanadium oxide film resistivity is stable and in the order of 300kΩ.

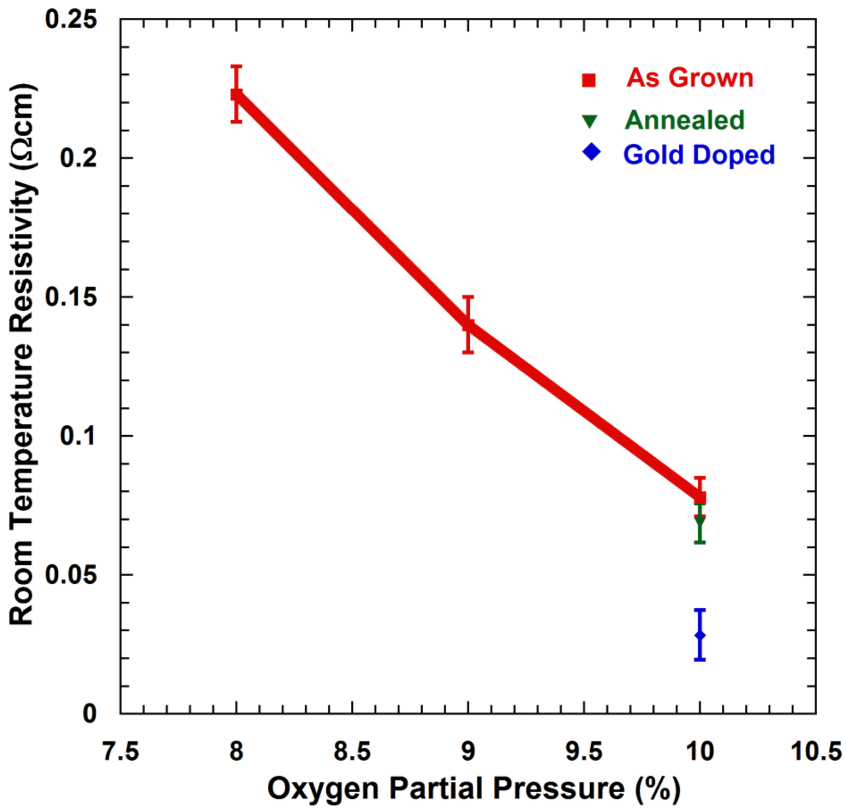

Figure 3.16 Oxygen partial pressure effect on room temperature resistivity

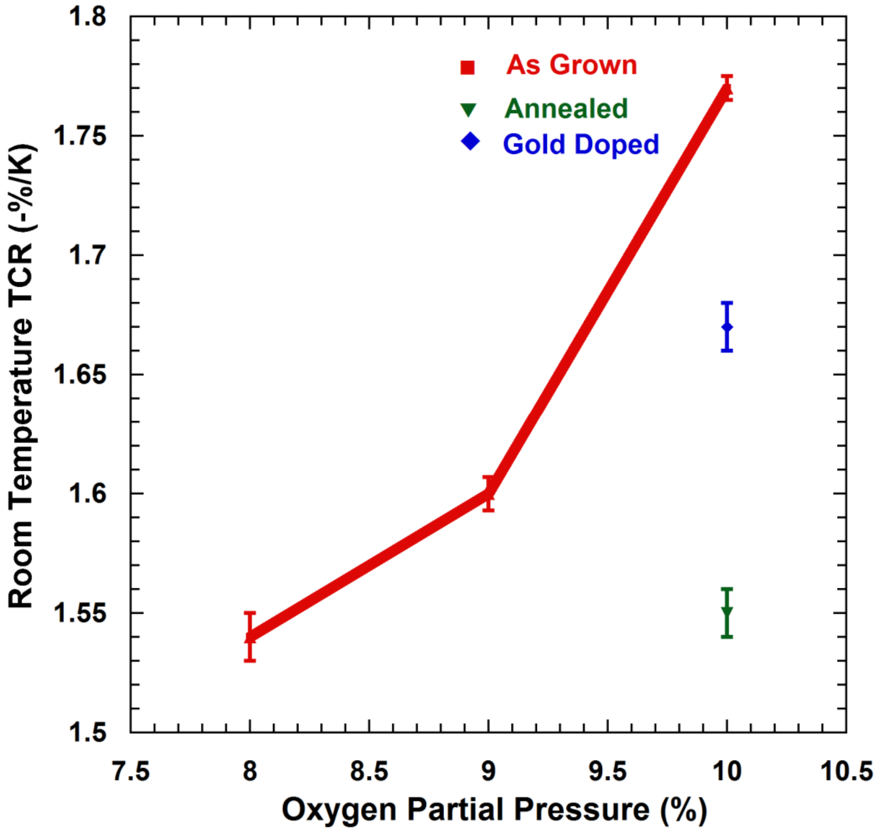

Figure 3.17 Oxygen partial pressure effect on room temperature TCR

Figure 3.16 and 3.17 reveal that there is a gradual increase in TCR and decrease in resistivity values from 8 to 10 % oxygen partial pressure. Where solid reverse triangles represent annealed samples and solid diamonds represent gold doped thin films. TCR value peaked at -1.77 % K^{-1} but resistivity value of this film comparatively high. In contrast, annealed or gold doped thin films have considerable low resistivity values with a slight difference in TCR values. Figure 3.18 shows the TCR change in as grown films between 300 and 350 K temperature. Room temperature TCR values of as grown films are -1.54, -1.60 and -1.77 %K^{-1} for the films that are produced in 8%, 9% and 10% oxygen partial pressures. TCR of all the films decrease at high temperatures and they all exhibit the same behavior in Figure 3.18.

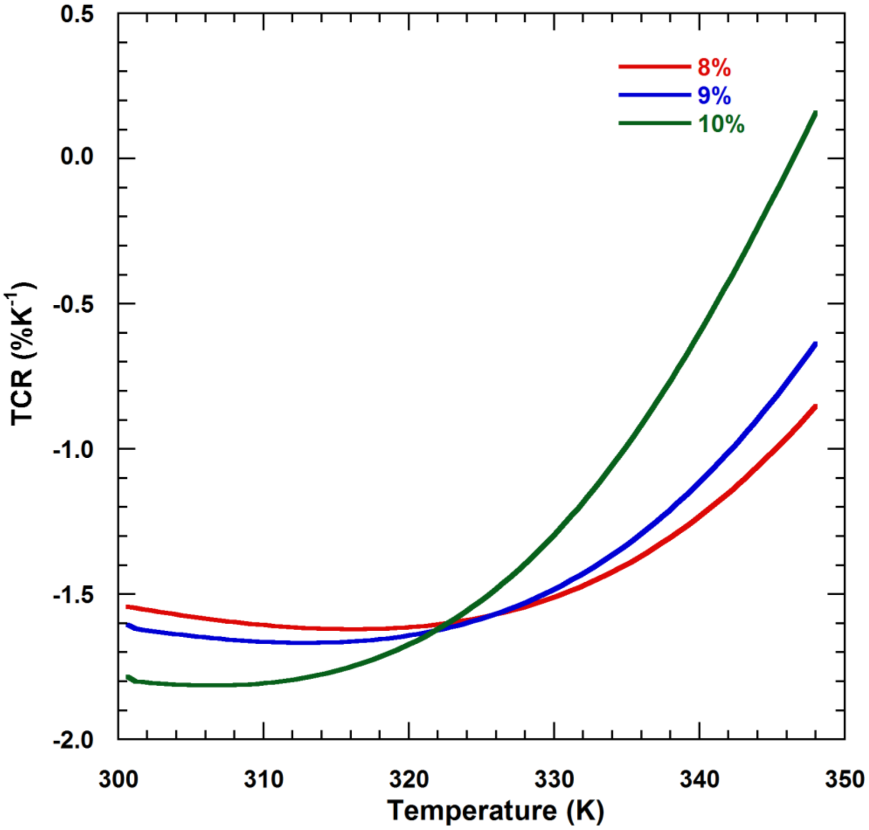

Figure 3.18 TCR change of the as grown films between 300 and 350 K

In addition to that, films in this dissertation have a different place in the literature. Cabarcos gave a comparison between TCR and resistivity values of VO_x thin films which were prepared by different techniques. Ideal VO_x thin films for bolometer applications must have the lowest resistivity and higher TCR values. They must be also stable and withstand complicated microfabrication steps. Films that were produced in this scope of the thesis were added in Fig. 3.19.

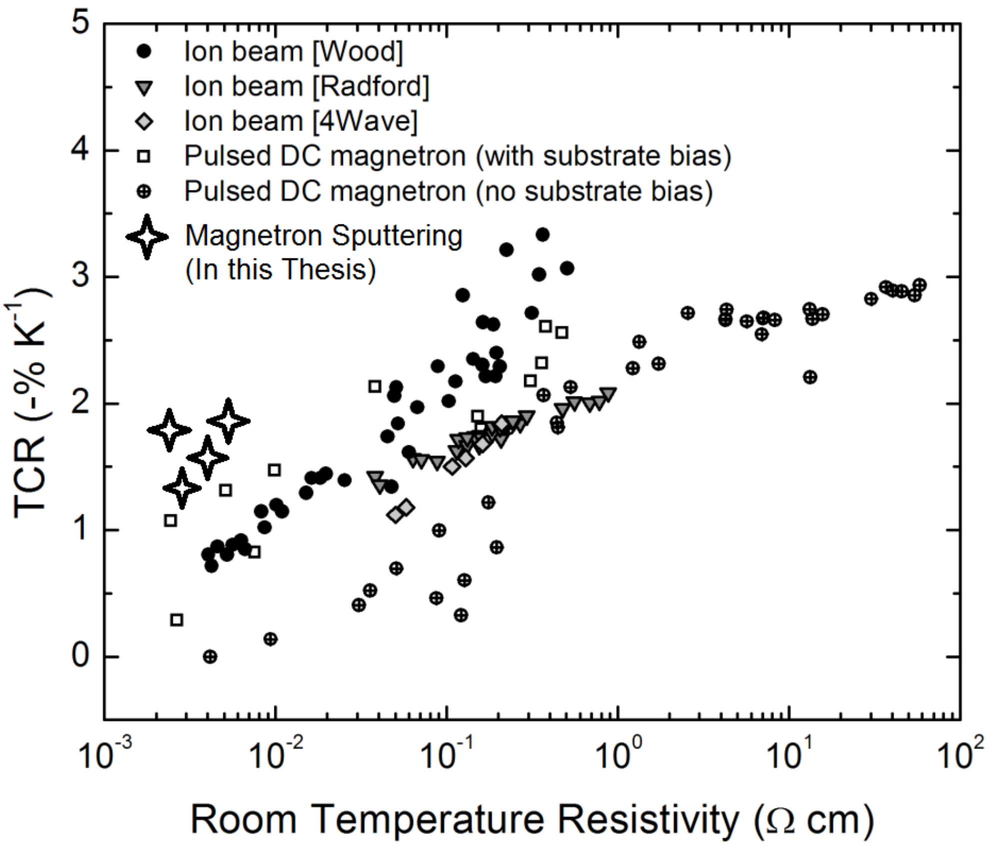

Figure 3.19 Resistivity and TCR relation of VO_x films which was obtained by different techniques. Redraw from Cabarcos' work (Cabarcos et al. 2011)

3.7 Simulation Results

Dimensions of bow tie antenna changed systematically and investigated values of different dimensions were given in Table 3.3. Related S11 results of these dimensions were given in Fig. 3.20, 3.21, 3.22 and 3.23. Optimized bow tie antenna characteristic was given in Fig. 3.24.

It was observed that increasing l, caused a shift to lower frequencies on resonance frequency. But reflection coefficient values increased considerably from 0.12 to 0.60. It was also observed that there was a second resonance at every 0.2 THz intervals. These resonance can be related to substrate. Reflection coefficient data related to main resonance values are shown in Table 3.3.

Table 3.3 Effect of geometrical lengths of bowtie antenna on resonance frequency and reflection coefficient

	l (µm)	w (µm)	d (µm)	k (µm)	Resonance Frequency (THz)	Reflection Coefficient
Effect of changing l	56	5	40	15	>0.78	<0.12
	66	5	40	15	>0.78	<0.12
	76	5	40	15	>0.78	<0.12
	86	5	40	15	0.78	0.12
	96	5	40	15	0.75	0.41
	106	5	40	15	0.72	0.60
Effect of changing w	96	2	40	15	0.70	0.29
	96	5	40	15	0.70	0.31
	96	10	40	15	0.70	0.35
Effect of changing d	96	5	30	15	0.76	0.36
	96	5	40	15	0.76	0.37
	96	5	50	15	0.75	0.37
Effect of changing k	96	5	40	5	0.72	0.45
	96	5	40	10	0.71	0.41
	96	5	40	15	0.69	0.29

On the other hand, increasing w did not cause any change in resonance frequency position. But reflection coefficient was changed from 0.29 to 0.35. Increasing arm width of the antenna also did not cause a significant change in resonance frequency position as well as reflection coefficient. Increasing bridge length k, caused a shift in the resonance frequency and it shifted towards lower frequencies. Reflection coefficient decreased considerably with increasing k values. A similar effect on resonance frequency was observed in the literature recently (Dong et al. 2012).

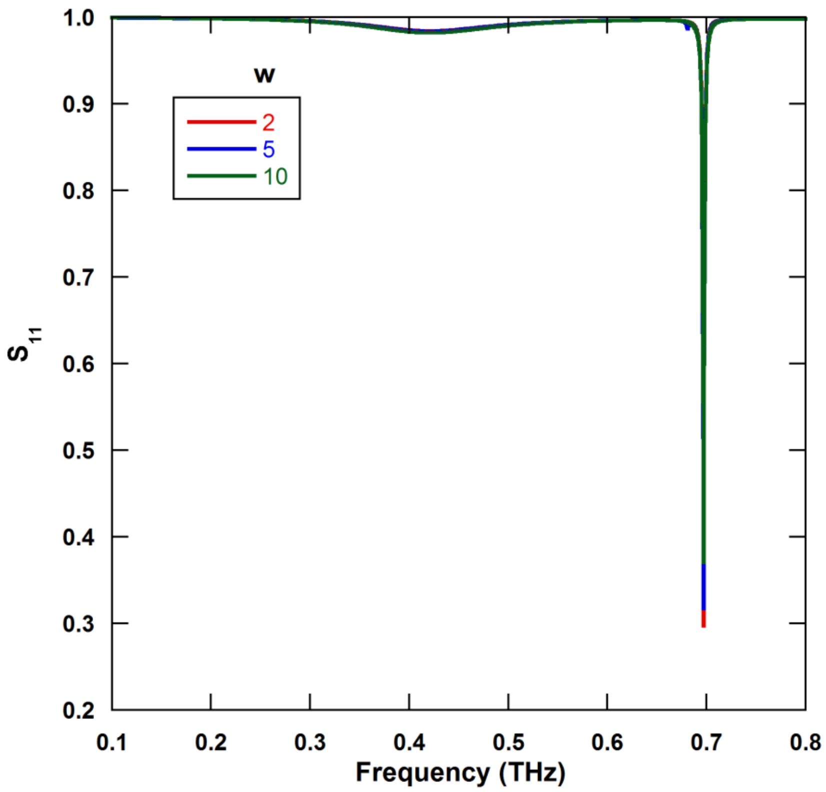

Figure 3.20 Effect of bridge width on resonance frequency and reflection coefficient

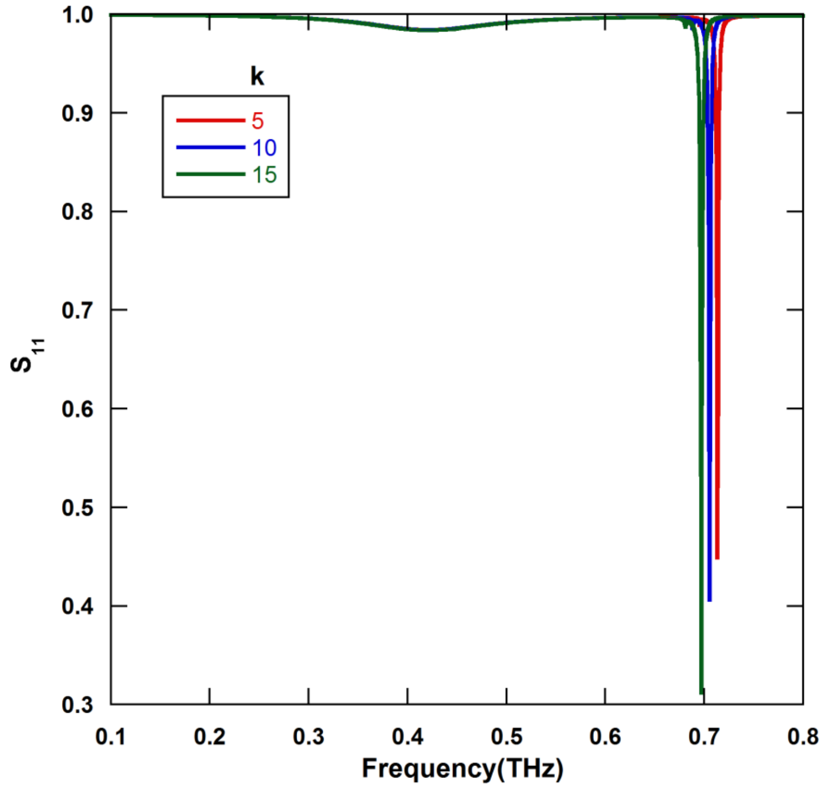

Figure 3.21 Effect of bridge length on resonance frequency and reflection coefficient

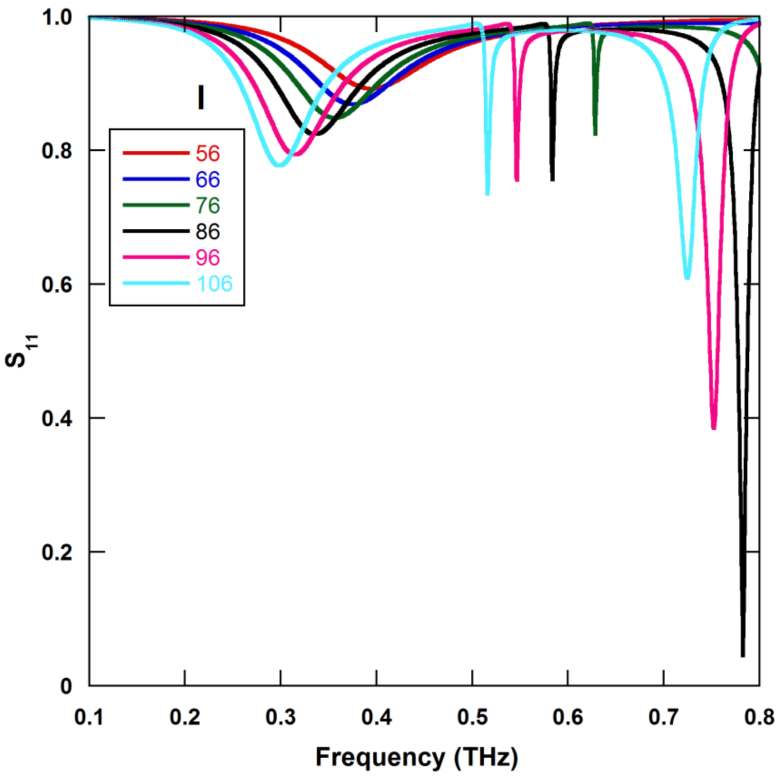

Figure 3.22 Effect of antenna arm's lengths on resonance frequency and reflection coefficient

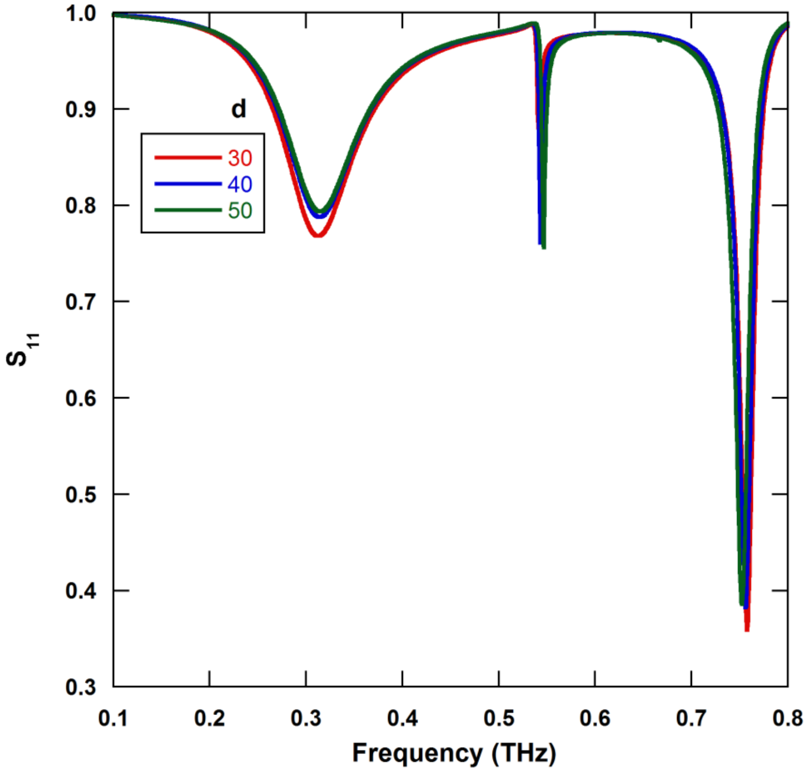

Figure 3.23 Effect of antenna arms width on resonance frequency and reflection coefficient

Plasmon resonances of bowtie antennas with these dimensions were investigated and effect of geometrical parameters were presented in the literature (Yang et al. 2011). Especially same behavior was observed about shifting at resonance frequency position.

Final design was made according to data in Table 3.3 and optimum geometry was achieved for 0.67 THz resonance frequency with reflection coefficient below 0.1. Related resonance and reflection coefficient over frequency are shown in Fig. 3.24.

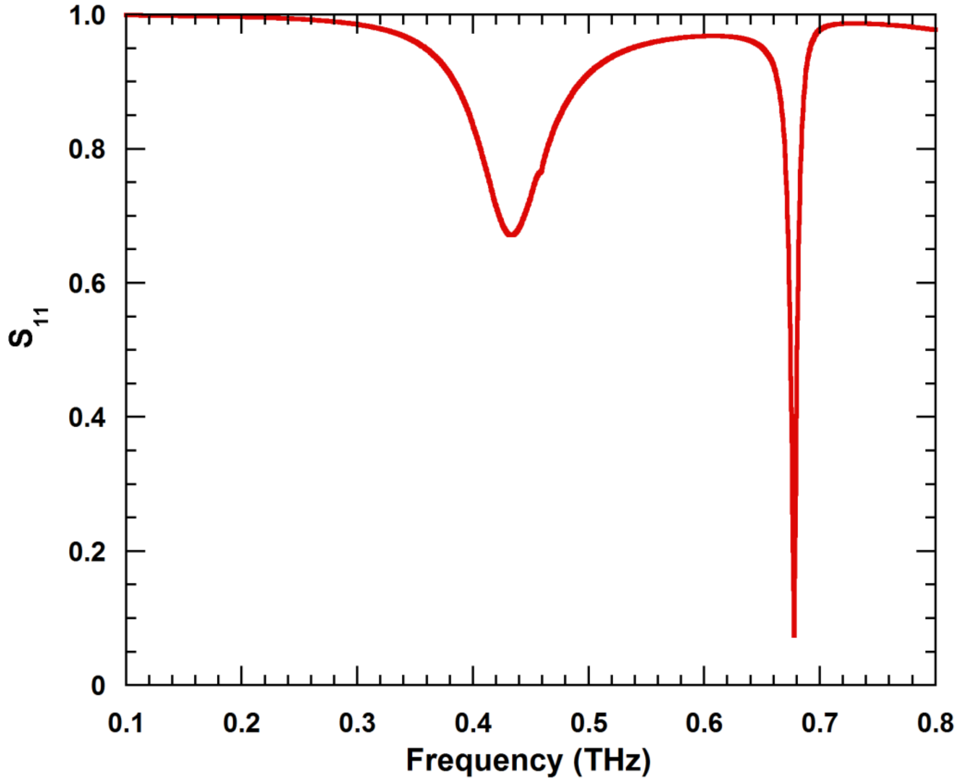

Figure 3.24 Simulation result for designed resonant bowtie antenna

Log periodic antenna simulation was also performed and the unit cell was used for simulation. Terahertz radiation was sent into gap between antenna arms. Top view of the log periodic antenna structure that was designed by CST MWS is shown Fig.3.25.

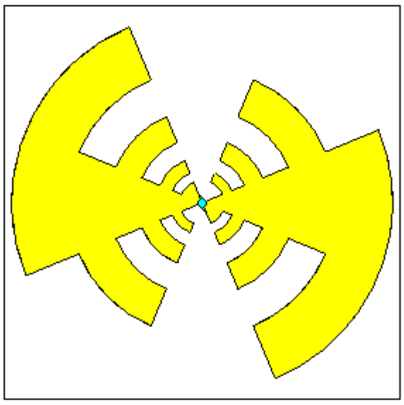

Figure 3.25 Top view of the designed log-periodic antenna structure

Designing was performed according to same goals used in bowtie antenna design. The width of the designed log-periodic antenna structure was 30 µm and τ=0.49. The resonance frequency of the designed log periodic antenna was 0.41 THz and reflection coefficient at this frequency was 0.12. It is observed that log periodic antenna structure shows wider bandwidth than bow tie antenna. Simulation result is shown in Fig. 3.26.

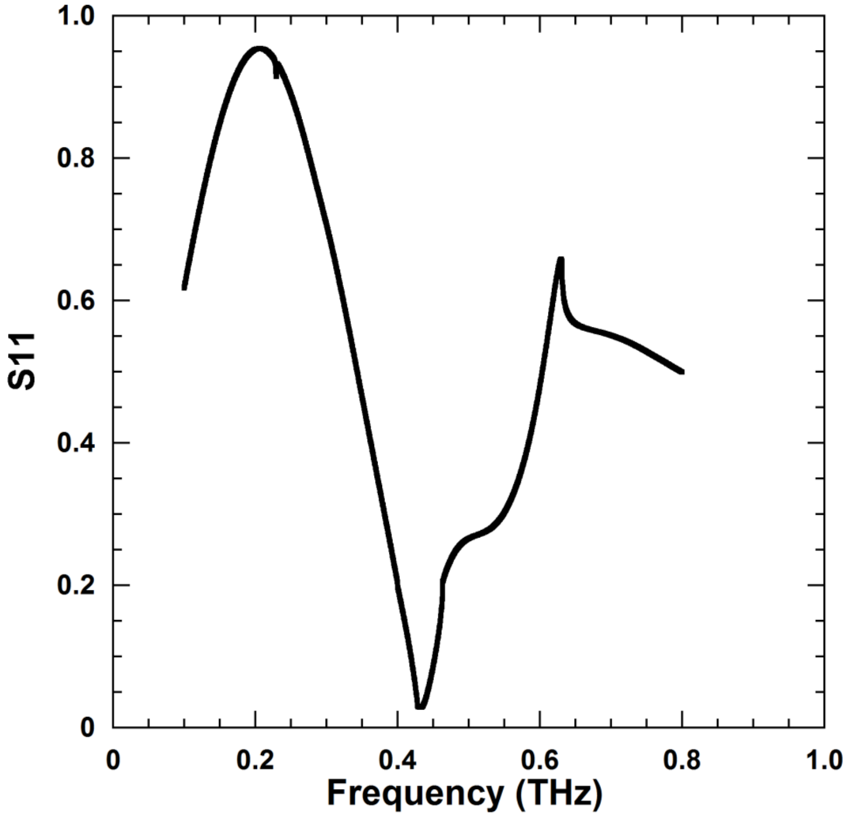

Figure 3.26 Resonance frequency and reflection coefficient of the designed antenna

3.8 Lithography Results

Lithography steps were divided into three and validation of theoretical expectation of these steps experimentally was tested by a preliminary work. Copper foil which has a thickness of 0.5 mm was sanded to obtain a smooth surface. Holes which have a diameter of 500 µm approximately were created with an injection needle. Gold wires which have a thickness of 17 µm were placed in the middle of these holes under a microscope. The steps of handmade creation of shadow mask were shown in Fig. 3.27.

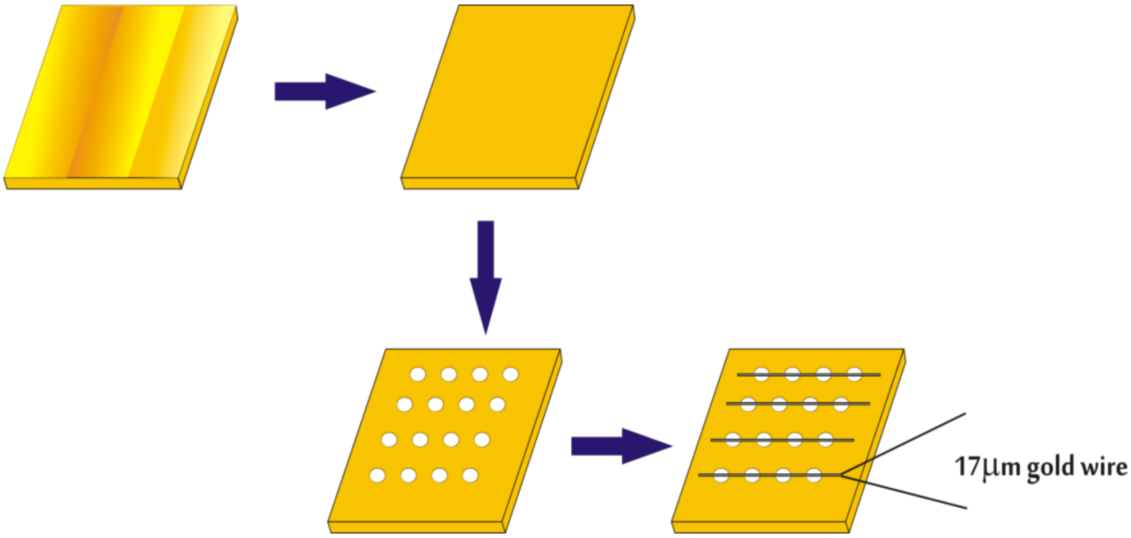

Figure 3.27 Handmade shadow mask creation

VO_x:Au thin films were coated with AZ5214E photoresist by a spin coater at 3000RPM. 7 seconds UV exposure was performed and then films were developed in NaOH solution immediately. Ion milling was performed to etch unprotected areas until reaching silicon substrate. After ion milling, KOH solution was used to perform wet etch silicon part of the structure and optical image and surface profilometer result of the final structure were shown in Fig. 3.28 and 3.29. As shown in Fig. 3.29 more than 1 µm dept was etched by KOH anisotropic silicon etching. Etch step and profile can be observed in Fig. 3.28 because of the etching mechanism of KOH. That means etched step has an angle. After this validation and optimization of KOH etch rates, designed antenna structures were drawn by Autocad.

Fabrication results of the related lithography steps were provided in Fig. 3.30 and 3.31. Contrary to expectations, pyramids and bubble shape structures formed even within few seconds in KOH solution. It was also observed that VO_x:Au film electrical properties changed after 10 seconds within KOH solution at wet etching process.

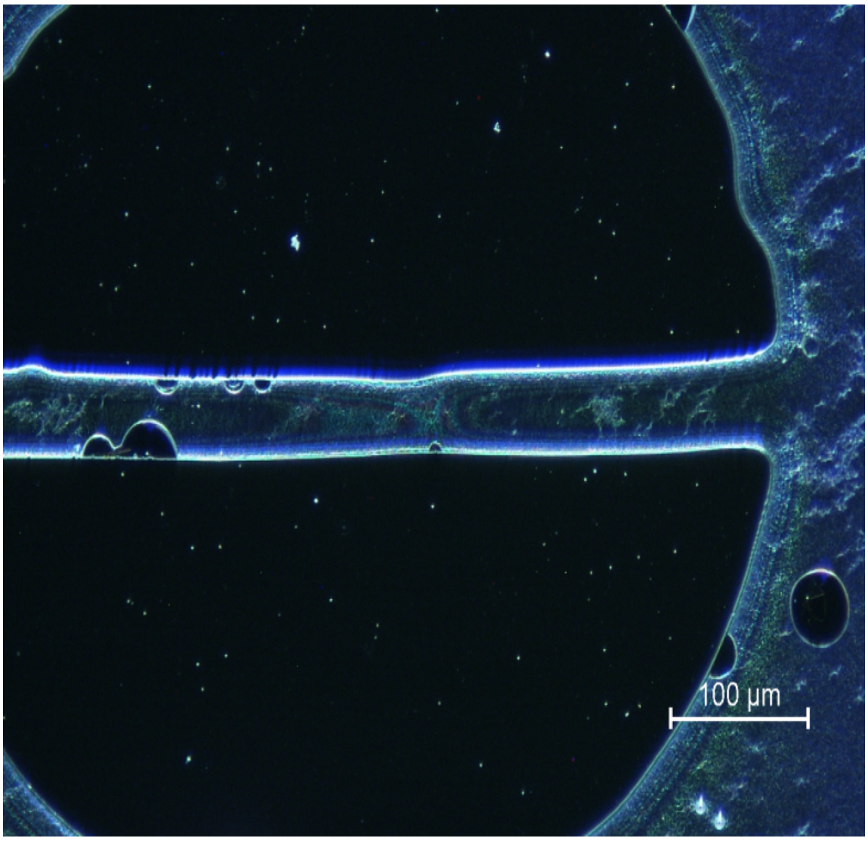

Figure 3.28 Preliminary work with handmade shadow mask to test and optimize KOH etching process

Figure 3.29 Surface analysis of the final structure in Fig. 3.28

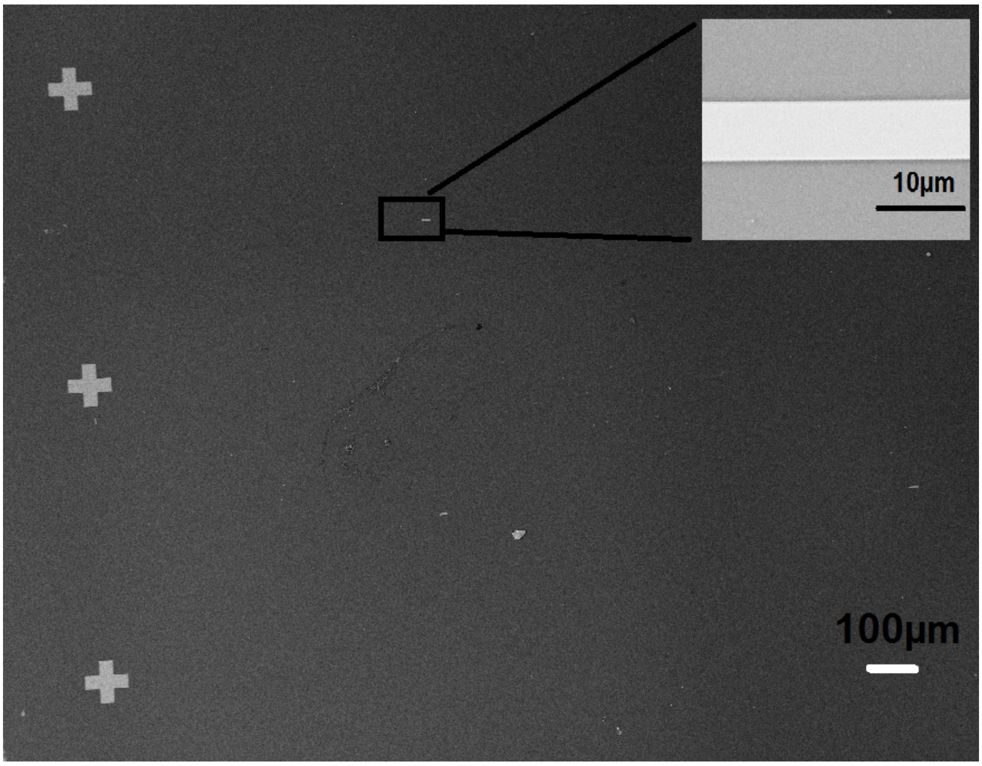

Figure 3.30 Final structure after the first stage of lithography

Designed bow tie array emerged at the end of the second step which is shown in Fig. 3.31.

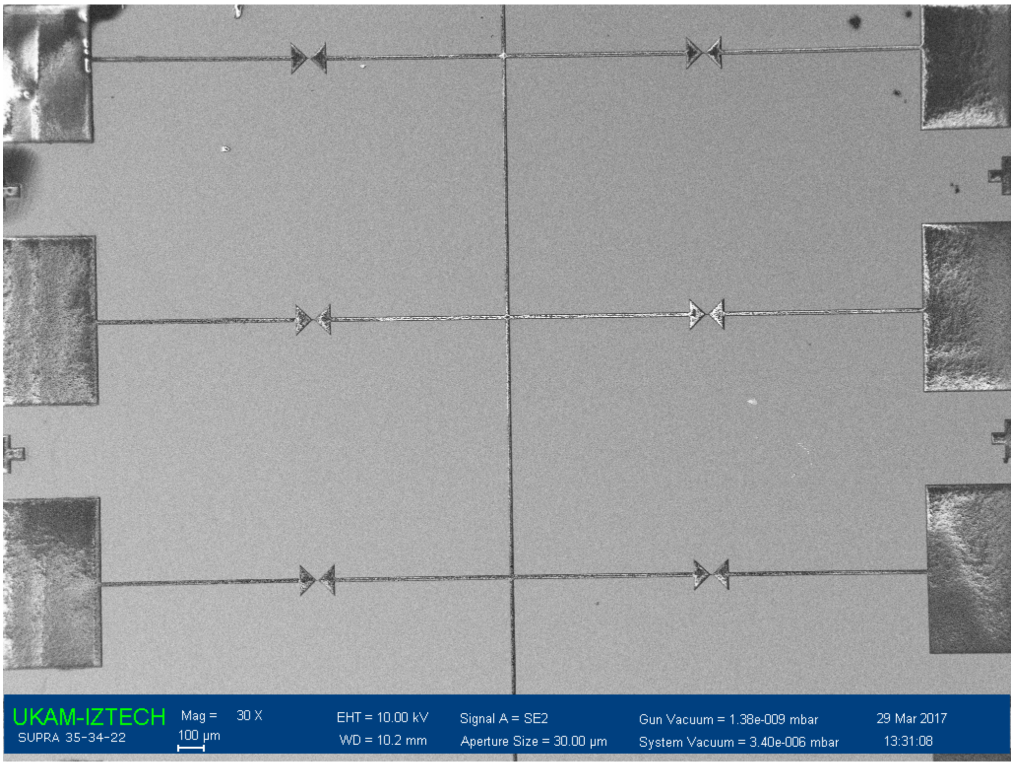

Figure 3.31 Final structure after the second stage of lithography

CHAPTER 4

CONCLUSIONS

In this dissertation, properties and applications of terahertz radiation were summarized in the introduction. Increasing demand for better THz detectors and sources was stated and unresolved problems as well as, key features for better detectors were underlined in motivation. In order to establish wide perspective about vanadium oxide thin films as an absorbing element, a literature review was given in the following section. Two crucial properties which are high TCR accompanied with low resistivity were specified to achieve better absorbing element for uncooled detectors.

In attempting to overcome existing problems in the literature for obtaining desired absorber element for uncooled THz bolometers, gold doping method was chosen. Polycrystalline VO_x:Au thin films were produced by dc magnetron sputtering system and degree of gold doping was optimized for the films which have the lowest resistivity accompanied with the highest TCR. Details of preparing VO_x:Au thin films with desired properties were given in Chapter 2. Structural characterization such as surface morphology of produced films and electrical characterization of these films were shown in Chapter 3. Another important focus of this thesis was to design resonant antenna on the optimized VO_x:Au thin films. Details of the simulations were explained in Chapter 2 and optimized parameters for antenna structure were presented in Chapter 3.

One of the essential achievement of this thesis was producing stable VO_x:Au thin film which has 0.0295 Ωcm resistivity and -1.67 % K^{-1} TCR. Along with low resistivity and suitable TCR values, optimized VO_x:Au thin films in this thesis have a distinctive place in the literature as shown in Fig. 3.19. According to equation 2.7 and previous works in infrared region (Smith et al. 2014) films which are produced in this thesis will provide lower Johnson noise in uncooled THz bolometer.

In order to achieve better film properties, silicon oxide layer was formed before sputtering process. Different oxidation methods such as dry and wet, were investigated in terms of quality and duration. It was observed that wet oxidation of silicon is faster than dry oxidation. Dry oxidation method was chosen and thickness of the oxide layer was carefully optimized. Conditions which are oxygen partial pressure during sputtering, post-annealing and gold doping were also investigated. Effect of these parameters on TCR and resistivity were studied. It is found that there is a narrow region in terms of oxygen partial pressure level and increment of oxygen partial pressure during sputtering process provides slightly higher TCR and lower resistivity in this narrow region. Further increment in oxygen partial pressure affect negatively on the film properties and caused resistivity increase along with TCR decrease. Surface degradation was observed during post-annealing of VO_x films hence gold doping method was chosen to decrease resistivity. It was found that gold doping is a better approach to decrease vanadium oxide thin film resistivity but it is also stated and exhibited that doping level must be optimized very precisely. Vanadium oxide film thickness is an important property for bolometer applications and it is already known that thickness of the vanadium oxide films also affects their growing mechanism. In this dissertation, vanadium oxide film thickness also optimized for achieving better electrical properties. Sputtering conditions such as oxygen partial pressure, duration and rotation speed of the sample holder were optimized. Hence, critical optimization of VO_x thin films for THz uncooled bolometers was done in terms of TCR, resistivity and surface smoothness. It will provide valuable information for researchers who would like to use vanadium oxide films for THz uncooled bolometer applications.

Another contribution of this thesis was optimization of an antenna structure for VO_x:Au films for THz region. Although plenty of research was performed in the infrared region, detailed antenna optimization for THz region of vanadium oxide films with SiO_2 support layer and air cavity were performed for the first time. In this thesis relation between geometrical parameters of the antenna and resonance properties as well as reflection coefficient at resonance frequency were investigated briefly. Affect of geometrical parameters such as length and width of antenna arms as well as the bridge. In the simulation part of the dissertation, the best design approach and simulation conditions were investigated and provided. Even cavity beneath absorber layer taken into account when simulations were performed. Antenna structures for these VO_x:Au thin films were optimized for THz region and bow tie antenna structure that has a resonance at 0.67 THz and reflection coefficient below 0.1 was achieved. Therefore all the details about optimization of an THz antenna for uncooled VO_x bolometer were provided. This result also will provide wider and valuable information to the researchers who would like to design and build an antenna structure on VO_x thin films that operate at THz region.

Meeting both expectations which are high TCR and low resistivity needed a formidable effort along with optimized antenna structure for THz region. A lithography step to construct bolometer arrays on vanadium oxide thin films was also proposed. In summary study in this thesis will be a guide to researchers who would like to construct an uncooled bolometer at THz range with vanadium oxide absorbing layer.

REFERENCES

Adler D., Feinleib J., Brooks H., and Paul W., 1967. "Semiconductor-to-Metal Transitions in Transition-Metal Compounds." *Physical Review* 155 (3): 851–60. doi:10.1103/PhysRev.155.851.

Ajmera S. K., Syllaios A. J., Tyber G. S., Taylor M. F., and Hollingsworth R. E. 2010. "Amorphous Silicon Thin-Films for Uncooled Infrared Microbolometer Sensors." In *Proc. SPIE*, 7660:766012. doi:10.1117/12.850545.

Balanis C. A. 1997. *Antenna Theory: Analysis and Design*. *John Wiley & Sons*. Third Edit. Hoboken, New Jersey: John Wiley & Sons, Inc. doi:10.1109/PROC.1984.12959.

Berg S., and Nyberg T. 2005. "Fundamental Understanding and Modeling of Reactive Sputtering Processes." *Thin Solid Films* 476 (2): 215–30. doi:10.1016/j.tsf.2004.10.051.

Biermann, S., Poteryaev A., Lichtenstein A. I., and Georges A. 2005. "Dynamical Singlets and Correlation-Assisted Peierls Transition in VO_2." *Physical Review Letters* 94 (2). doi:10.1103/PhysRevLett.94.026404.

Budai J. D., Hong J., Manley M. E., Specht E. D., Chen W. L., Tischler J. Z., Abernathy D. L., et al. 2014. "Metallization of Vanadium Dioxide Driven by Large Phonon Entropy." *Nature* 515 (7528), 535–39. http://dx.doi.org/10.1038/nature13865.

Cabarcos, Orlando M., Hitesh a. Basantani, S. S. N. Bharadwaja, Jing Li, Bryan D. Gauntt, Sami Antrazi, Elizabeth C. Dickey, David L. Allara, and Mark W. Horn. 2011. "Comparison of Ion Beam and Magnetron Sputtered Vanadium Oxide Thin Films for Uncooled IR Imaging." *Spie* 8012: 80121K. doi:10.1117/12.884377.

Cavalleri A., Rini M., Chong H. H. W., Fourmaux S., Glover T. E., Heimann P. A., Kieffer J. C., and Schoenlein R. W. 2005. "Band-Selective Measurements of Electron Dynamics in VO2 Using Femtosecond near-Edge X-Ray Absorption." *Physical Review Letters* 95 (6). doi:10.1103/PhysRevLett.95.067405.

Changhong C., Yi X., Zhao X., and Xiong B. 2000. "Preparation and Properties of

Vanadium Dioxide Thin Films for Uncooled Microbolometer." In *25th International Conference on Infrared and Millimeter Waves*, 145–46. IEEE. doi:10.1109/ICIMW.2000.892973.

Chen R. H., Jiang Y. L., and Li B. Z. 2014. "Influence of Post-Annealing on Resistivity of VOx Thin Film." *IEEE Electron Device Letters* 35 (7): 780–82. doi:10.1109/LED.2014.2326691.

Chen S., Ma H., Wang S., Shen N., Xiao J., Zhou H., Zhao X., Li Y., and Yi X. 2006. "Vanadium Oxide Thin Films Deposited on Silicon Dioxide Buffer Layers by Magnetron Sputtering." *Thin Solid Films* 497 (1–2): 267–69. doi:10.1016/j.tsf.2005.07.221.

Cheng Q., and Almasri M. 2009. "Silicon Germanium Oxide (Si X Ge 1-X O Y) Infrared Material for Uncooled Infrared Detection." In *Proc. SPIE*, 7298:72980K. doi:10.1117/12.818866.

Choi S. B., Kyoung J. S., Kim H. S., Park H. R., Park D. J., Kim B., Ahn Y. H., et al. 2011. "Nanopattern Enabled Terahertz All-Optical Switching on Vanadium Dioxide Thin Film." *Applied Physics Letters* 98 (7): 71105. doi:10.1063/1.3553504.

Committee, Antennas, Ieee Antennas, and Propagation Society. 2014. "IEEE Standard for Definitions of Terms for Antennas IEEE Antennas and Propagation Society." *IEEE Std 145-2013 (Revision of IEEE Std 145-1993)* 2013: 50. doi:10.1109/IEEESTD.2014.6758443.

Cui Y., and Ramanathan S. 2011. "Substrate Effects on Metal-Insulator Transition Characteristics of Rf-Sputtered Epitaxial VO2 Thin Films." *J. Vac. Sci. Technol. A* 29 (4): 41502–7. doi:10.1116/1.3584817.

Dai J., Wang X., He S., Huang Y., and Yi X. 2008. "Low Temperature Fabrication of VOx Thin Films for Uncooled IR Detectors by Direct Current Reactive Magnetron Sputtering Method." *Infrared Physics and Technology* 51 (4): 287–91. doi:10.1016/j.infrared.2007.12.002.

Dong R., Nie Y., Yao S., Jiang Y., Meng J., and Yang Y. 2012. "Plasmonic Resonance of Bowtie Antennas and Their Geometry Dependence." 8562:85621L.

doi:10.1117/12.999703.

Fieldhouse N., Pursel S. M., Horn M. W., and Bharadwaja S. S. N. 2009. “Electrical Properties of Vanadium Oxide Thin Films for Bolometer Applications: Processed by Pulse Dc Sputtering.” *Journal of Physics D: Applied Physics* 42 (5): 55408. doi:10.1088/0022-3727/42/5/055408.

Girish K., and Ray K. P. 2003. *Broadband Microstrip Antenna*. Norwood, MA: Artech House, Inc.

González F. J., Abdel-Rahman M., and Boreman G. D. 2003. “Antenna-Coupled VOx Thin-Film Microbolometer Array.” *Microwave and Optical Technology Letters* 38 (3). 235–37. doi:10.1002/mop.11024.

Guo H., Meyrath T. P., Zentgraf T., Liu N., Fu L., Schweizer H., and Giessen H. 2008. “Optical Resonances of Bowtie Slot Antennas and Their Geometry and Material Dependence.” *Optics Express* 16 (11): 7756. doi:10.1364/OE.16.007756.

Gurvitch M., Luryi S., Polyakov A., and Shabalov A. 2010. “Treating the Case of Incurable Hysteresis in VO2.” *Future Trends in Microelectronics: From Nanophotonics to Sensors and Energy*, 395–409. doi:10.1002/9780470649343.ch33.

Han P. Y., and Zhang X. C. 2001. “Free-Space Coherent Broadband Terahertz Time-Domain Spectroscopy.” *Measurement Science and Technology* 12 (11): 1747–56. doi:10.1088/0957-0233/12/11/301.

Han Y. H., Kim K. T., Shin H. J., Moon S., and Choi I. H. 2005. “Enhanced Characteristics of an Uncooled Microbolometer Using Vanadium-Tungsten Oxide as a Thermometric Material.” *Applied Physics Letters* 86 (25). doi:10.1063/1.1953872.

Hancox I., Rochford L. A., Clare D., Sullivan P., and Jones T. S. 2011. “Utilizing N-Type Vanadium Oxide Films as Hole-Extracting Layers for Small Molecule Organic Photovoltaics.” *Applied Physics Letters* 99 (1): 13304. doi:10.1063/1.3607478.

Hanlon T. J., Coath J. A., and Richardson M. A. 2003. “Molybdenum-Doped Vanadium

Dioxide Coatings on Glass Produced by the Aqueous Sol–gel Method." *Thin Solid Films* 436 (2): 269–72. doi:https://doi.org/10.1016/S0040-6090(03)00602-3.

Jagtap V. S., Dégardin A. F., and Kreisler A. J. 2012. "Low Temperature Amorphous Growth of Semiconducting Y-Ba-Cu-O Oxide Thin Films in View of Infrared Bolometric Detection." In *Thin Solid Films*, 520:4754–57. doi:10.1016/j.tsf.2011.10.127.

Jansen C., Wietzke S., Peters O., Scheller M., Vieweg N., Salhi M., Krumbholz N., Jördens C., Hochrein T., and Koch M. 2010. "Terahertz Imaging: Applications and Perspectives." *Appl. Opt.* 49 (19). OSA: E48--E57. doi:10.1364/AO.49.000E48.

Jiazhen Y., Yue Z., Wanxia H., and Mingjin T. 2008. "Effect of Mo-W Co-Doping on Semiconductor-Metal Phase Transition Temperature of Vanadium Dioxide Film." *Thin Solid Films* 516 (23): 8554–58. doi:10.1016/j.tsf.2008.05.021.

Jin P., Nakao S., and Tanemura S. 1998. "Tungsten Doping into Vanadium Dioxide Thermochromic Films by High-Energy Ion Implantation and Thermal Annealing." *Thin Solid Films* 324 (1–2): 151–58. doi:https://doi.org/10.1016/S0040-6090(98)00362-9.

Kakiuchida H., Jin P., Okada M., and Tazawa M. 2007. "Optical Characterization of Titanium–Vanadium Oxide Films." *Japanese Journal of Applied Physics* 46, 621.

Ko C., and Ramanathan S. 2009. "Dispersive Capacitance and Conductance across the Phase Transition Boundary in Metal-Vanadium Oxide-Silicon Devices." *Journal of Applied Physics* 106 (3). doi:10.1063/1.3186024.

Li J., Yuan N., and Xie J. 2005. "Annealing Characteristics of the Vanadium Oxide Films Prepared by Modified Ion Beam Enhanced Deposition." *Applied Surface Science* 243 (1–4): 437–42. doi:10.1016/j.apsusc.2004.09.103.

Liu H., Zhong H., Karpowicz N., Chen Y., and Zhang X. 2007. "Terahertz Spectroscopy and Imaging for Defense and Security Applications." *Proceedings of the IEEE* 95 (8): 1514–27. doi:10.1109/JPROC.2007.898903.

Liu L., Xu H., Percy R. R., Herald D. L., Lichtenberger A. W., Hesler J. L., and R. M. Weikle. 2009. "Development of Integrated Terahertz Broadband Detectors

Utilizing Superconducting Hot-Electron Bolometers." *IEEE Transactions on Applied Superconductivity* 19 (3): 282–86. doi:10.1109/TASC.2009.2018268.

Liu L., Kang L., Mayer T. S., and Werner D. H. 2016. "Hybrid Metamaterials for Electrically Triggered Multifunctional Control." *Nature Communications* 7, 13236. doi:10.1038/ncomms13236.

Lu X. H., Kang L., Chen J., Zhong Y. Y., He N., Zhang L. B., Jin B. B., et al. 2008. "A Terahertz Detector Operating at Room Temperature." *Proc. SPIE* 7277: 72770N–72770N–7. doi:10.1117/12.821570.

Luukanen A., Grönberg L., Helistö P., Penttilä J. S., Seppä H., Sipola H., Dietlein C. R., and Grossman E. N. 2006. "An Array of Antenna-Coupled Superconducting Microbolometers for Passive Indoors Real-Time THz Imaging." *Proc. SPIE*. doi:10.1117/12.669044.

Lv Y., Hu M., Wu M., and Liu Z. 2007. "Preparation of Vanadium Oxide Thin Films with High Temperature Coefficient of Resistance by Facing Targets D.c. Reactive Sputtering and Annealing Process." *Surface and Coatings Technology* 201 (9–11): 4969–72. doi:10.1016/j.surfcoat.2006.07.211.

Metcalf P. A., Guha S., Gonzalez L. P., Barnes J. O., Slamovich E. B., and Honig J. M. 2007. "Electrical, Structural, and Optical Properties of Cr-Doped and Non-Stoichiometric V_2O_3 Thin Films." *Thin Solid Films* 515, 3421–25. doi:https://doi.org/10.1016/j.tsf.2006.10.003.

Moreno M., Kosarev A., Torres A., and Ambrosio R. 2007. "Fabrication and Performance Comparison of Planar and Sandwich Structures of Micro-Bolometers with Ge Thermo-Sensing Layer." *Thin Solid Films* 515, 7607–10. doi:10.1016/j.tsf.2006.11.172.

Morin F. J. 1959. "Oxides Which Show a Metal-to-Insulator Transition at the Neel Temperature." *Physical Review Letters* 3 (1). American Physical Society: 34–36. doi:10.1103/PhysRevLett.3.34.

Morozov D., Mauskopf P. D., Ade P., Ridder M., Khosropanah P., Bruijn M., Kuur J. V., Hoevers H., Gao J. R., and Griffin D. 2011. "Ultrasensitive TES Bolometers for Space-Based FIR Astronomy." *IEEE Transactions on Applied*

Superconductivity 21, 188–91. doi:10.1109/TASC.2010.2089585.

Nagatsuma T., Horiguchi S., Minamikata Y., Yoshimizu Y., Hisatake S., Kuwano S., Yoshimoto N., Terada J., and Takahashi H. 2013. "Terahertz Wireless Communications Based on Photonics Technologies." *Optics Express* 21 (20): 23736. doi:10.1364/OE.21.023736.

Nagel M., Bolivar P. H., Brucherseifer M., Kurz H., Bosserhoff A., and Büttner R. 2002. "Integrated THz Technology for Label-Free Genetic Diagnostics." *Applied Physics Letters* 80 (1): 154–56. doi:10.1063/1.1428619.

Oak Ridge Laboratory. 2015. "Insulator-to-Metal Transition of Vanadium Dioxide." https://science.energy.gov/bes/highlights/2015/bes-2015-03-a/.

Ouchi T., Kajiki K., Koizumi T., Itsuji T., Koyama Y., Sekiguchi R., Kubota O., and Kawase K. 2014. "Terahertz Imaging System for Medical Applications and Related High Efficiency Terahertz Devices." *Journal of Infrared, Millimeter, and Terahertz Waves* 35 (1): 118–30. doi:10.1007/s10762-013-0004-5.

Oksuzoglu R. M., Bilgiç P., Yıldırım M., and Deniz O. 2013. "Influence of Post-Annealing on Electrical, Structural and Optical Properties of Vanadium Oxide Thin Films." *Optics & Laser Technology* 48, 102–9. doi:10.1016/j.optlastec.2012.10.001.

Ozyuzer L., Koshelev A. E., Kurter C., Gopalsami N., Li Q., Tachiki M., Kadowaki K., et al. 2007. "Emission of Coherent THz Radiation from Superconductors." *Science* 318 (5854): 1291–93. doi:10.1126/science.1149802.

Ozyuzer L., Simsek Y., Koseoglu H., Turkoglu F., Kurter C., Welp U., Koshelev A. E., et al. 2009. "Terahertz Wave Emission from Intrinsic Josephson Junctions in High-Tc Superconductors." *Supercond. Sci. Technol.* 22 (11): 114009 doi:10.1088/0953-2048/22/11/114009.

Podraza N. J., Gauntt B. D., Motyka M. A., Dickey E. C., and Horn M. W. 2012. "Electrical and Optical Properties of Sputtered Amorphous Vanadium Oxide Thin Films." *Journal of Applied Physics* 111 (7). doi:10.1063/1.3702451.

Radu I. P., Martens K., Mertens S., Adelmann C., Shi X., Tielens H., Schaekers M., et al. 2011. “Vanadium Dioxide as a Memory Material.” In *Silicon Compatible Materials, Processes, And Technologies for Advanced Integrated Circuits and Emerging Applications*, 35:233–43. doi:10.1149/1.3568865.

Rampelberg G., Schutter B. D., Devulder W., Martens K., Radu I., and Detavernier C. 2015. “In-Situ X-Ray Diffraction Study of the Controlled Oxidation and Reduction in the V-O System for the Synthesis of VO_2 and V_2O_3 Thin Films.” *J. Mater. Chem. C* 3. Royal Society of Chemistry: 11357–65. doi:10.1039/C5TC02553B.

Rauly D., Monfardini A, Colin A., and Febvre P. 2008. “Design of Two-Band 150-220 GHz Superconducting Bolometric Detection Structure.” *PIERS Online* 4 (6): 671–75. doi:10.2529/PIERS071220141852.

Rogalski A. 2012. “Progress in Focal Plane Array Technologies.” *Progress in Quantum Electronics* 36 (2–3): 342–473. doi:10.1016/j.pquantelec.2012.07.001.

Root M. J. 2011. “Resistance Model for Lithium-Silver Vanadium Oxide Cells.” *Journal Of The Electrochemical Society* 158 (12): A1347–53. doi:10.1149/2.049112jes.

Saijo H., Morimoto M., Yamashita M., Tonouchi M., and Hangyo M. 1999. “Terahertz Radiation from Log-Periodic Antennas.” In *Technical Digest. CLEO/Pacific Rim ’99. Pacific Rim Conference on Lasers and Electro-Optics*, 2:451–52. IEEE. doi:10.1109/CLEOPR.1999.811515.

Semerci T., Demirhan Y., Miyakawa N., Wang H. B., and Ozyuzer L. 2016. “Thin Film like Terahertz Bolometric Detector on Bi2212 Single Crystal.” *Optical and Quantum Electronics* 48 (6): 340. doi:10.1007/s11082-016-0612-0.

Shie J. S., Chen Y. M., Mang O. Y., and Chou B. C. S. 1996. “Characterization and Modeling of Metal-Film Microbolometer.” *Journal Of Microelectromechanical Systems* 5 (4): 298–306.

Smith E. M., Ginn J. C., Warren A. P., Long C. J., Panjwani D., Peale R. E., and Shelton D. J. 2014. “Linear Bolometer Array Using a High TCR VOx-Au Film.” *Proc. SPIE 9070, Infrared Technology and Applications* 4 (1): 90701Z. doi:10.1117/12.2050434.

Soltani M., Chaker M., Haddad E., Kruzelecky R. V., and Margot J. 2004. “Effects of Ti-W Codoping on the Optical and Electrical Switching of Vanadium Dioxide Thin Films Grown by a Reactive Pulsed Laser Deposition.” *Applied Physics Letters* 85 (11): 1958–60. doi:10.1063/1.1788883.

Son L. N., Tachiki T., and Uchida T. 2012. “High TCR of VO_x Thin Films Fabricated by Metal-Organic Decomposition for Bolometer Detectors.” In *2012 37th International Conference On Infrared, Millimeter, And Terahertz Waves (IRMMW-THz)*. International Conference on Infrared Millimeter and Terahertz Waves.

Stutzman W. L. and Thiele G. A. 1998. *Antenna Theory and Design*. Second edition John Wiley & Sons, Inc. http://www.wiley.com/college.

SURA. 2006. “Electromagnetic Spectrum.” http://www.sura.org/commercialization/terahertz.html#EMS_Chart.

Syllaios A. J., Schimert T. R., Gooch R. W., McCardel W. L., Ritchey B. A., and Tregilgas J. H. 2000. “Amorphous Silicon Microbolometer Technology.” *MRS Proceedings* 609. doi:10.1557/PROC-609-A14.4.

Tonks L., and Langmuir I. 1929. “A General Theory of the Plasma of an Arc.” *Physical Review* 34 (6). American Physical Society: 876–922. doi:10.1103/PhysRev.34.876.

Tonouchi M. 2007. “Cutting-Edge Terahertz Technology.” *Nature Photonics* 1 (2): 97–105. doi:10.1038/nphoton.2007.3.

Turkoglu F., Ozyuzer L., Koseoglu H., Demirhan Y., Preu S., Malzer S., Simsek Y., Wang H. B., and Muller P. 2013. “Emission of the THz Waves from Large Area Mesas of Superconducting $Bi_2Sr_2CaCu_2O_{8+\delta}$ By the Injection of Spin Polarized Current.” *Physica C: Superconductivity and Its Applications* 491: 7–10. doi:10.1016/j.physc.2013.01.014.

Wang B., Lai J., Li H., Hu H., and Chen S. 2013. “Nanostructured Vanadium Oxide Thin Film with High TCR at Room Temperature for Microbolometer.” *Infrared Physics & Technology* 57, 8–13. doi:10.1016/j.infrared.2012.10.006.

Wang B., Lai J., Zhao E., Hu H., and Chen S. 2012. “Research on VO_x Uncooled Infrared Bolometer Based on Porous Silicon.” *Frontiers of Optoelectronics* 5 (3):

292–97. doi:10.1007/s12200-012-0224-7.

Wang H., Yi X., and Chen S. 2006. “Low Temperature Fabrication of Vanadium Oxide Films for Uncooled Bolometric Detectors.” *Infrared Physics & Technology* 47 (3): 273–77. doi:http://dx.doi.org/10.1016/j.infrared.2005.04.001.

Wei X., Li S., Gou J., Dong X., Yang X., Li W., Wang T., Wu Z., Jiang Y., and Chen Z. 2014. “Preparation and Characteristics of Vanadium Oxide Thin Films by Controlling the Sputtering Voltage.” *Optical Materials* 36 (8): 1419–23. doi:10.1016/j.optmat.2014.02.021.

Wood R. A. 1993. “Uncooledthermal Imaging with Monolithic Silicon Focal Planes.” In *Proc. SPIE Vol. 2020*, 21:322–29. doi:10.1111/j.1744-618X.2010.01158.x.

Wood R. A. 1995. “Use of Vanadium Oxide in Microbolometer Sensors.” Google Patents. https://www.google.com/patents/US5450053.

Woodward R. M., Cole B. E., Wallace V. P., Pye R. J., Arnone D. D., Linfield E. H., and Pepper M. 2002. “Terahertz Pulse Imaging in Reflection Geometry of Human Skin Cancer and Skin Tissue.” *Physics in Medicine and Biology* 47 (21): 3853–63. doi:10.1088/0031-9155/47/21/325.

Yang Y., Singh R., and Zhang W. 2011. “Anomalous Terahertz Transmission in Bow-Tie Plasmonic Antenna Apertures.” *Optics Letters* 36 (15): 2901. doi:10.1364/OL.36.002901.

Yang Z., Ko C., and Ramanathan S. 2011. “Oxide Electronics Utilizing Ultrafast Metal-Insulator Transitions.” *Annaul Review of Materials Research* 41 (1): 337–67. doi:10.1146/annurev-matsci-062910-100347.

Yuce H., 2015. "Characterization of vanadium oxide thin films grown by magnetron sputtering technique" Dissertation, http://openaccess.iyte.edu.tr/handle/11147/4585

VITA

Hakan Alaboz
Izmir Institute of Technology
Materials Science and Engineering
Department
Urla, Izmir/Turkey

email hakan.alaboz@gmail.com

phone +905335429312

Date of birth: February 27, 1983

Education

Ph.D.	Materials Science and Engineering, Izmir Institute of Technology
M. Sc.	Physics Engineering, Ankara University
B. Sc.	Physics Engineering, Ankara University

Teaching Experience:

Undergraduate level courses; Freshmen Physics,

Modern Physics Lab., Electric Lab.,
Waves and Optics Lab. and Mechanics Lab. IZTECH (2013-2016)

Reviewer Experience:

Vacuum	(2016)
IOP Nanotechnology	(2017)

List of Publications:

1) G. Aygun, H. Yuce, H. Alaboz, Y. Demirhan, M. Ozdemir, L. Ozyuzer, Physica Scripta, 92, 114007, 2017
2) H. Alaboz, Y. Demirhan, H. Yuce, G. Aygun, L. Ozyuzer, Optical and Quantum Electronics, 49, 239, 2017
3) Y. Demirhan, H. Alaboz, M. A. Nebioglu, B. Mulla, M. Akkaya, H. Altan, C. Sabah, L. Ozyuzer, Superconducting Science and Technology, DOI: 10.1088/1361-6668/aa6fbe, 2017
4) M. A. Nebioglu, T. Takan, H. Altan, Y. Demirhan, H. Alaboz, L. Ozyuzer, C. Sabah, Modern Physics Letters B, 31, 1750074, 2017
5) Y. Demirhan, H. Alaboz, L. Özyüzer, M. A. Nebioğlu, T. Takan, H. Altan, C. Sabah, Optical and Quantum Electronics, 48, 170, 2016
6) Y. Demirhan, H. Saglam, F. Turkoglu, H. Alaboz, L. Ozyuzer, N. Miyakawa, K. Kadowaki, Vacuum, 120, 89, 2015
7) H. Olgar, H. Alaboz, (available in arxiv.org), 2015